

Some pages of this thesis may have been removed for copyright restrictions.

If you have discovered material in Aston Research Explorer which is unlawful e.g. breaches copyright, (either yours or that of a third party) or any other law, including but not limited to those relating to patent, trademark, confidentiality, data protection, obscenity, defamation, libel, then please read our [Takedown policy](#) and contact the service immediately (openaccess@aston.ac.uk)

Channel Characteristics for Intra-Vehicle Wireless Communications

Mohd Nur Irfan Bin Mohd Yusoff

A thesis presented for the degree of
Doctor of Philosophy

Aston University

June 2020

©Mohd Nur Irfan Bin Mohd Yusoff, 2020

Mohd Nur Irfan Bin Mohd Yusoff asserts his moral right to be identified as the
author of this thesis

“This copy of the thesis has been supplied on condition that anyone who consults
it is understood to recognise that its copyright belongs to its author and that no
quotation from the thesis and no information derived from it may be published
without appropriate permission or acknowledgement.”

Aston University
Channel Characteristics for Intra-Vehicle Wireless Communications
Mohd Nur Irfan Bin Mohd Yusoff
Doctor of Philosophy, 2020

Vehicles are continuously being improved to enhance the driving experience by integrating new technologies. Recent luxury vehicles may have over 70 Electronic Control Units (ECU) and 2200 cables. It is estimated that the number of ECUs and connections between ECUs and sensors will continuously increase to meet growing network requirements. The wire harness is the third most expensive component in a vehicle, reducing the number of cables through wireless communications would consequently result in space, cost, and fuel savings. However, the behaviour of the intra-vehicle channel and suitable wireless network technologies for an intra-vehicle network have not been fully addressed.

In this research, the intra-vehicle narrowband loss performance in non-line-of-sight and line-of-sight condition was investigated and compared through real field tests. The results indicate that fading behaviour is primarily caused by small-scale rather than large-scale fading. An empirical-based path loss model is proposed with its parameters extracted from the real field test measurements. Further analysis of the small-scale fading through Rician K -factor reveals the dependence of the K -factor with distance and locations. These investigations suggest that for a narrowband system whereby the bandwidth of the transmitted signal is lower than the coherence bandwidth; the channel can be modelled using Rician fading. Furthermore, the wideband and ultra-wideband channel was characteristics through a real field tests. The results demonstrate that the multipath fading of intra-vehicle channel is much worse than other type of environments such as factory workshops and hospitals.

Finally, the time-varying characteristics of the intra-vehicle channel, tested under various scenarios, suggest that the channel's coherence time is primarily impacted by passenger motion in the vehicle. Considering both the channel loss and time-varying characteristics, the performance trade-off's of the cooperative communication system against retransmission was evaluated.

Keywords: channel characteristics, intra-vehicle, wireless communications, automotive

To my loving parents,

Acknowledgements

This journey would not have been possible without the help and support from many people. First and foremost, I would like to express my gratitude to my supervisor Dr Xiaohong Peng, for his guidance, enthusiasm and patience throughout these years. I am forever indebted for his continuous support through this challenging journey. I would also like to extend my gratitude to Prof. Jack Hynds for his valuable industrial insight and support during my research.

Many thanks to my colleague in the research group, Steven Knowles and Mala Sadik, with whom I have shared my thoughts and also for their assistance. I would also like to extend my thanks to Tristan Fleet for always offering a helping hand.

I would like to give my sincere thanks to my parents and wife for their support and encouragement throughout this journey.

Last but not least, I would like to thank Aston University and Jaguar Land Rover for the financial support and assistance. This journey might never happened without their support.

Contents

Thesis Summary	1
Dedication	2
Acknowledgements	3
Acronym	8
List of figures	12
List of tables	16
1 Introduction	17
1.1 Research objectives	18
1.2 Contributions	19
1.3 List of publications	20
1.4 Structure of thesis	21
2 Fundamentals of wireless communication channels	22
2.1 The mechanism of radio propagation	23
2.2 Fading manifestation	24
2.2.1 Large-scale fading	25
2.2.2 Small-scale fading	27
2.3 Channel modelling	28

2.3.1	Amplitude statistics	29
2.3.2	Multipath channels	30
2.4	Summary and conclusions	32
3	Intra-vehicle wireless networks (IVWN)	33
3.1	Vehicle networks	33
3.1.1	CAN	34
3.1.2	LIN	35
3.1.3	FlexRay	35
3.1.4	MOST	35
3.1.5	LVDS	36
3.1.6	Automotive ethernet	36
3.2	Vehicle network architecture	37
3.2.1	Future network requirements	40
3.3	Wireless network in vehicles	40
3.3.1	Channel investigation and its models	41
3.4	Summary and conclusions	43
4	Narrowband channel characteristics of IVWN	44
4.1	Introduction	44
4.2	Testbed setup	46
4.2.1	Calibration procedure	47
4.2.2	Measurement procedure and scenario	48
4.3	Experimental results and data analysis	50
4.3.1	Path loss	50
4.3.2	Large-scale fading	52
4.3.3	Small-scale fading	58
4.3.4	Rician fading channels (K -factor)	60

4.4	Summary and conclusions	64
5	Wideband channel characteristics of IVWN	66
5.1	Introduction	66
5.2	Testbed setup	67
5.2.1	Measurement campaign and procedures	67
5.3	Experimental results and data analysis	69
5.3.1	Power delay profile	69
5.3.2	RMS delay spread	75
5.3.3	Coherence bandwidth	78
5.4	Summary and conclusions	80
6	Electromagnetic interference (EMI)	82
6.1	EMC standards	84
6.1.1	CISPR-25	85
6.2	Testbed and experiment	90
6.3	Result and analysis	92
6.3.1	Impulsive noise	92
6.3.2	Investigation on the impulsive noise radiated in the engine compartments	97
6.3.3	Characterising the measured EMI	97
6.4	Summary and conclusions	105
7	Time-varying and cooperative communication in IVWN	107
7.1	Time-varying channel characteristic	108
7.1.1	Testbed setup: Time variation measurement	110
7.1.2	Experimental results and data analysis	113
7.2	Cooperative relaying in IVWSN	116

7.2.1	Testbed setup: Cooperative relaying and retransmission scheme	118
7.2.2	Performance evaluation	120
7.3	Summary and conclusions	123
8	Conclusions and future work	125
8.1	Summary	125
8.2	Future work	127
	Bibliography	130

Acronym

ADAS advanced driver assistance systems

AF amplify-and-forward

ADC analogue to digital converter

APDP averaged power delay profile

APD Amplitude probability distribution

CSMA carrier-sense multiple access

CR carrier resolution

CIR channel impulse response

CDF Cumulative distribution function

CISPR Comité International Spécial des Perturbations Radioélectriques

CAN control area network

DF decode-and-forward

dBm decibel-milliwatts

dB decibel

ECU electronic control units

EMI electromagnetic interference

EMC electromagnetic compatibility

EMCD electromagnetic interference directive

EU European union

ETSI European Telecommunications standards institute

FSPL free-space path loss

FCC federal communications commission

FCF frequency correlation function

FIR finite impulse response

GHz gigahertz

Gbps gigabit per second

Hz hertz

IDFT inverse discrete fourier transform

IVWN intra-vehicle wireless network

IET institution of engineering and technology

IEC international electrotechnical commision

ISO international organization for standardization

Kbps kilobit per second

KS kolmogorov-smirnov

LOS line-of-sight

LVDS low-voltage differential signaling

LIN local interconnect network

LAN local area network

MOST media oriented systems transport

Mbps megabit per second

Msps mega samples per second

MHz megahertz

MIMO multiple-input and multiple-output

MATLAB matrix laboratory

ms milliseconds

NLOS non line of sight

ns nanoseconds

OCB outside the context of a basic service set

PDP power delay profile

QAM quadrature amplitude modulation

RLV relative loss variation

rms root mean square

Rx receiver

SDR software defined radio

SoC system on chip

TSN time sensitive networking

TV television

TDMA time-division multiple access

TT-CAN time triggered control area network

Tx transmitter

UNECE united nations economic commission of europe

USRP universal software radio peripheral

UWB ultra-wideband

UART Universal Asynchronous Receiver/Transmitter

Wi-Fi Wireless Fidelity

List of Figures

2.1	Received power against distance.	25
2.2	Fading channel manifestation.	26
2.3	Small-scale fading.	27
2.4	Different channel modelling approaches.	28
2.5	An example of a channel impulse response (<i>CIR</i>).	31
3.1	A simplified vehicle network architecture [40].	39
4.1	Block diagram of experimental testbed.	46
4.2	A diagram of equipment calibration setup.	47
4.3	A diagram of equipment calibration setup.	48
4.4	Measurement locations.	49
4.5	Measured path loss, mean path loss and loss due to large-scale fading at 2.4 GHz.	53
4.6	Measured path loss, mean path loss and loss due to large-scale fading at 5.9 GHz.	53
4.7	1α -spread (in dB) vs. signal length $2L$ using the Lee method for 2.4 GHz.	55
4.8	1α -spread (in dB) vs. signal length $2L$ using the Lee method for 5.9 GHz.	56

4.9	1α -spread (in dB) vs. signal length $2L$ using the generalized Lee method for 2.4 GHz.	56
4.10	1α -spread (in dB) vs. signal length $2L$ using the generalized Lee method for 5.9 GHz.	57
4.11	The CDF of large-scale fading and log-normal fit at 2.4 GHz.	58
4.12	The CDF of large-scale fading and log-normal fit at 5.9 GHz.	58
4.13	The cumulative distribution function (CDF) of relative loss variation (RLV) for Small-scale fading β_s and Rician fit.	59
4.14	The cumulative distribution function (CDF) of relative loss variation (RLV) for Small-scale fading β_s and Rician fit.	60
4.15	Estimated Rician K -factor against distance for 2.4 GHz.	63
4.16	Estimated Rician K -factor against distance for 5.9 GHz.	63
5.1	The testbed setup block diagram.	68
5.2	Transmitter and receiver locations.	69
5.3	Location of firewall within the engine compartment.	70
5.4	The frequency response $H(f)$ of location number 2, 24 and 48.	70
5.5	The PDP of all 49 locations.	73
5.6	A normalized PDP of all 49 locations in 2D.	73
5.7	A heat-map of 49 PDP	73
5.8	The first peak power at $t = 0$ of all 49 locations versus distance.	74
5.9	Power delay profile of the 49th location.	74
5.10	The $APDP(t)$ with Two-component power law fit.	75
5.11	RMS delay spread against different location.	76
5.12	rms delay spread against distance.	77
5.13	Frequency correlation function of the 21st location.	79
5.14	The coherence bandwidth at different locations.	80

5.15	The coherence bandwidth against distance.	81
6.1	CISPR-25 class 5 peak and quasi-peak limits.	86
6.2	CISPR-25 class 5 average limits.	86
6.3	CISPR-25 class 5 peak and quasi-peak limits in dBm.	87
6.4	CISPR-25 class 5 average limits in dBm.	88
6.5	Estimated received average noise power based on CISPR-25.	89
6.6	Estimated received peak noise power based on CISPR-25.	89
6.7	Engine-compartment measurement (Test 1).	91
6.8	Engine compartment measurement (Test 2).	91
6.9	Time-series measurement performed at location 1 when the engine is turned off and on.	93
6.10	Time-series measurement at 433 MHz for the engine, passenger and boot compartment.	94
6.11	Time-series measurement at 2.4GHz for the engine, passenger and boot compartment.	94
6.12	Probability density of the time-series measurement at 433 MHz.	95
6.13	Probability density of the measurement at 2.4 GHz.	96
6.14	Burst length and burst gap of impulsive noise.	98
6.15	Distribution of EMI burst length at 433 MHz.	99
6.16	Distribution of EMI burst length at 2.4 GHz.	100
6.17	Distribution of EMI burst length at 5.9 GHz.	100
6.18	Distribution of EMI burst gap at 433 MHz.	101
6.19	Distribution of EMI burst gap at 2.4 GHz.	102
6.20	Distribution of EMI burst gap at 5.9 GHz.	102
6.21	<i>APD</i> of location 2 at 433 MHz.	104
6.22	<i>APD</i> of location 2 at 2.4 GHz.	104

6.23	<i>APD</i> of location 2 at 5.9 GHz.	105
7.1	The time variation measurement (Test 1) experiment setup.	110
7.2	The measured received signal power (dBm) against time (s) of the antenna located on the driver side.	112
7.3	The measured received signal power (dBm) against time (s) of the antenna located on the passenger side.	112
7.4	The autocorrelation of the measured received power for antennas located on the driver side and passenger side.	114
7.5	The coherence time against time in seconds.	115
7.6	Transmitter, relay and receiver node in cooperative relaying configuration.	117
7.7	The cooperative and retransmission (Test 2) experimental setup. . .	118
7.8	The testbed event diagram.	120
7.9	The percentage of packet received for direct, cooperative relaying and retransmission.	121
7.10	The number of consecutive packet losses against time in seconds for direct, retransmission, and cooperative relaying.	121
7.11	The distribution of the number of consecutive packet losses for direct, retransmission, and cooperative relaying.	122

List of Tables

3.1	A summary of network protocol specifications.	34
3.2	A summary of domain latency and bandwidth requirements [37]. . .	38
3.3	SAE functional classifications.	38
4.1	USRP settings at 2.4 GHz and 5.9 GHz	49
4.2	Estimated loss exponent and reference path loss.	52
5.1	A table of <i>rms</i> measurement campaign in different environments . .	77
6.1	USRP settings at 433 MHz, 2.4 GHz and 5.9 GHz	91
6.2	The peak EMI measured in the engine, passenger and boot compart- ments of a Land Rover Discovery Sport.	96
6.3	The peak EMI measured in the engine, passenger and boot compart- ments of a Skoda Fabia.	96
6.4	Peak EMI measured at five locations and different frequencies. . . .	98
7.1	USRP settings for N_s , R_L and N_d nodes.	120

Chapter 1

Introduction

A vehicle network architecture contains multiple buses and point-based networks which enable the transfer of information between electronic control units (ECUs). Historically, additional network buses are added to support the growing number of sensors and ECUs; in consequence, this leads to increased network complexity [1]. The number of ECU in a vehicle has increased considerably from 75 ECUs in 2010 to 150 ECUs in 2019 [2,3]. In addition, the total cost of sensors and electronic devices in vehicles is rapidly increasing wherein 2020, it is responsible for 40% of the cost of a vehicle, as compared to 18% in 2000 [4]. The wire-harness system is the third most expensive and heaviest component behind the engine and chassis. In a luxury vehicle, the wire harness can weight as much as 60 kg [5].The increasing network complexity and cost has attracted significant research attention, where various wired network solution has been proposed [1].

A wireless solution can provide significant benefits to a vehicle, where it can lead to cost and weight savings by reducing the size of the wire harness. Additionally, implementing a wireless solution could ease the design and installation of a vehicular network, which is a time-consuming and labour-intensive process. There are

relatively few studies conducted on the topic of wireless communications as compared to wired communications in a vehicle. Several wireless network solutions have been proposed in the literature, which focuses on low data-rate wireless communications. In recent years, the introduction of new technologies such as advanced driving assistance systems (ADAS) and autonomous driving has changed vehicle network requirements, increasing the demand for a high-bandwidth, low-latency, and deterministic network in vehicles.

Currently, wireless communications in a vehicle are limited to navigation and infotainment applications and yet to be integrated into other systems such as vehicle control and sensing. Wireless communications must operate reliably in a vehicle environment which is affected by severe multipath fading. Moreover, the fast increasing number of electronic devices and vehicle electrification pose new challenges for wireless communications due to the increased radiated electromagnetic interference (EMI). A further understanding of the characteristics of intra-vehicle channels is needed before applying the suitable technologies that can establish reliable and sustainable wireless connectivity in this challenging environment.

1.1 Research objectives

Replacing the current wired networks in vehicles requires thorough knowledge and an accurate understanding of vehicle channel characteristics. This study aims to identify and investigate various factors that could impact the performance of wireless communications in a vehicle. The results will facilitate the design of wireless intra-vehicle communication for a unique vehicle environment. Currently, there are no wireless intra-vehicle network standards available, nor is there a definite answer on which technology is most suitable for the vehicle environment. Therefore, it is beneficial to investigate vehicle channel properties from a broad perspective. A series

of measurement campaign was conducted to investigate and analyse the channel properties.

This investigation on vehicle channel properties can be categorised into three aspects: 1) channel loss, 2) electromagnetic interference (EMI), 3) time-varying channel characteristic. In the first part, the narrowband, wideband and UWB channel characteristic is analysed by evaluating the propagation loss, small-scale and large-scale fading, delay spread, and coherence bandwidth of the channel. In the second part, the impact of radiated EMI on wireless communications in vehicles is performed by reviewing the current automotive standard on electromagnetic compatibility (EMC) and as well as characterising the EMI in vehicles. In the final part, the time-varying characteristic in a vehicle environment is investigated by evaluating the channel coherence time.

1.2 Contributions

The primary contributions of this thesis can be summarised as follows:

- A path-loss model for intra-vehicle narrowband communication is presented together with its large-scale and small-scale fading statistics. This study highlights the method of extracting fading components and the level of influence from each of these components over the overall loss performance at various frequencies.
- A Rician K -factor analysis of the small-scale fading is presented, where the result shows a near-Rayleigh condition.
- The appropriate averaging window length for extracting large-scale fading in the vehicle environment is presented.

- The vehicle multipath characteristics in non-line-of-sight are analysed by evaluating the root-mean-squared (*rms*) delay spread and coherence bandwidth. In addition, this work presents the dependency of *rms* delay spread and coherence bandwidth with location and distance.
- The electromagnetic interference (EMI) at 433 MHz, 2.4 GHz, and 5.9 GHz on several locations in a vehicle is presented. The impulsive noise is characterised according to its likelihood of occurring, burst length, and burst gap.
- The time-varying nature of the vehicle in motion was characterised in term of its fading and coherence time. The result suggests the vehicle can be treated as a slow fading channel.
- The performance evaluation of cooperative relaying in comparison to direct transmission and retransmission scheme was presented.

1.3 List of publications

- Irfan Yusoff, Xiaohong Peng "Impacts of Channel Loss and Electromagnetic Interference on Intra-Vehicle Wireless Communications," 2020 IEEE 91st Vehicular Technology Conference (VTC2020-Spring), Antwerp, Belgium, 2020.
- Irfan Yusoff, Xiaohong Peng "The Multipath Characteristic of an Intra-Vehicle Channel under the Non-Line-of-Sight Condition," 2020 IEEE 91st Vehicular Technology Conference (VTC2020-Spring), Antwerp, Belgium, 2020.
- Steven Knowles Flanagan, Xiaohong Peng, Jianhua He, Irfan Yusof "Empirical Investigation of SDR-based DSRC Communication," 2020 IEEE 91st Vehicular Technology Conference (VTC2020-Spring), Antwerp, Belgium, 2020.
- Irfan Yusoff, Xiaohong Peng, Jack Hynds "Loss Performance of Intra-Vehicle Channels for Narrowband Signal Transmission," 2020 The Ninth International

Conference on Advances in Vehicular Systems, Technologies and Applications (VEHICULAR 2020), Porto, Portugal, 2020.

- Irfan Yusoff, Xiaohong Peng "On the Rician K -factor of Intra-Vehicle Fading Channels," 2020 IEEE 31st Annual International Symposium on Personal, Indoor and Mobile Radio Communications (PIMRC), London, UK, 2020.

1.4 Structure of thesis

In Chapter 2, the fundamentals of wireless communications, including multipath propagation characteristics and fading mechanisms is presented; it serves as a foundation for the remainder of the thesis. Chapter 3 covers the current development of wired vehicle network architecture. It also describes the state-of-art of wireless communications in a vehicle.

Chapter 4 discusses the analysis of the results on the narrowband characteristics of a vehicle, regarding its large-scale and small-scale fading components. The analysis of small-scale fading is further expanded with a Rician K -factor analysis. Chapter 5 investigates wideband channel characteristics in non-line-of-sight conditions, with the multipath channel statistics extracted and analysed. Topics related to electromagnetic interference (EMI), including a review of current electromagnetic compatibility (EMC) standards, are discussed in Chapter 6. In Chapter 7, the time-varying nature of an occupied vehicle was investigated. Furthermore, the performance of wireless transmission using cooperative relaying, as well as direct transmission and retransmission scheme was evaluated. Finally, the thesis is summarised and concluded in Chapter 8.

Chapter 2

Fundamentals of wireless communication channels

Wireless communications had far-reaching societal impacts. The transfer of information no longer must be done through a physical medium. The electromagnetic theory published in 1861 by James Clerk Maxwell established the foundation of our understanding of electromagnetic wave propagation. Today, wireless communications are utilised in many devices, from TVs and computers to mobile phones. In wireless communications, a channel ($H(t)$) describes the characteristics of the path between a transmitter and receiver. Electromagnetic wave propagation is highly dependent on the type of transmission medium through which the wave travels [6]. It is critical to understand the channel characteristics because they impact the performance of wireless communication systems.

2.1 The mechanism of radio propagation

The characteristics of the propagation channel governs the level and quality of the received signal. Similar to other forms of electromagnetic energy, radio waves also experience reflection, refraction, and diffraction [7]. In an ideal free-space environment - a vacuum environment where a wave is free from obstacles and obstructions, the signal strength of a transmitted radio signal travelling between a transmitter and receiver will be attenuated as a function of distance [8]. In wireless communications, the attenuation loss due to the influence of the medium in which the signal travels is known as path loss. The free-space path loss (*FSPL*) equation is commonly used to model and describe path loss as a function of distance, which is given in [9] as:

$$FSPL(d) = \frac{P_t G_t G_r}{P_r} = \frac{P_t G_t G_r \lambda^2}{(4\pi)^2 d^2 L} \quad (2.1)$$

where P_r is the received power, P_t is the transmitted power, L is the system loss factor, G_r is the receiver antenna gain, G_t is the transmitter antenna gain, d is the separation distance between transmitter and receiver in meters, and λ is the signal wavelength in meters. According to Eq. 2.1, the signal transmitted between the transmitter and receiver has an inverse-square law function.

For an environment that is relatively free from obstructions, the *FSPL* equation is adequate in estimating the performance of a wireless system. However, this equation is inadequate for an environment with a dense multipath. Multipath propagation is an inherent feature of a wireless communication channel, in which a received signal is a superposition of several delayed copies of the transmitted signal. In other words, a received signal is a combination of power received from two or more reflected paths. Several phenomena (for example, reflection, absorption, diffraction, and scattering) are responsible for the creation of multipath [7].

Reflection

Reflection occurs when the radio electromagnetic wave hits the smooth surface of an object with a dimension that is larger than the wavelength (λ) of the transmitted radio wave. A transmitted wave results in a specular reflection with reduced power due to the absorption characteristics of the material which it has come into contact. In practice, reflection happens when a transmitted signal interacts with the ground surface, buildings, walls, floors, ceilings, and other objects in the environment.

Diffraction

Diffraction occurs when radio waves interact with objects or obstacles with sharp edges or wedges. The radio waves bend around the obstruction, reducing field strength.

Scattering

The scattering phenomenon occurs when radio waves come into contact with rough surfaces, which causes a transmitted wave to scatter into multiple specular reflections.

2.2 Fading manifestation

In a multipath environment, a radio signal arrives at the receiver in multiple copies from different directions. Depending on the amplitude and phase of the signal, this can cause constructive or destructive interference [9]. When the received signal strength is measured as a function of distance or time, the random fluctuations in received signal strength, as demonstrated in Fig.2.1 are known as multipath fading [8]. Fading manifestations can be broadly classified into two primary groups:

large-scale fading and small-scale fading, as shown in Fig.2.2 [10]. Large-scale is typically attributed to prominent or large features and objects. Whereas, small-scale fading refers to rapid changes in amplitude, with changes in separation distance as small as half a wavelength, as shown in Fig.2.3. A received signal $r(t)$ when described as a function of time, can be expressed as a combination of large-scale $m(t)$ and small-scale $r_0(t)$ component, as given by [10]:

$$r(t) = m(t)r_0(t) \quad (2.2)$$

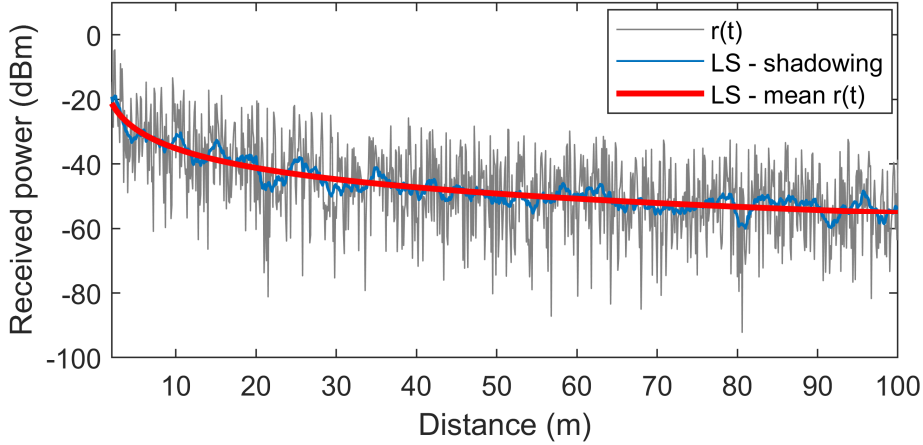


Figure 2.1: Received power against distance.

2.2.1 Large-scale fading

Large-scale fading describes the slow changes in received signal strength, or path loss with distance, when averaged across multiple wavelengths. In the literature, the phenomenon is described as being caused by the interaction between the transmitted signal and prominent or large features such as buildings [11]. Large-scale fading statistics are expressed in terms of mean path loss (L_m) which can be evaluated through linear regression, and a log-normally (X_α) distributed variation about the

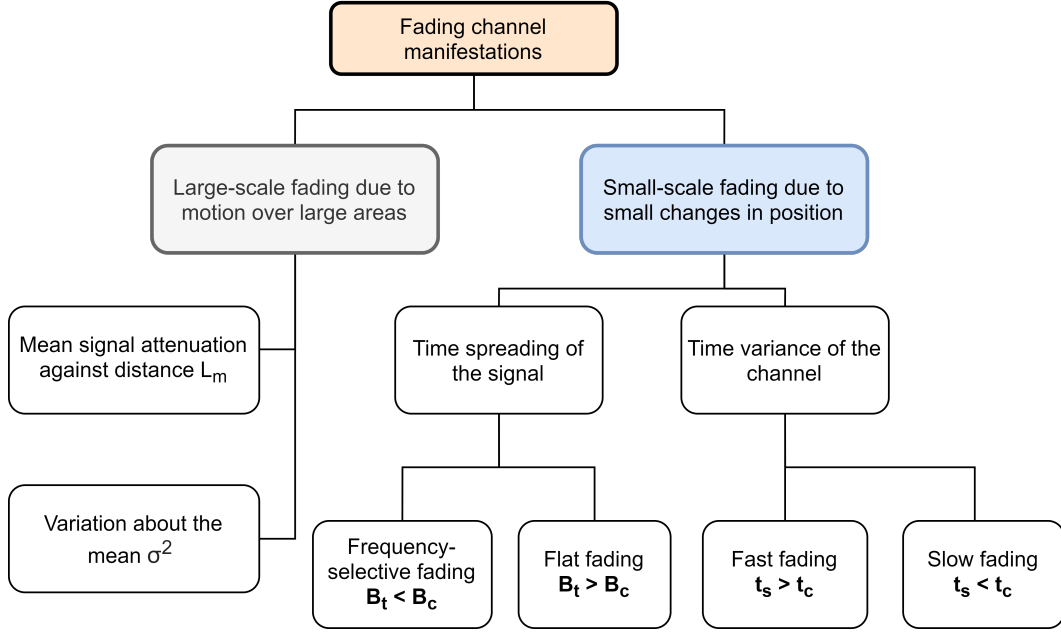


Figure 2.2: Fading channel manifestation.

mean, as given by [9, 12]:

$$L_p = L_m + X_\alpha \quad (2.3)$$

where the combined loss often stated in dB is denoted by L_p . The mean path loss (L_m) which is typically modelled by the generalised Friis equation also known as the log-distance path-loss model, is given by [9]:

$$L_m = L_{ref}(d_0) + 10n \log_{10}\left(\frac{d}{d_0}\right) \quad (2.4)$$

where the terms L_{ref} , n , d , d_0 represents the path loss at a reference distance, the path loss exponent, the distance between the transmitter and receiver antennas, and the chosen reference distance.

2.2.2 Small-scale fading

Small-scale fading is divisible into two categories: signal dispersion and time-variant behaviour of the channel [10]. The manifestation can be analysed in either the time or frequency domains. In a heavy multipath environment, a received signal is a combination of multiple signals reflected from the environment. In environment with numerous reflected paths, a small change in distance leads to a change in the distance travelled on each reflected paths. Hence, this causes a change in phase and amplitude of the reflected signal which result in a rapid fluctuation in the received signal strength amplitude, as shown in Fig.2.3.

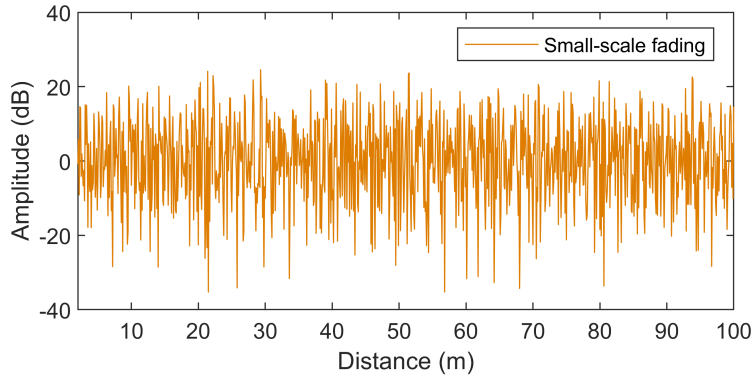


Figure 2.3: Small-scale fading.

Coherence bandwidth (B_c) is a channel parameter, in which the channel is assumed to be linear in gain and phase for a range of frequencies [9]. A time-invariant channel can be classified as frequency-selective fading or flat fading [13]. A channel is deemed to be frequency-selective when the bandwidth of the transmitted signal (B_t) is larger than the coherence bandwidth (B_c) of the channel. In contrast, a channel is deemed to be flat fading when the bandwidth of the transmitted signal (B_t) is smaller than the coherence bandwidth (B_c) of the channel.

In a time-variant channel, a channel is classified as a slow-fading channel when

the symbol length (t_s) in time is lower than the coherence time (t_c) of the channel [14]. In contrast, the channel is deemed to be fast-fading when the coherence time is shorter than the symbol length in time.

2.3 Channel modelling

A wireless channel is modelled using mathematical or empirical approaches to evaluate the performance of various wireless technologies. Improving our knowledge and understanding of a channel facilitates the design of wireless technologies that are suitable for such an environment. Broadly, channel modelling can be classified into two categories: deterministic and empirical, as shown in Fig.2.4 [15].

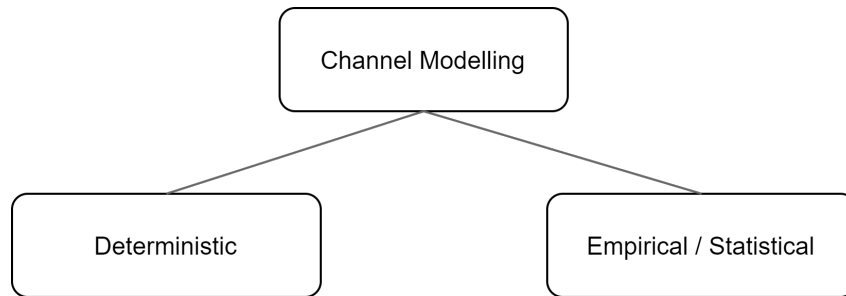


Figure 2.4: Different channel modelling approaches.

A deterministic model uses mathematical approaches where the physical environment is mapped in detail, and the channel is characterised using techniques such as ray-tracing, ray-launching, and electromagnetic field solvers. The accuracy of a model is highly dependent on the detailed representation of the environment [16]. The disadvantage of the deterministic method is that the complexity increases with the number of objects and structures within the environment. As an example, modelling a communication channel on an offshore platform at the sea is much simpler than modelling a channel operating in a dense city environment.

A channel could also be modelled using statistical or empirical approaches. The

empirical method is less complicated and yields a more accurate representation of a channel because it accounts for materials and detail feature of the structures. There are various approaches, ranging in complexity from simple path-loss measurements to channel-response measurements.

2.3.1 Amplitude statistics

The received signal is a combination of multiple reflected signals as a consequence of interaction with a multipath environment. The interaction of the signal with the environment can cause the signal to vary with time and distance. The envelope amplitude of small-scale fading is commonly modelled as a statistical distribution, usually as a Rician or Rayleigh distribution function [17].

Rayleigh

Rayleigh distribution is used to describe small-scale fading with no specular component. In other words, the channel is modelled as an environment without a line-of-sight (*LOS*) path. The Rayleigh distribution is expressed as [18]:

$$P(r) = \frac{r}{\sigma^2} \exp\left(-\frac{r^2}{2\sigma^2}\right) \quad (2.5)$$

where r is the amplitude of the signal and σ is the standard deviation of the signal.

Rician

In some scenarios, a direct line-of-sight (*LOS*) path between the transmitter and receiver may exist. In this situation, the Rician distribution is more appropriate for describing the fading statistics. Rician fading is usually described using two parameters (A^2 and σ^2) known as the Rician K -factor, as given by [19, 20]:

$$K = \frac{|A|^2}{2\sigma^2} \quad (2.6)$$

where K is the ratio of the dominant component (A^2) to the scattered component (σ^2). As the amplitude of the dominant component approaches zero, the Rician distribution approaches the Rayleigh distribution. In addition to Rician and Rayleigh distributions, other distributions that have been used to model the amplitude statistics of small-scale fading include the Nakagami and Weibull distributions.

2.3.2 Multipath channels

In wireless communications, multipath propagation is modelled as a Channel Impulse Response (CIR), also known as Finite Impulse Response (FIR) filter in linear systems. A channel can be characterised as a time-dependent impulse response $h(t, \tau)$ or a frequency-dependent $H(\omega, \tau)$ impulse response [21]. In a time-invariant system, the output of the system $y(t)$ for a given input $x(t)$ can be determined using a time-dependent impulse response [22]:

$$y(t) = \int_{+\infty}^{-\infty} h(t, \tau)x(t - \tau)d\tau \quad (2.7)$$

The interaction between the transmitted signal with the environment causes multiple delayed copies to be received on the receiver. The received signal consist of a time-delayed, attenuated and phase-shifted copy of the transmitted signal, as represented in Fig.2.5. The channel when assumed to be time-variant $h(t, \tau)$ or time-invariant $h(t)$ over a small time interval can be represented as [23, 24]:

$$h(t, \tau) = \sum_{i=1}^N a_i(t)e^{-j\phi_i}\delta(\tau - \tau_i) \quad (2.8)$$

where $a_i(t)$, $\delta(\tau)$ and ϕ_i represents the amplitude of a multipath, the Dirac delta

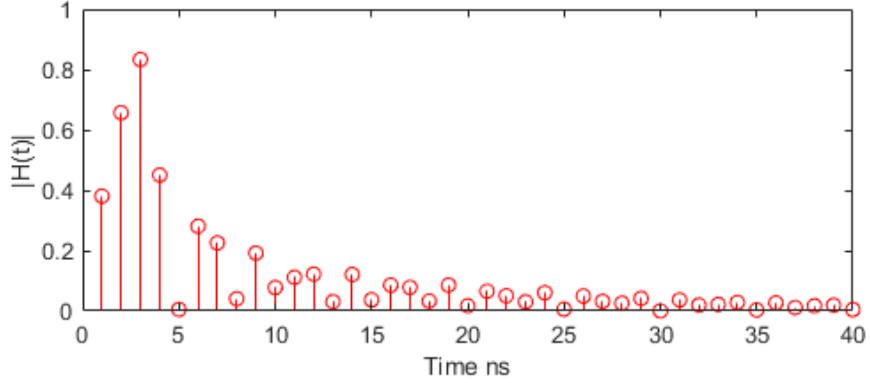


Figure 2.5: An example of a channel impulse response (*CIR*).

function and the i th phase angle, respectively.

The power delay profile ($PDP(t)$) is commonly used to analyse the multipath characteristics of a wireless channel. The PDP is the square magnitude of the channel impulse response (*CIR*), as expressed in [9]:

$$PDP(t) = |h(t)|^2 \quad (2.9)$$

The multipath of an environment is characterised by parameters such as root mean square (*rms*) delay spread (τ_{rms}), mean excess delay ($\bar{\tau}$) and maximum delay spread (τ_{max}). The parameters are calculated using the extracted $PDP(t)$. The mean excess delay ($\bar{\tau}$) of a channel is evaluated by [25]:

$$\bar{\tau} = \frac{\sum_k a_k^2 \tau_k}{\sum_k a_k^2} \quad (2.10)$$

where a_k and τ_k represent the measured PDP gain and time of the k th path, respectively. The *rms* delay spread τ_{rms} is evaluated from the $\bar{\tau}$ as given by [25]:

$$\tau_{rms} = \sqrt{\bar{\tau}^2 - \bar{\tau}^2} \quad (2.11)$$

The coherence bandwidth (B_c) measures a range of frequencies where the signal is strongly correlated [9]. The rms delay spread of a channel is inversely proportional to B_c , and for a frequency correlation function of 0.9 can be evaluated by [9]:

$$B_c \approx \frac{1}{50\tau_{rms}} \quad (2.12)$$

Furthermore, for a frequency correlation function of 0.5, the B_c can be evaluated by:

$$B_c \approx \frac{1}{5\tau_{rms}} \quad (2.13)$$

2.4 Summary and conclusions

This chapter has presented the fundamentals of radio propagation, including propagation mechanisms and an overview of fading manifestations. Fading channel manifestations are classified into two categories: large-scale and small-scale fading. Small-scale fading can be further categorised into two groups, which cause time-spreading of the transmitted signal or time-variance of the channel due to movements. A wireless channel modelling can be broadly classified as a deterministic or an empirical based model, each of which has its own benefits and drawbacks. In summary, this chapter has provided fundamental background, serving as a foundation for the remainder of this thesis.

Chapter 3

Intra-vehicle wireless networks (IVWN)

3.1 Vehicle networks

The current generation of vehicles is much more complicated than those of decades ago. In the early years, vehicle controls and monitoring were based on mechanical actuators. The demand for fuel efficiency, increased safety and better driving experience has led to many innovations in automotive technology [26]. Modern vehicles are equipped with a multitude of sensors such as temperature, speed and proximity sensors that provide essential information about the vehicles. A vehicle network architecture comprises multiple bus- and point-based networks that support various communication requirements. Historically, additional buses or direct point-to-point links have been added to support new sensors and ECUs, which has the vehicle network to grow in complexity.

Bus-based networks such as CAN (Control Area Network) were later introduced to support the growing demand for bandwidth. In 2011, it was reported that a

luxury vehicle could have as many as 60–75 ECUs with 6 CAN networks and 6 LIN networks [2]. Today, the number of ECUs in a luxury vehicle could exceed 100, and it is estimated that the number of sensors and ECUs will continue to grow in the near future.

There are several automotive network technologies available today such as CAN, FlexRay, LIN, MOST, LVDS and Automotive Ethernet [1]. Each of the technologies is designed to support a wide range of requirements. A summary of specifications for each of the network technology is shown in Table 3.1.

Table 3.1: A summary of network protocol specifications.

Technology	Bitrate	Topology	Protocol
LIN	19.2 Kbps	Point-to-point	Serial
CAN	1 Mbps	Bus-based	CSMA
FlexRay	20 Mbps	Point-to-point	TDMA
MOST	150 Mbps	Ring topology	TDMA
LVDS	655 Mbps	Point-to-point	Serial
100BASE-T1	100 Mbps	Bus-based	TDMA
1000BASE-T1	1000 Mbps	Bus-based	TDMA

3.1.1 CAN

The CAN bus, which employs Carrier Sense, Multiple Access with Collision Resolution (CSMA/CR), is the most widely used and popular vehicle network technology. The CAN standard was originally developed in 1983 at Robert Bosch GmbH, and extended in 1991 to allow extended frame format [27]. The CAN bus network can be differentiated into two categories: high-speed and low-speed. The high-speed CAN is used in applications with a data rate of up to 1 Mbps. The low-speed CAN, also known as fault-tolerant CAN, is used in applications with a data rate of up to 125 Kbps. The main difference between the two categories is the method of termi-

nating cables. The latest standard, released in 2016, supports a data rate up to 5 Mbps [28]. A variation of the CAN standard with time-triggered and deterministic features, known as TT-CAN, has been introduced to support new vehicle network requirements.

3.1.2 LIN

The LIN or Local Interconnect Network (LIN) standard was developed in the 1990s by the LIN Consortium [29, 30]. The network was developed as an inexpensive and simple single wire solution with a standardised data rate of 9.6 kbps or 19.2 kbps. The network operates similarly to the commonly used UART (Universal asynchronous receiver– transmitter). The LIN standard is typically used to connect localised sensors such as a vehicle door module sensor to an ECU.

3.1.3 FlexRay

FlexRay’s development started in 1999 with the aim of developing a deterministic network, robust and able to support high-bandwidth applications. FlexRay incorporates time-division multiple access (TDMA) with a maximum data rate of 10 Mbps [2]. The network is typically used in safety-critical domains such as the drivetrain where deterministic timing is crucial for safety. The price per controller in a FlexRay system is relatively higher than in a CAN system, which is a consequence of precise timing and implementation complexity.

3.1.4 MOST

The Media-Oriented Systems Transport (MOST) system is an optical fibre-based solution which provides immunity to electromagnetic interference [31]. The network was developed to support high-bandwidth infotainment applications. MOST has a

synchronous ring topology with a fixed, configurable data rate at 25, 50 and 150 Mbps. Although MOST offers advantages from synchronised timing, robustness and high bandwidth, its complexity imposes high implementation and design costs. In recent years, automotive Ethernet has become more favourable than MOST due to its similar bandwidth and relatively cheap implementation.

3.1.5 LVDS

The Low-Voltage Differential Signal (LVDS) standard is a point-to-point network solution originally developed by National Semiconductor to support increasing demand for higher bandwidth [32]. The standard specifies a maximum data rate of 655 Mbps; however, data rates above 1 Gbps are common [1]. In vehicles, the LVDS is used for high-bandwidth applications such as vehicle cameras.

3.1.6 Automotive ethernet

For decades, Ethernet has been the standard local area network (LAN) technology for personal computers, but was not used in vehicles. This is mainly due to not meeting the automotive electromagnetic interference (EMI) requirements. In addition, there is concern that, at high data rates, Ethernet networks would produce too much noise, interfering with other devices within the vehicle. Apart from that, standard Ethernet could not guarantee latency down to the microsecond level as required for safety-critical applications.

In 2011, Broadcom announced the BroadR-Reach PHY automotive Ethernet standard. Automotive Ethernet operates over two wires in contrast to the standard eight-wire shielded Ethernet, which reduces cost and weight. BroadR-Reach PHY is specified to operate at up to 100 Mbps without needing additional cable shielding [33]. Today, BroadR-Reach PHY is used in high data rate applications such as radar

and cameras. In recent years, 1 Gbps and 10 Gbps Ethernet have been tested and developed, with discussion on looking towards beyond 10 Gbps. As an extension to the automotive Ethernet standard, there is growing interest in the automotive industry on time-sensitive networking (TSN), which allows real-time communication over Ethernet [34].

3.2 Vehicle network architecture

Vehicle network architecture design considers several factors such as space, weight, and, most importantly, cost [35, 36]. Although there is a wide range of network technologies available, CAN buses are still widely used as they are inexpensive.

Vehicle functions are generally grouped into functional domains. Fig.3.1 shows a typical vehicle network architecture. The vehicle's electronics are divided into domains with different network requirements, i.e. Powertrain, Chassis, Body and Comfort, Driver Assistance and Driver Safety, and Human-machine interface [37]. The powertrain components relates to providing mechanical energy for the vehicle such as the engine, wheels and transmission. The chassis components support the powertrain, and include steering, suspension and brakes. Body and comfort components address air conditioning, heater, seat controls, windows, etc. Driver assistance and driver safety components relate to vehicle navigation, parking sensors and ADAS. Lastly, the human-machine interface components provide interfaces between passenger and vehicle, such as the infotainment system. Each domain will have its own specific requirement and latency. Table 3.2 summarises a typical domain requirement.

A vehicle network architecture implements multiple network technologies. For example, the powertrain and chassis-related controls and sensors are linked to the ECU through a CAN bus network. For body-related controls such as the door

Table 3.2: A summary of domain latency and bandwidth requirements [37].

Domain	Latency	Bandwidth
Powertrain	< 10 us	Low
Chassis	< 10 us	Low
Body and comfort	< 10 ms	Low
Driver assistance and driver safety	< 1 ms	20 - 100 Mbps (for each camera)
Human-machine interface	< 10 ms	Varies between systems

Table 3.3: SAE functional classifications.

Classification	Bitrate	Applications
Class A	< 10 kbps	Convenience features, sensor and button interfaces
Class B	10 kbps - 125 kbps	General information transfer, body electronics, comfort
Class C	125 kbps - 1 Mbps	Real-time control, power-train etc.
Class D	1-10 Mbps	Drive-by-wire or x-by-wire, active safety
Infotainment	> 10 Mbps	Infotainment, video streaming etc.

module, LIN networks are used. These networks are linked together through a multi-protocol gateway or bridge as a means for information to be translated into other network protocols.

The SAE, previously known as the Society of Automotive Engineers, has published a functional classification standard for vehicle networks [38,39] based on function and speed as Classes A, B, C, D and infotainment, as summarised in Table.3.3.



Figure 3.1: A simplified vehicle network architecture [40].

3.2.1 Future network requirements

In recent years, medium-class vehicles have come to be equipped with features for safety and driver assistance. The demand for such features has increased the size and complexity of in-vehicle networks in a cost-sensitive market. Therefore, new design methods for efficient realisation are needed while meeting the automotive industry's stringent reliability requirements.

In recent years, there has been increasing interest in low-latency and deterministic vehicle networks, with the increasing network requirements being mainly to support infotainment and advanced driving assistance systems (ADAS) for future vehicles. The automotive industry is currently focusing on automotive Ethernet [41–44]. In addition, there is also growing interest in distributed computing networks that process information through a distributed ECU using a low latency network [45].

It is clear, there are growing computing design requirements for vehicles now, and in the future. As bandwidth and the number of ECUs increased, vehicle networks have become more complex and heavy due to the practice of adding further networks to support the growing demand. Configuration complexity, cost, weight, space and reliability will be paramount in vehicle network research and design.

3.3 Wireless network in vehicles

Vehicles are equipped with a multitude of sensors and electronic devices. The number of electronic devices in a vehicle has increased significantly over the decades, as has the cost of those devices: in 2000, electronics constituted up to 18% of the total cost of the vehicle [4]. By 2018, the cost proportion had increased to 40% [4].

It has been reported that the wire-harness system of a vehicle can be the third-

most expensive and heaviest component, behind the engine and chassis. The number of cable and cost per vehicle is increasing [5,46]. In a luxury vehicle, the wire harness can weigh up to 60 kg; in a more typical vehicle, the weight is estimated to be 35–42 kg [5]. Increases in the harness’s weight and cost could be mitigated by introducing a wireless network solution into future intra-vehicle network architecture. A wireless network solution offers significant benefits as it can reduce weight and physical space needs. In turn, weight and space reductions will lead to improved fuel efficiency. Furthermore, introducing a wireless solution will ease the time-consuming and labour-intensive processes of designing and installing a vehicular network. Another benefit of a wireless network is the possibility to upgrade it, as no significant modification and re-cabling are required. In consequence, wireless networking could lead to modular electronic architecture.

An article published in IET Computing & Control Engineering Journal in 2001, titled “Vehicles without Wires” by G. Leen and D. Heffernan [47], was one of the first attempts to look at the possibility of using commercially ready wireless technology for intra-vehicle networks. One concern for designing wireless intra-vehicle networks is whether the wireless solution would be able to achieve the same performance as the wired network solution, especially in terms of network reliability. This can, however, be achieved by understanding the characteristics of intra-vehicle channels before applying suitable technologies to establish reliable and sustainable wireless connectivity in this environment.

3.3.1 Channel investigation and its models

The vehicle is a confined environment with a reflective structure and objects. A wireless network solution must operate under this challenging operational condition. There have been several studies investigating the channel characteristic of

a vehicle environment. The research can be categorised into three groups by the bandwidth of the wireless technology examined: narrowband, wideband and ultra-wideband. Throughout the years, research on the wireless intra-vehicle network has focused mainly on the ultra-wideband (UWB) régime. This is demonstrated by the far greater number of studies on UWB systems [48–71] than on narrowband systems [72–81]. The trend toward UWB started with the authorisation of unlicensed UWB operation by the Federal Communications Commission (FCC) [82]. The use of UWB for vehicle network is preferred due to its better performance in heavy multipath environments than narrowband solutions can typically achieve [69]. Although it is compelling to implement a UWB solution for vehicle network, the maximum transmission power allowed for UWB systems is significantly lower than for narrowband systems [83]. As a consequence, UWB is more prone to electromagnetic interference (EMI) [84]. Currently, there are no standards nor a definite answer on which technology is most suitable for such an environment. Therefore, it is beneficial to investigate intra-vehicle channel prospects from a broad perspective.

Vehicle chassis are typically made from metal, which can be modelled as a reverberation chamber [71,81,85–87]. NLOS and LOS conditions do not have a significant influence on extracted channel parameters [79], but, for narrowband communication, the multiplicity of transmission paths results in a higher number of deep fading locations than UWB produces in the same environment [88].

Channel conditions are sensitive to many factors, e.g. transmitter and receiver movement, or objects that reflect, scatter or diffract waves within the environment [14]. A preliminary investigation has shown strong correlation of channel variation with passenger movement [74,89,90]. In comparison, external environmental factors have a negligible or small impact on the channel [54, 55, 79]. In addition, other factors such as engine vibrations and road conditions have a relatively small impact

on the channel, in comparison with the occupants' movements [91,92].

3.4 Summary and conclusions

In this chapter, the background and state of the art of wired vehicle network and its architecture were discussed. Today's vehicle is much more complicated than that of decades past, now involving a multitude of sensors and different networks within the vehicle. The cost of vehicle electronics, including the wire harness, has increased significantly throughout the years, and demand is increasing for more cost-effective and higher-bandwidth networks. As bandwidth requirements and implementation costs make wired systems prohibitive, a wireless technology may prove increasingly useful. Wireless technologies offer significant benefits, allowing the wire harness to be reduced or eliminated from vehicle network architecture. In addition, current wireless network performance has become comparable to its wired counterpart. For example, a 802.11ax wireless LAN system-on-chip (SoC) can achieve a data rate of up to 4.8 Gbps, and is already commercially available [93]. Currently, there are no standards nor a definite answer on which technology is most suitable for such an environment. Therefore, it is beneficial to investigate channel from a broad perspective by comparing the channel performance at varying bandwidth. A suitable wireless technology can be chosen by understanding the channel properties of a vehicle.

Chapter 4

Narrowband channel characteristics of IVWN

4.1 Introduction

Vehicles contain multiple ECUs that communicate with each other through a bus- or point-to-point-based network. The network technology chosen is based on specific performance requirements. For example, control-related applications require high reliability and low latency, whereas infotainment and camera-based advanced driver assistance systems (ADAS) applications may require a higher bandwidth with less stringent latency requirements. Thus, any wireless network solution needs to address these varying network requirements.

To achieve this goal, the properties of intra-vehicle wireless channels need to be thoroughly investigated to develop appropriate technologies and protocols that can ensure the transmission performance required.

The aim of this work is to gain a better understanding of the characteristics of intra-vehicle channels in passenger and boot compartments for narrowband wireless

signals. In particular, this should be in terms of their distance-dependent attenuation factor and fading property at two different frequencies: 2.4 and 5.9 GHz. These frequencies are selected as they cover the 2.4 GHz unlicensed band and 5.9 GHz dedicated short-range communications (IEEE 802.11p) band.

The extent of influence from each of these components on the overall loss performance at different frequencies is demonstrated. This work reveals the location/distance-based loss performance and fading phenomenon in both small- and large-scale aspects. Simultaneously, it will be shown how they collectively contribute to the loss performance in such a complicated environment. Furthermore, the Rician K -factor of small-scale fading is investigated using the moment-based estimator method. The results provide a better understanding of intra-vehicle channel behaviour, especially the spatial fading characteristics in this complex and unique environment.

Work on narrowband performance has been largely overlooked compared to ultra-wideband (UWB) transmission, as demonstrated by the number of available published works [57]. It is essential to understand the narrowband behaviour of the intra-vehicle channel. This is because the signal bandwidths of potential intra-vehicle wireless technologies (i.e. Bluetooth, Zigbee, and Wi-Fi) are lower than the coherence bandwidth of the channel.

Although there have been some investigations on the propagation characteristics of narrowband signals in intra-vehicle wireless channels, most are more focused on the general behaviour of this type of channel, such as channel coherence bandwidth, frequency diversity, and power delay profile. Some exemplar works include a simple analytical multi-ray model with field measurements [73], and an analysis of the potential benefit of frequency diversity for intra-vehicle wireless applications [76]. A further study [74] examines channel coherence time and channel loss statistics at 915 MHz and 2.4 GHz, but without considering distance-related loss performance. In

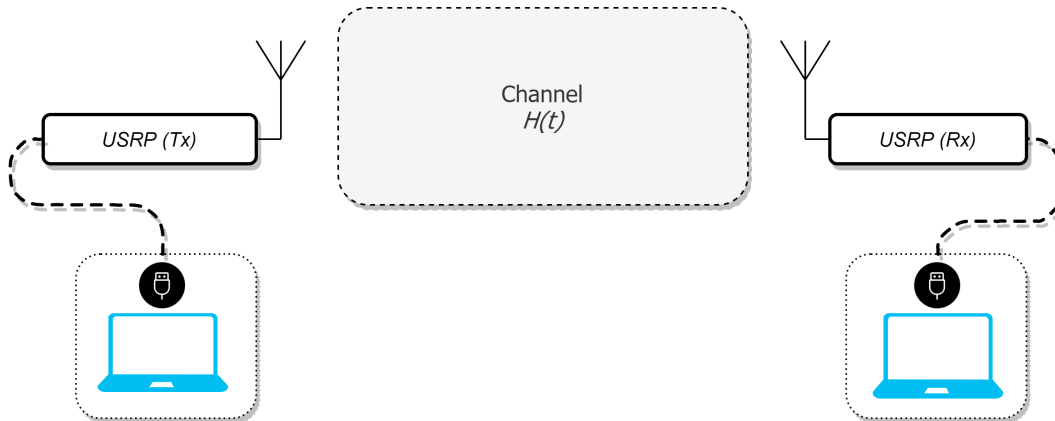


Figure 4.1: Block diagram of experimental testbed.

in addition, both UWB and narrowband channel models were presented for the engine compartment in [94], which can vary considerably from the passenger compartment in propagation characteristics.

This chapter is organised into multiple subsections. The testbed setup, configurations, and scenarios are described in Section 4.2. The components (mean path loss, large-scale fading, and small-scale fading) are described in Section 4.3. Finally, the chapter is summarised in Section 4.4.

4.2 Testbed setup

A testbed was developed using two Universal Software Radio Peripheral (USRP) B210 devices from National Instruments, as shown in Fig.4.1. The two USRPs were attached to a laptop with one used as a transmitter and the other as a receiver. The USRPs were connected to omnidirectional antenna from Linx Technologies and Taoglas Limited when performing the 2.4 and 5.9 GHz measurements, respectively.

Application codes were individually written for the transmitter and receiver, which performed the signal generation and measurement processes. The transmitter application code (written in Python) generates a continuous waveform, which is then

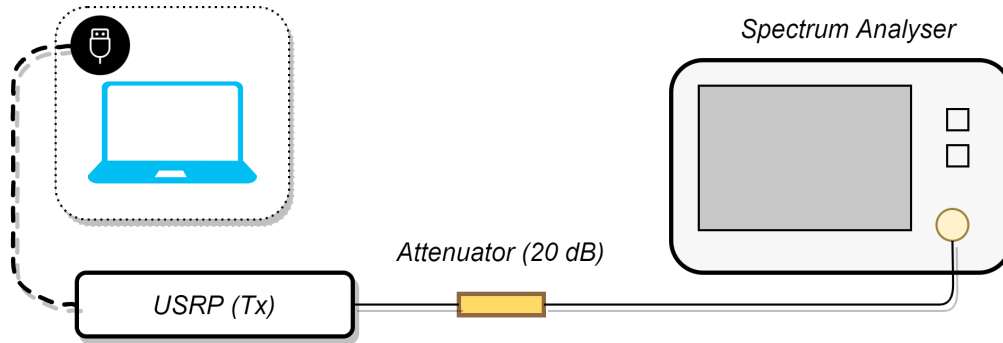


Figure 4.2: A diagram of equipment calibration setup.

transferred to the connected USRP for signal transmission. The receiver application code configures the USRP to the required settings and stores the received waveform samples. The captured samples were further processed, whereby the received voltage was converted to received power in dBm within MATLAB.

4.2.1 Calibration procedure

The supplied USRPs were not factory calibrated. To compensate for loss and measurement errors, each USRP was individually calibrated using a spectrum analyser (Tektronix). The transmitter was calibrated with the setup shown in Fig.4.2. The transmitter USRP transmits a continuous wave at the chosen frequency, while the spectrum analyser measures the received power. The measurement was repeated for different USRP gain settings. Similarly, the receiver was calibrated with the setup shown in Fig.4.3. The receiver was calibrated by measuring the losses between the front end of the USRP and the analogue-to-digital converter (ADC). The transmitter power level was varied while the receiver power measured from the USRP was recorded. The loss was calculated by deducting the transmitted power from the received power.

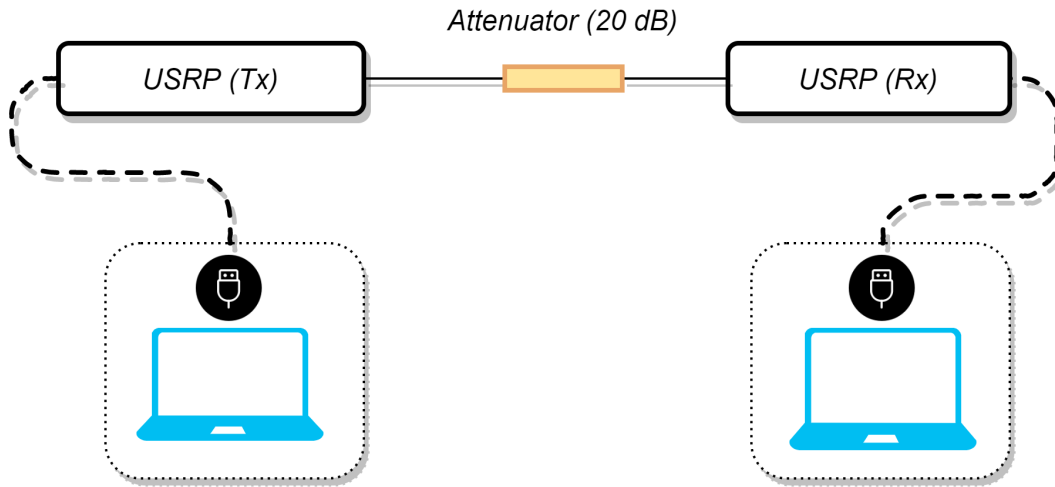


Figure 4.3: A diagram of equipment calibration setup.

4.2.2 Measurement procedure and scenario

The test was performed in the passenger and boot compartments of a Land Rover Discovery vehicle. The transmitter USRP was configured to transmit a baseband signal modulated by a carrier wave at the chosen frequency of either 2.4 or 5.9 GHz. The USRP output power was set as -1 and -5 dBm for the 2.4 and 5.9 GHz measurements, respectively. The receiver recorded the received signal waveforms for over a 10 s period, which resulted in a total of 100 million received samples in the time domain for each testing location. The measurements were repeated three times for each of the test locations. The related settings are summarised and specified in Table 4.1.

To minimise the impact from interference and to ensure the chosen channel was free from interference, a frequency spectrum scan was performed before taking measurements. The vehicle was maintained in a stationary position (without mobility condition involved) throughout the test with the engine and electric power turned off. Objects and human movement were kept away from the vicinity of the vehicle

Table 4.1: USRP settings at 2.4 GHz and 5.9 GHz

Frequency Setting	2.45 GHz	5.9 GHz
Antenna	ANT-2.4-LCW-SMA	TG.35.8113
Tx Power	-0.8 dBm	-5.18 dBm
Tx Gain Setting	73	73
Rx Gain Setting	35	60
Bandwidth	1 Hz	1 Hz
Sample Rate	10Msps	10Msps
Update Rate	1Msps	1Msps

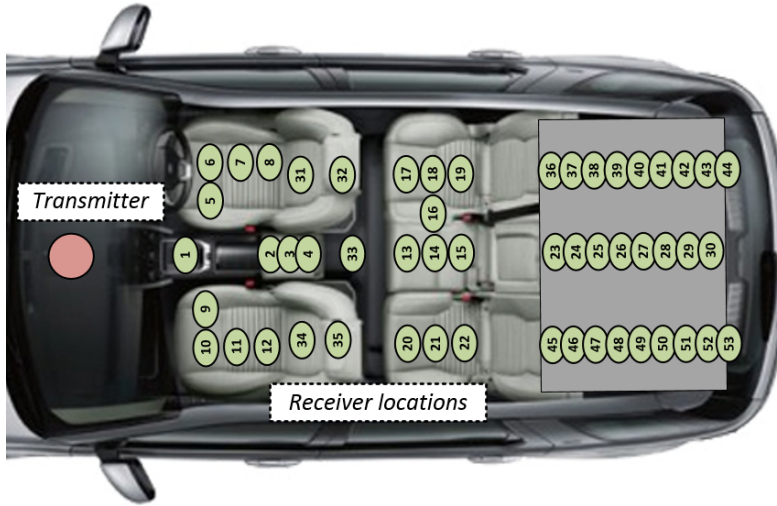


Figure 4.4: Measurement locations.

throughout the tests to mitigate for error caused by external factors. The antenna were vertically polarised throughout the tests with the transmitter and receiver aligned towards the back and front of the vehicle, respectively. The transmitter was placed at a fixed location on the dashboard of the vehicle, whereas the receiver USRP was moved to a different location after each measurement. Measurement points for the transmitter and receiver are presented in Fig. 4.4. It was ensured that locations were more than one wavelength apart, and clearly marked.

All necessary information (such as the height and relative distance of the lo-

cation) was recorded and used to calculate the separation distance between the transmitter and receiver antenna. The recorded results were processed in MATLAB in the form of complex numbers and then used to extract the received power in dBm.

4.3 Experimental results and data analysis

Propagation loss of the radio signal transmitted between receivers is typically described as path loss L . To calculate the path loss (or attenuation loss) from the collected data, the known transmission power T_x was subtracted from the measured received power R_x as follows:

$$L = T_x - R_x \quad (4.1)$$

4.3.1 Path loss

There are various different models used to represent the characteristic of loss in an environment. One such model is the log-distance path loss model (also known as the Friis equation). In this study, intra-vehicle path loss behaviour was modelled using the log-distance path loss model with additional terms representing small- and large-scale variation or fading. The combined path loss, denoted by L_p , is expressed (all in dB) as follows:

$$L_p = L_m + \Psi_\alpha + \beta_s \quad (4.2)$$

where the term L_m represents the mean path loss, Ψ_α is large-scale fading, and β_s is small-scale fading.

The mean path loss L_m is defined by the generalised Friis equation comprising

two parts: 1) the loss at a reference distance, d_0 , from the transmitter, and 2) the loss logarithmically increasing with distance, which is described by [9], as follows:

$$L_m = L_{ref}(d_0) + 10n \log_{10}\left(\frac{d}{d_0}\right) \quad (4.3)$$

where the terms L_{ref} , n , d , d_0 represent the path loss at a reference distance, the path loss exponent, the distance between the transmitter and receiver antenna, and the chosen reference distance, respectively.

The mean path loss L_m was estimated using the least square linear regression method [95]. Base on Eq.(4.3), mean loss values for the 53 receiver locations, $L_{m,i}$ were obtained as follows:

$$L_{m,i} = L_{ref,i} + 10n_i x_i \quad \text{for } i = 1, 2, \dots, 53. \quad (4.4)$$

where

$$x_i = \log_{10}\left(\frac{d_i}{d_0}\right), \quad (4.5)$$

$$n_i = \frac{\sum_{i=1}^{53} (x_i - \bar{x})(L_i - \bar{L})}{\sum_{i=1}^{53} (x_i - \bar{x})^2}, \quad \text{and} \quad (4.6)$$

$$L_{ref,i} = \bar{L} - n_i \bar{x} \quad (\bar{L} = \frac{\sum_{i=1}^{53} L_i}{53}). \quad (4.7)$$

Here, d_i and L_i represent the distance of the i th location (in meters) and the instance path loss of the i th location (in dB), respectively.

Path loss and estimated mean path loss, which represent the first path loss component, L_m , were produced as shown in Fig.4.5 for 2.4 GHz and Fig.4.6 for 5.9 GHz. The extracted parameters for both 2.4 and 5.9 GHz are presented in Table 4.2, together with the loss at the reference distance, L_{ref} . Path loss for both frequencies

Table 4.2: Estimated loss exponent and reference path loss.

Frequency (GHz)	n	L_{ref} (dB)
2.4	2.212	37.04
5.9	1.289	50.43

exhibits a different loss characteristic, whereby at 5.9 GHz the overall path loss is higher than at 2.4 GHz. For comparison purposes, the results of the Friis model (or the free-space loss model) (L_f and $n = 2$) are also presented in Fig. 4.5 and Fig. 4.6, according to:

$$L_f = 20\log_{10}\left(\frac{d}{d_0}\right) + 20\log_{10}(f) + 20\log_{10}\left(\frac{4\pi}{c}\right) \quad (4.8)$$

where f and c represent signal frequency and the speed of light, respectively. These results indicate that the mean path loss of the intra-vehicle narrowband transmission exhibits a varied relationship with the free-space loss. At 2.4 GHz, the mean loss is lower than the free-space loss by a range of 2–4 dB over a distance of 3 m in the vehicle (as shown in Fig. 4.5). However, when the frequency was increased to 5.9 GHz, the mean loss increased significantly compared with the free-space loss for most of the test range, as shown in 4.6. It was also observed that the path loss performance inside vehicles (in terms of the scale of variation), is mainly attributed to the multipath fading effect, which will be examined in detail in the following subsections.

4.3.2 Large-scale fading

Large-scale modelling is an important characteristic when designing a wireless system. In this study, large-scale fading (also known as shadowing) represents the local average slow fading characteristics of the received signal. The received signal

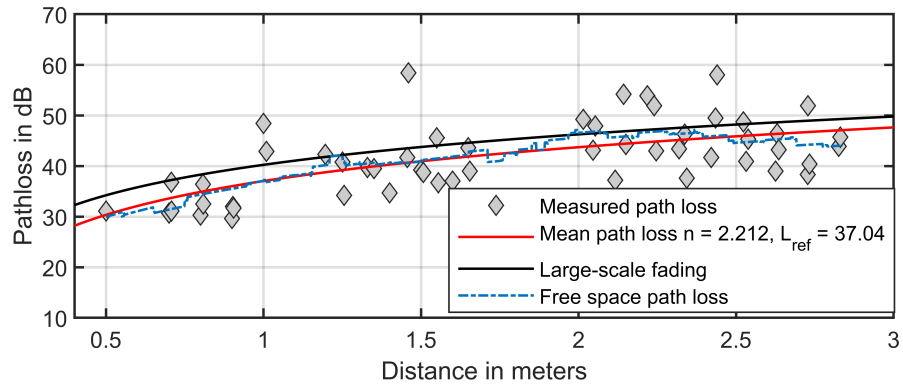


Figure 4.5: Measured path loss, mean path loss and loss due to large-scale fading at 2.4 GHz.

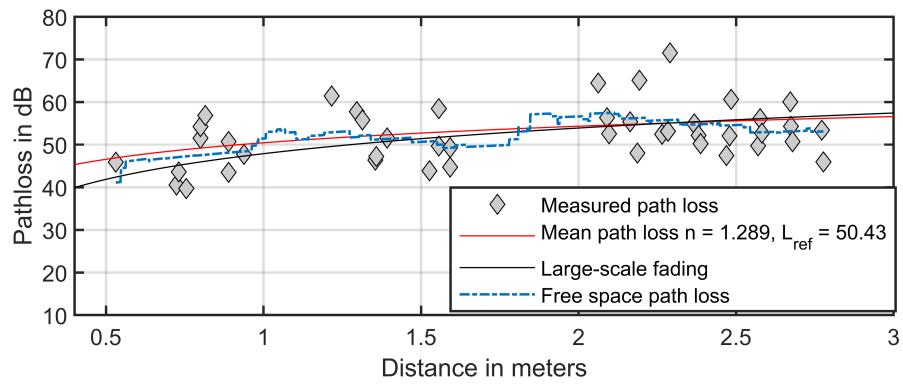


Figure 4.6: Measured path loss, mean path loss and loss due to large-scale fading at 5.9 GHz.

envelope is a combination of the local mean of slow varying signal (large-scale fading) $\Psi_\alpha(x)$ with a fast-varying component (small-scale fading) $\beta_s(x)$, expressed as follows:

$$r(x) = \Psi_\alpha(x)\beta_s(x) \quad (4.9)$$

The large-scale fading component can be extracted from $r(x)$ by spatially averaging the received signal with an appropriate averaging length $2L$. The appropriate length for different carrier frequencies and environment such as indoor and outdoor has been investigated [96]. However, to the best of our knowledge, there are no published work on determining the appropriate averaging length for an intra-vehicle environment. Lee has provided an analytical recommendation in estimating the appropriate $2L$ [97]. Based on Eq. (4.9), the estimated local mean $\hat{r}(x)$ can be obtained by using the following equation, as per [97]:

$$\hat{r}(x) = \frac{1}{2L} \int_{x-L}^{x+L} \Psi_\alpha(y)\beta_s(y)dy \quad (4.10)$$

where $2L$ represents the signal length, which is defined as the length of distance covered by a set of signal samples used to appropriately average the signal data for analysing fading properties. The term $\hat{r}(x)$ will be close to the true mean $\Psi_\alpha(x)$ when $2L$ is properly chosen. The large-scale fading component Ψ_α can be extracted from the measured received signal using the moving mean method, with the metric given by:

$$\Psi_\alpha = \frac{1}{2L} \sum_{i=1}^{2L} l_i \quad (4.11)$$

where l_i is the path loss of the i th signal sample. To find $2L$, Lee introduced the $1\alpha - spread$ parameter, which represents the scale of signal variation around the

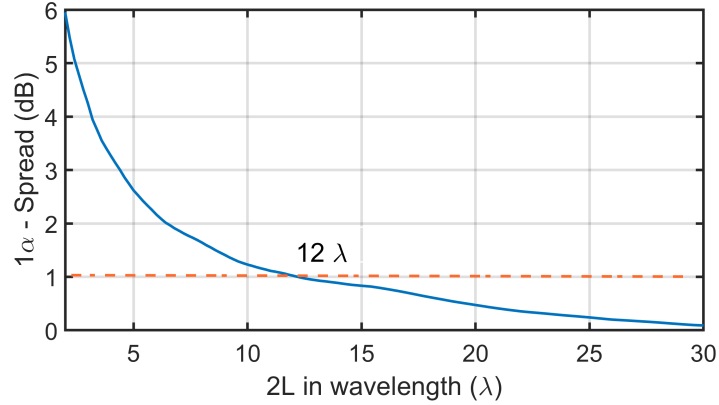


Figure 4.7: 1α -spread (in dB) vs. signal length $2L$ using the Lee method for 2.4 GHz.

true mean, as follows:

$$1\alpha - spread = 20 \log_{10} \frac{\Psi_{\alpha}(x) + \alpha_{\hat{\Psi}}}{\Psi_{\alpha}(x) - \alpha_{\hat{\Psi}}} \quad (4.12)$$

where $\alpha_{\hat{\Psi}}$ is the standard deviation of Ψ_{α} . The $1\alpha - spread$ parameter for both 2.4 and 5.9 GHz frequencies were plotted against signal length $2L$ in wavelength (λ) according to Eqs. (4.11) and (4.12), as shown in Figs. 4.7 and 4.8, respectively. According to the Lee method [97], the upper bound of $2L$ is defined as the value when the $1\alpha - spread$ is equal to 1 dB, which was shown to be 12λ and 17λ for 2.4 GHz and 5.9 GHz, respectively. The estimated $2L$ using this method provides the upper bound limit where the large-scale fading component will not be smoothed out during the averaging process. However, this method only provides an estimate where the true or optimum signal length will be less than the wavelength at 1-dB $1\alpha - spread$. The method of estimating the lower bound of $2L$ is discussed in [96]. A vehicle with a similar dimension as the vehicle tested will be able to use the upper bound estimated in this work to extract the large-scale fading component.

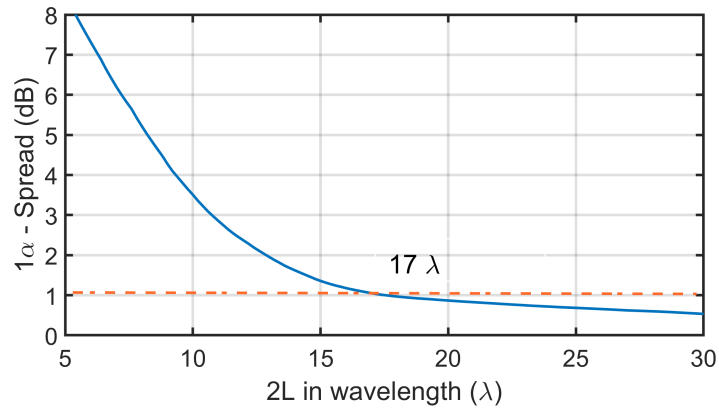


Figure 4.8: 1α -spread (in dB) vs. signal length $2L$ using the Lee method for 5.9 GHz.

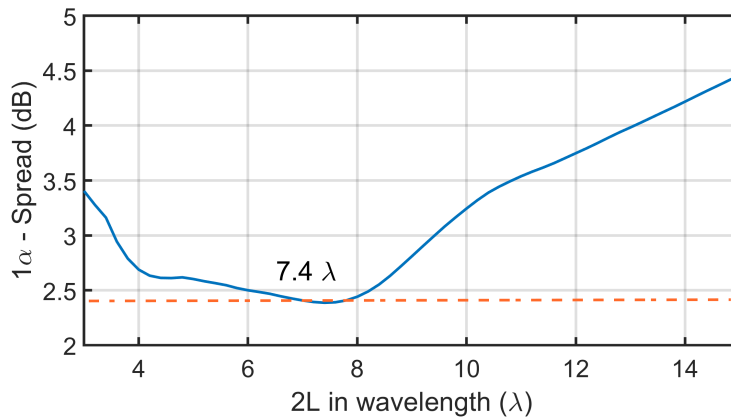


Figure 4.9: 1α -spread (in dB) vs. signal length $2L$ using the generalized Lee method for 2.4 GHz.

Optimum signal length ($2L$)

We can determine the optimum signal length that helps to maximise the accuracy of the channel model built from the testbed measurements. This can be achieved by applying the generalised Lee method [98], in which Ψ_α given in Eq. (4.11), is replaced by $\hat{\Psi}_\alpha$, the averaged Ψ_α over the signal length. This is shown as follows:

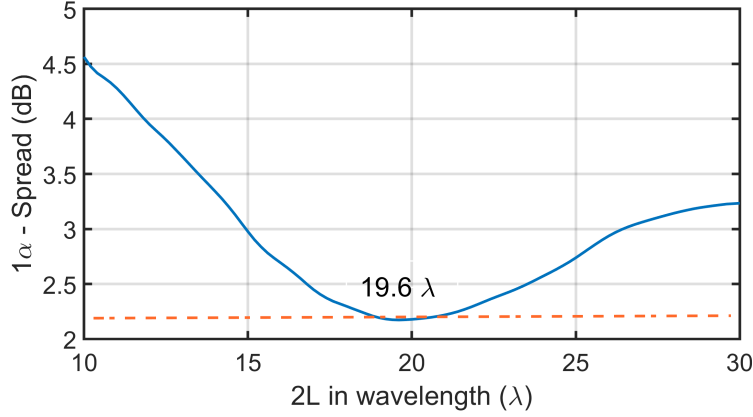


Figure 4.10: 1α -spread (in dB) vs. signal length $2L$ using the generalized Lee method for 5.9 GHz.

$$\hat{\Psi}_\alpha = \frac{1}{2L} \sum_{i=1}^{2L} \Psi\alpha_i \quad (4.13)$$

Here, the $1\alpha - spread$ in the generalised Lee method is expressed as follows:

$$1\alpha - spread = 20 \log_{10} \frac{\hat{\Psi}_\alpha(x) + \alpha_{\hat{\Psi}}}{\hat{\Psi}_\alpha(x) - \alpha_{\hat{\Psi}}} \quad (4.14)$$

By applying Eqs.(4.14) and (4.13) to the measured received signal, the $1\alpha - spread$ vs signal length $2L$ in wavelength (λ) was plotted, as shown in Fig. 4.9 and 4.10. The optimum signal length $2L$ which corresponds to the lowest $1\alpha - spread$ value available is obtained as 7.4λ and 19.6λ for 2.4 and 5.9 GHz, respectively.

Having determined the optimum signal length, the large-scale fading component Ψ_α for 2.4 and 5.9 GHz were extracted from the measured path loss L_p , as shown in Figs. 4.5 and 4.6, respectively. The statistical property of Ψ_α , in terms of the relative loss variation (RLV), can be represented by a cumulative density function (CDF) as depicted in Figs. 4.11 and 4.12. This is found to follow a log-normal distribution (normal in dB).

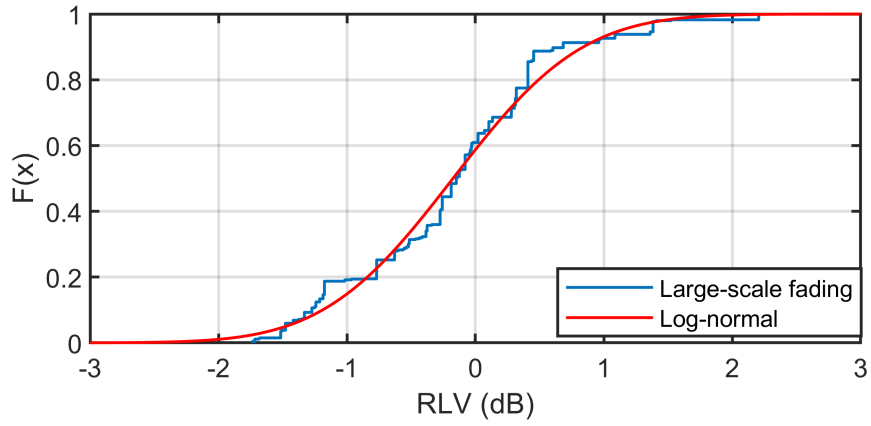


Figure 4.11: The CDF of large-scale fading and log-normal fit at 2.4 GHz.

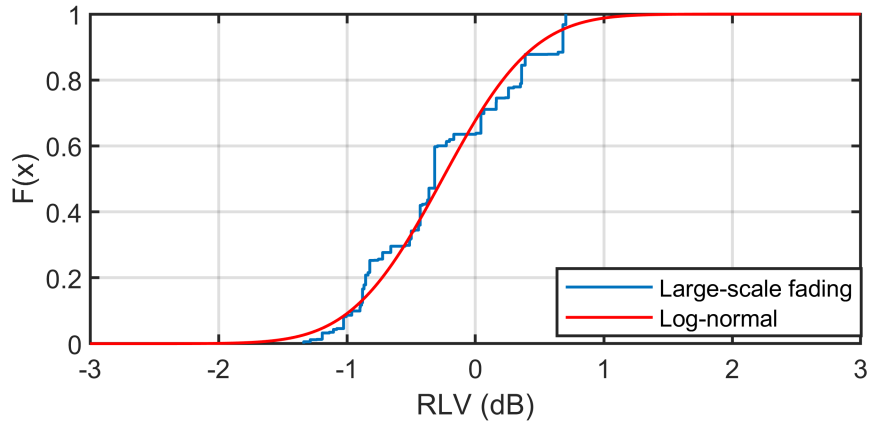


Figure 4.12: The CDF of large-scale fading and log-normal fit at 5.9 GHz.

4.3.3 Small-scale fading

Small-scale fading is defined as the variation of received signal power over a short time period or a short distance less than a few wavelengths. According to Eq. (4.15), the small-scale fading component β_s is obtained by deducting the large-scale fading component Ψ_α and the mean path loss L_m , as follows:

$$\beta_s = L_p - L_m - \Psi_\alpha \quad (4.15)$$

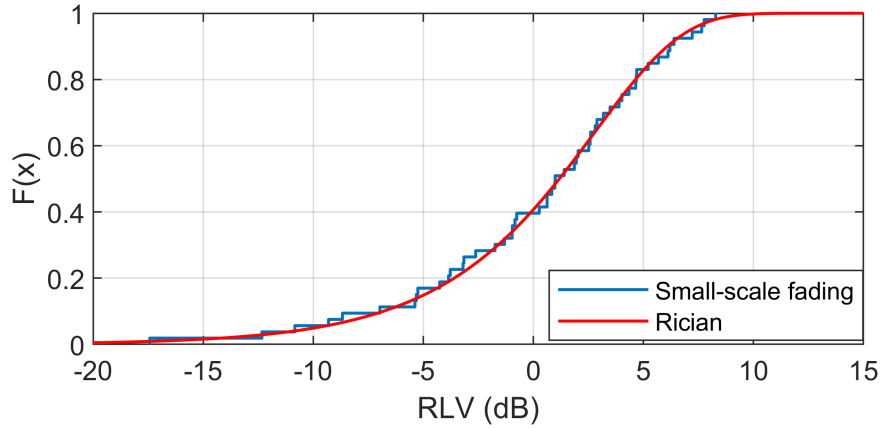


Figure 4.13: The cumulative distribution function (CDF) of relative loss variation (RLV) for Small-scale fading β_s and Rician fit.

The CDF of the relative loss variation (RLV) of small-scale fading β_s for 2.4 and 5.9 GHz are shown in Figs. 4.13 and 4.14, respectively. The small-scale fading on both frequencies demonstrated much greater variation (approximately 25 dB in RLV) compared to large-scale fading Ψ_α (approximately 2–4 dB in RLV), as shown in Figs. 4.11 and 4.12. In addition, the deepest fade at both 2.4 and 5.9 GHz was found to be approximately 17 dB below the mean path loss L_m .

By comparing the CDFs for both large- and small-scale fading, it is evident that small-scale fading was dominant in contributing to the overall path loss in the intra-vehicle environment. The RLV caused by small-scale fading was significantly higher, reaching as much as 18 dB.

The CDF of small-scale fading β_s at 2.4 and 5.9 GHz demonstrated similar distribution pattern. A two-sample Kolmogorov–Smirnov (KS) test was performed on the small-scale fading samples, which resulted in a probability value (ρ -value) of 0.9. The high ρ -value signifies that small-scale fading between the two frequencies was highly correlated. In other words, small-scale fading does not change when the carrier frequency is changed from 2.4 GHz to 5.9 GHz or vice versa.

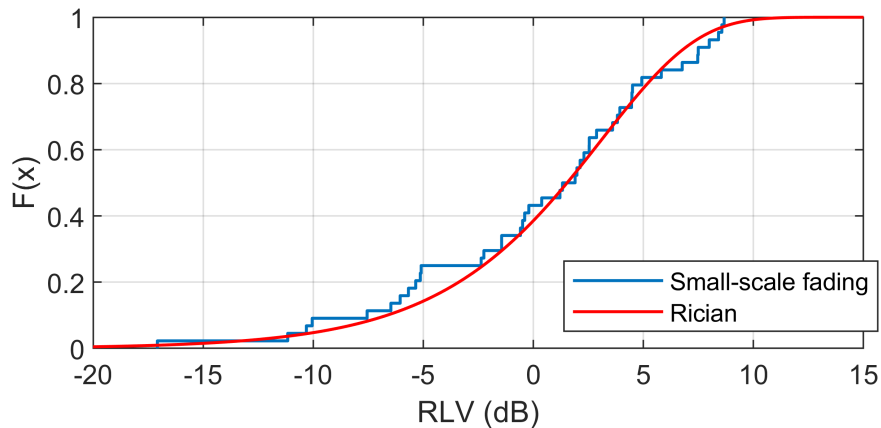


Figure 4.14: The cumulative distribution function (CDF) of relative loss variation (RLV) for Small-scale fading β_s and Rician fit.

4.3.4 Rician fading channels (K -factor)

A vehicle can be considered a confined environment with challenging operating conditions. As a result, wireless communications inside a vehicle are exposed to multipath fading scenarios, and in some cases, no direct transmission paths can be established (referred to as the Rayleigh channel condition), while in other scenarios the channel behaviour can be described as Rician, where one direct transmission path and other scattered paths co-exist. The Rician K -factor represents the ratio between the power in the direct path and the power in the other scattered paths, which reflects the true channel statistics [9].

It is important to know under which conditions the channel should be regarded as Rayleigh or Rician with a specific K -factor, as this will help to determine realistic channel behaviour and to select the most appropriate technologies to address the challenges of intra-vehicle communications.

Few published results explicitly address the Rician K -factor for intra-vehicle fading channels. In [94], a propagation channel model for the engine compartment was presented, involving large-scale fading with a normal distribution and small-

scale fading with a Rician distribution. To characterise small-scale fading with the Rician K -factor, the authors used two distance ranges (<450 and ≥ 450 mm). This resulted in only two K -factors being available for the small-scale model that was derived. The approach used in this study (utilising the moment-based estimator [99]) meant that a range of K -factors corresponding to varying distances (from 0.5 to 2.8 m) could be obtained to reflect fading scenarios in a real-world environment realistically.

In [100] and [78], the authors investigated the potential impact of the coexistence of Zigbee and Bluetooth, or Zigbee only, by presenting a small-scale fading model with a brief Rician K -factor analysis. However, their results were based on a small number of measurement locations (just four locations in [100]) in the vehicle. In contrast, the results for the K -factor analysis in this work were produced from 53 different locations across the passenger and boot compartments in a vehicle, to ensure a convincing and accurate small-scale fading model could be achieved. In addition, [78] assessed the variability of small-scale fading in the time domain, while here we examine this property in the spatial domain to reveal the location-based channel property.

The intra-vehicle small-scale fading β_s profile was investigated using Rician K -factor analysis. The Rician K -factor is commonly described as the ratio of the dominant path to the specular or multipath component, as given by [101]:

$$K = \frac{|A|^2}{2\sigma^2} \quad (4.16)$$

where $|A|^2$ is the power of the dominant part of the received signal and $2\sigma^2$ is twice the signal power of the diffuse part.

The small-scale fading component β_s is obtained by deducting the large-scale fading component Ψ_α and the mean path loss L_m from the measured path loss L_p .

To derive the Rician K -factor from the measured path loss, the moment-based estimator introduced in [99] which does not require the signal phase information was used to estimate the K -factor. The moment-based estimator provides a simple parameter γ that can be used to work out the K -factor, as follows:

$$K = \frac{\sqrt{1-\gamma}}{1-\sqrt{1-\gamma}} \quad (4.17)$$

where γ is given by [99] as follows:

$$\gamma = \frac{V[\beta_{s,i}]}{(E[\beta_{s,i}])^2} \quad (4.18)$$

where $V[.]$, $E[.]$ represent the variance of the small-scale component of the received signal power $\beta_{s,i}$ and the expected value or mean of $\beta_{s,i}$, respectively.

Based on Eqs. (4.17) and (4.18), we calculated the K -factor for the intra-vehicle channel investigated in this study using the obtained field measurements. We first extracted the small-scale fading component β_s from Eq. (4.15), and then applied Eqs. (4.17) and (4.18) to obtain $K = 0.576$, which can be regarded as the average K -factor of the channel. As this K -factor suggests, the intra-vehicle channels can generally be treated as a near-Rayleigh channel when $K \approx 0$.

To reveal the relationship between the K -factor, the separation distance d , and other environmental conditions such as line-of-sight (LOS), the parameter γ_i ($i=1,2,\dots,53$) was calculated using Eq. (4.18). Each γ_i corresponds to one of the 53 measurement points and was calculated using 6 samples of the received signal power ($\beta_{si}, \dots, \beta_{s(i+6)}$) collected at and around the specific location point. With each γ_i calculated, the estimated K -factor for the separation distance d between the corresponding location point and the transmitter was obtained by applying Eq. (4.17).

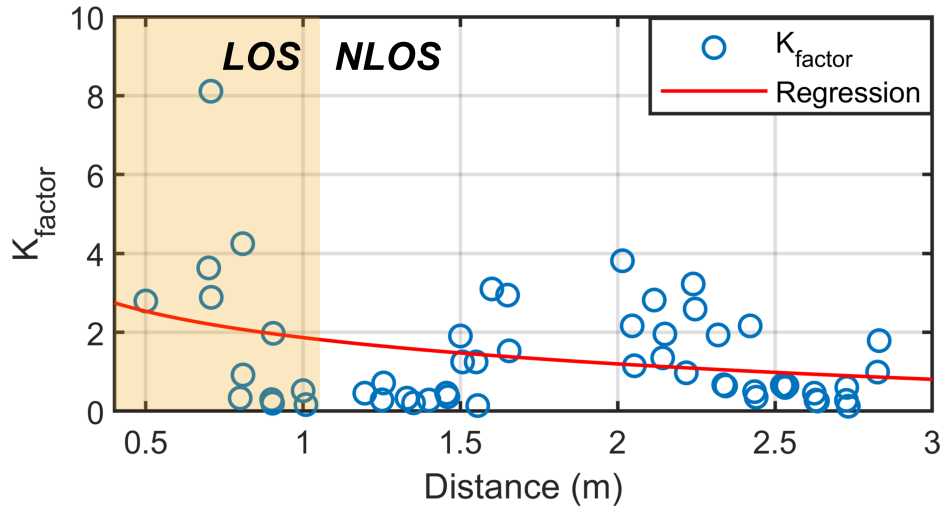


Figure 4.15: Estimated Rician K -factor against distance for 2.4 GHz.

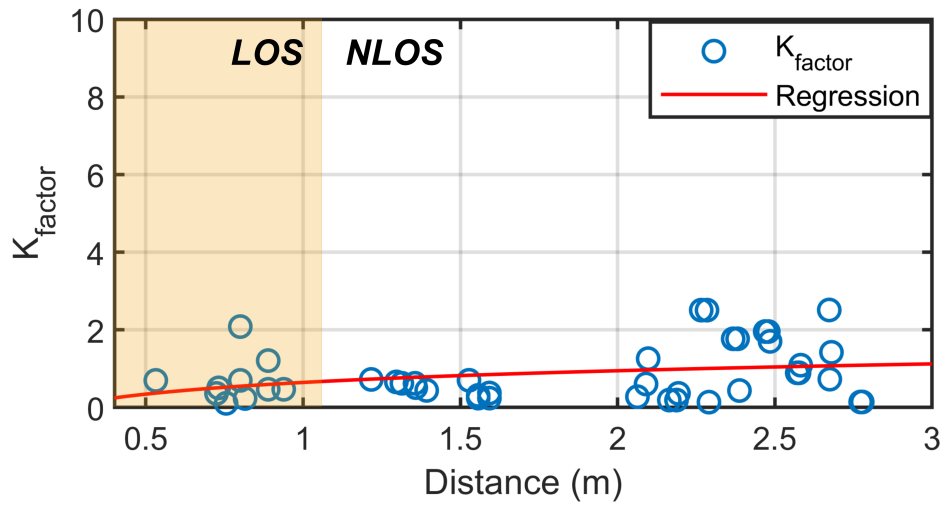


Figure 4.16: Estimated Rician K -factor against distance for 5.9 GHz.

The distance-based K -factors for 2.4 and 5.9 GHz are presented in Figs. 4.15 and 4.16, respectively. The 2.4 GHz K -factors under the LOS condition (highlighted in the shaded area) have relatively higher values than those in the non-LOS area (unshaded). This result demonstrates that the K -factor of the intra-vehicle channels at 2.4 GHz was correlated with the separation distance. Therefore, the channel demonstrates more Rician behaviour within a shorter separation distance; however, this tends to become more Rayleigh-like when the distance increases.

Conversely, the 5.9 GHz K -factors show the opposite result, where there is an inverse correlation between K -factors and distance. The decreasing relationship of K -factor with distance at 5.9 GHz, was found to be similar to a study conducted in a tunnel environment at 5.8 GHz [102]. This behaviour can be explained by the atmospheric loss experienced by the signal, which increases with frequency. Although the distance travelled by the scattered component which interacts with the environment is similar, however, the atmospheric loss will be higher at 5.9 GHz than at 2.4 GHz. In other words, the ratio of direct path component against the diffuse multipath component increases with distance. The analysed K -factors at both frequencies shows a low K -factor values where some locations have a K -factor value lower than 1 (near Rayleigh).

4.4 Summary and conclusions

The propagation characteristic of narrowband signals at 2.4 and 5.9 GHz in the intra-vehicle wireless channels were presented. Various channel parameters were extracted from the received signal power measurements, such as the distance-related attenuation loss (mean loss), and large- and small-scale fading statistics, which jointly contribute to the overall path loss. In addition, this work demonstrates that the small-scale fading effect is does not change when the carrier frequency is

changed from 2.4 GHz to 5.9 GHz or vice versa. However, the similarity of small-scale fading at lower (i.e. 433 MHz) and higher (i.e. millimeter wave) frequency has not been investigated. Further investigation is required to determine the correlation of small-scale fading between different frequency bands.

It was determined that multipath fading has a significant impact on the path loss performance of narrowband signals compared to attenuation-related loss, which has a varying relationship with free-space loss depending on the selected operating frequency. The small-scale fading is much more influential on path loss in this environment.

Intra-vehicle channel properties (in terms of the channel loss model and associated fading components) were characterised by the Rician K -factor. Based on the analysis of the K -factor as a function of separation distance, it was demonstrated that channel behaviour varies at 2.4 GHz from Rician to Rayleigh as the separation distance increases and the LOS condition changes. In general, this work demonstrate that the intra-vehicle channel can be treated as near-Rayleigh channel. In addition, we have also derived the upper bound and optimum signal length of $2L$ to extract the large-scale fading component from the measured losses appropriately.

Following this investigation, other properties of the intra-vehicle channel can be explored, such as channel frequency response as a function of distance or location, which can help to identify suitable transmission technologies for this environment.

Chapter 5

Wideband channel characteristics of IVWN

5.1 Introduction

An intra-vehicle network contains multiple buses, each with a different set of requirements to support particular applications. For example, the infotainment system needs high bandwidth with less stringent latency requirement, whereas the Advanced Driver Assistance System (ADAS) requires high reliability with low latency. Therefore, wireless communications in a vehicle will need to meet a wide range of requirements in terms of reliability, robustness, bandwidth, latency, and efficiency. To design a wireless communication suited to the vehicle environment, a good understanding of the conditions and properties of intra-vehicle channels is necessary.

A vehicle is a complex environment for wireless communications that experiences heavy multipath propagation. A measurement campaign was conducted to investigate the multipath properties of a vehicle, specifically the multipath properties

of the intra-vehicle channel under non-line-of-sight (NLOS) conditions. There have been several works published on wideband and ultra-wideband intra-vehicle channel characteristics. Some investigations and channel models have been proposed for different areas of a vehicle [57, 61, 66]. The large-scale fading statistics of a wideband channel has been studied in [50, 80]. In addition the K -factor of wideband and ultra-wideband channel of an intra-vehicle channel is studied in [100, 103]. To the best of our knowledge, there are no published works on the variability of multipath propagation and its dependence on location. This investigation reveals the channel dependence properties characterising the multipath behaviour in the intra-vehicle channel.

This chapter discusses the measurement campaign performed in the vehicle. Section 5.2 describes the testbed and settings for collecting measurements. The results and analysis, including the power delay profile, root mean squared (*rms*) delay spread, and coherence bandwidth, are presented in Section 5.3. Section 5.4 provides the chapter summary and conclusions.

5.2 Testbed setup

The test was conducted on a four-door Suzuki Swift. A total of 49 locations were selected for measurement ensuring each section of the vehicle was covered. There were 12 measured locations in the boot compartment, 21 in the back-passenger section, and 16 in the front part of the vehicle.

5.2.1 Measurement campaign and procedures

We designed the testbed using Universal Software Radio Peripheral (USRP) products from National Instruments, as shown in Fig.5.1. Each USRP was connected to an omnidirectional antenna from Taoglas Limited and attached to a laptop for signal

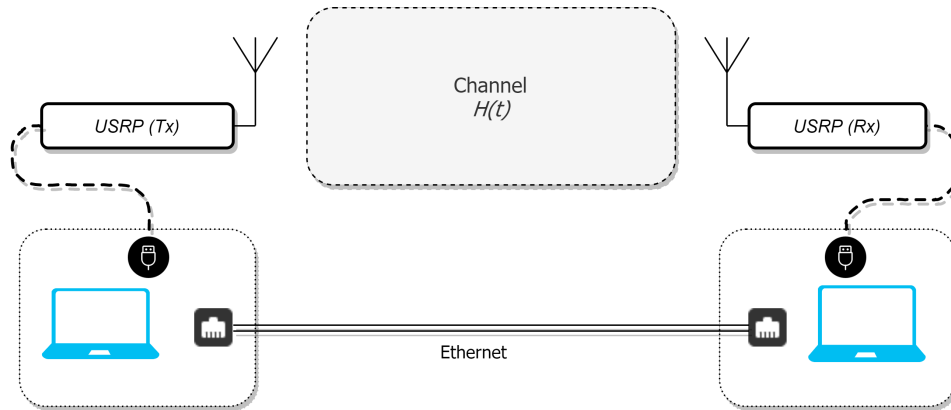


Figure 5.1: The testbed setup block diagram.

generation and processing. An application layer code was written in Python to perform the signal processing and synchronisation of the two USRPs. The testbed was developed as a portable tool to measure frequency response. The step frequency, frequency band, and transmitter power of the USRP were configurable. The testbed was calibrated in the laboratory with an Agilent Network Analyser.

The transmitter was configured to perform a frequency sweep from 2 to 3 GHz in intervals of 333 kHz, resulting in a bandwidth of 1 GHz. The transmitter power level was set to transmit at 0 dBm.

Throughout the measurement, the vehicle is set in parked condition with the engine ignition in off position. The area around the vehicle was also kept out of any large objects and human movement throughout the tests. The transmitter antenna was placed in front of the engine block as shown in Fig.5.2 with the hood fully closed during measurement. The location was chosen as the engine compartment is known to be densest with sensors. A wireless node located in the engine compartment will have its line-of-sight (LOS) path obstructed by the vehicle firewall, typically made of sheet metal, as shown in Fig.5.3. The receiver was moved to a different location after each measurement. The locations were numbered starting from the

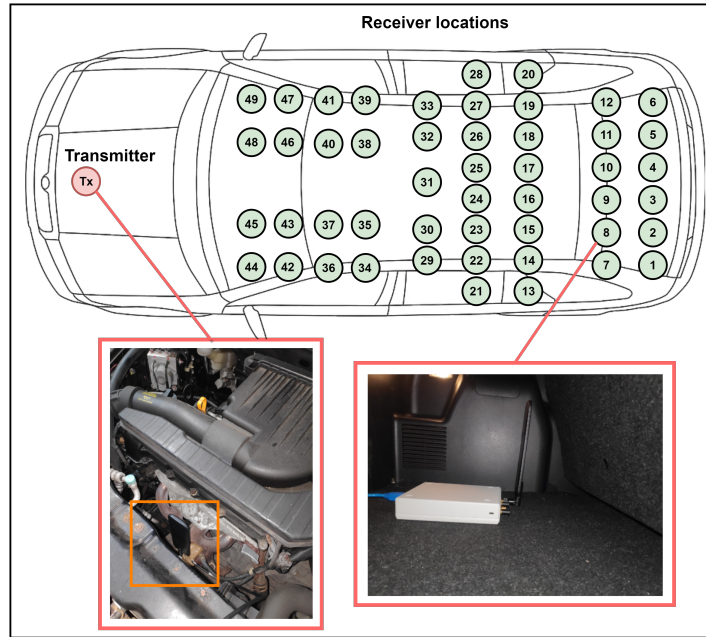


Figure 5.2: Transmitter and receiver locations.

boot compartment to the front of the vehicle. The distance between the measured location point and the transmitter decreased with location number.

5.3 Experimental results and data analysis

5.3.1 Power delay profile

The measurement campaign resulted in a total of 49 frequency response measurements. Fig.5.4 indicates the frequency response at three different locations was highly frequency-selective. A similar pattern was seen on all the measured locations.

The power delay profile (*PDP*), which is the square of the magnitude of the channel impulse response (CIR), represents the distribution of signal power over a multipath channel as a function of time. The techniques of measuring a channel

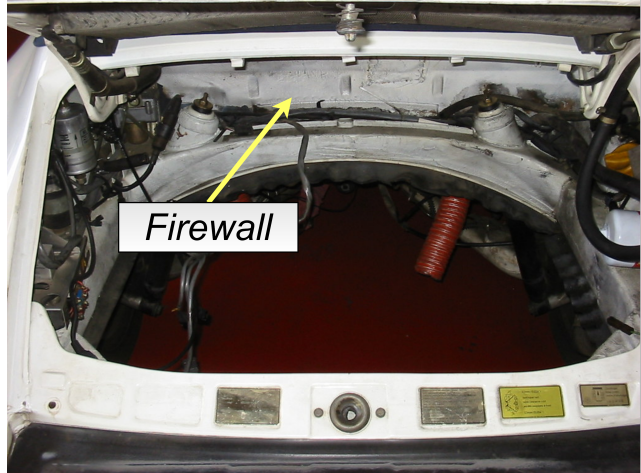


Figure 5.3: Location of firewall within the engine compartment.

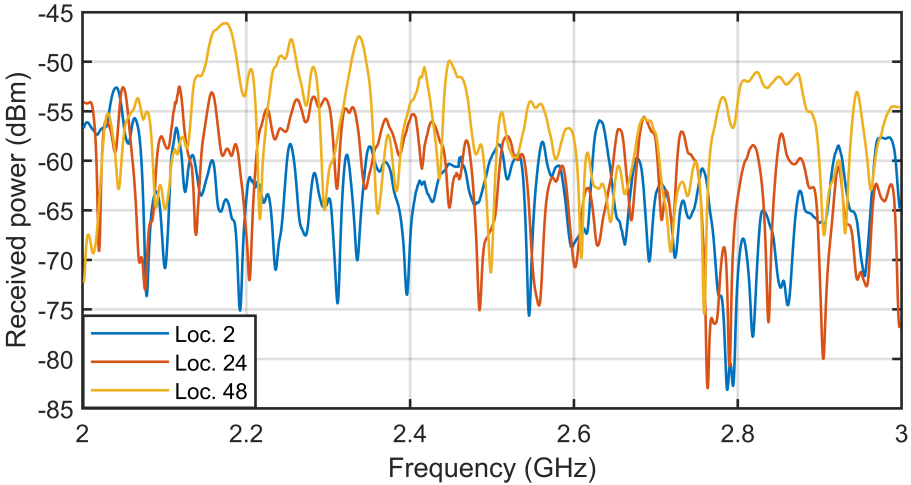


Figure 5.4: The frequency response $H(f)$ of location number 2, 24 and 48.

PDP can be categorised into two categories: time-domain measurement and frequency domain measurement [104]. One method of a time-domain approach is the direct RF pulse. In this method, a signal generator is used to transmit a pulse, and the received signal is then measured using an oscilloscope [9]. On the other hand, the frequency-domain measurement can be performed using the frequency sweep technique where a signal is transmitted and measured incrementally at each frequency [104]. The duality property of Fourier Transform allows measurement in one domain (i.e. time or frequency) to be represented in the other domain [105]. Hence, measurement conducted in the frequency-domain can be converted to the time-domain.

In this work, due to the availability of equipment, the frequency domain technique was used to measure the channel. The *PDP* at time t and location i is estimated from the frequency domain measurement $H(f)$ using the inverse discrete Fourier transform (IDFT) with a Hanning window $W(f)$ as described in Eq.(5.1).

$$PDP(t, i) = |IDFT[H(f, i).W(f)]|^2 \quad (5.1)$$

A three-dimensional view of the *PDP* as a function of time and location number is presented in Fig.5.5. From visual observation, the *PDP* decays exponentially with time t in a comparable trend at each location. The trend is further analysed with the *PDP* of each location normalised to the peak, as shown in Fig.5.6. The shaded area (or at time $> 500\text{ns}$) with low power shown in Fig.5.6 is the noise floor. These result suggests the general behaviour of the *PDP* under our tested condition was similar throughout the vehicle.

In Fig.5.7, the *PDP* heat-map shows higher impulse response power with shorter distances to the transmitter. This is evident by the heat-map colour brightening as location number increases. In addition, the first peak power at time $t = 0$, which

represents the direct wave (i.e. direct propagation between the transmitter and receiver) was extracted and plotted as a function of distance, as shown in Fig.5.8. As expected, the plot indicates that the first peak power decreased with distance.

In a dense multipath environment, such as an industrial environment [106, 107] or a hospital [108], the *PDP* is typically found to arrive in multiple clusters. In the environment tested, the *PDP* arrived as a single cluster. *PDP* Clusters can be identified by the significant peaks in the *PDP*.

Because all 49 locations exhibit a similar *PDP* shape, the *PDP* of the tested condition can be averaged and modelled as a simple two-term time-dependent power-law model. The averaged power delay profile *APDP* is calculated in linear form, as given by:

$$APDP(t) = E[PDP(t, i)] \quad (5.2)$$

where $E[.]$ represents the average *PDP*(t) of all 49 locations. In the process of estimating the *APDP* from *PDP*, the computation included only the first 500ns, which was considered the optimum time to remove noise from the *PDP*, as shown in Fig.5.9. The identification of this threshold was made through visual inspection.

The two term power-law parameters as given in Eq.(5.3) was extracted through linear regression-based method. The *APDP* and the two-term power law fit is plotted in Fig.5.10.

$$PDP(dB) = k.t^\beta \quad \text{for } t < t_m \quad (5.3)$$

The extracted parameters are $k = -2.223$ and $\beta = 0.449$ for time t less than 500ns (t_m).

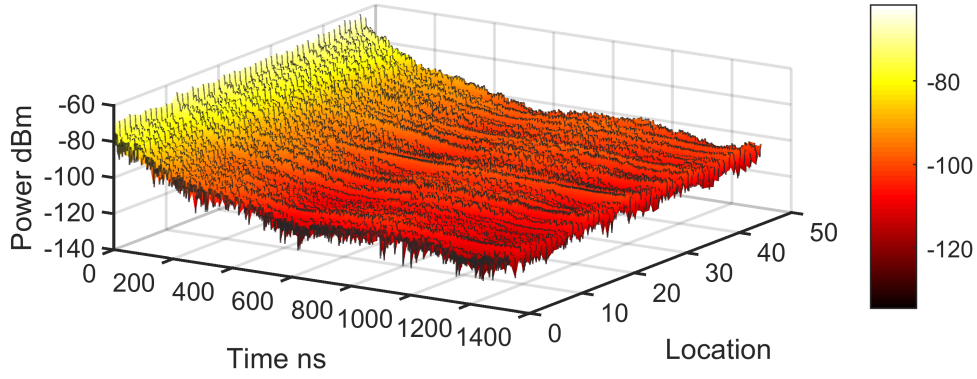


Figure 5.5: The *PDP* of all 49 locations.

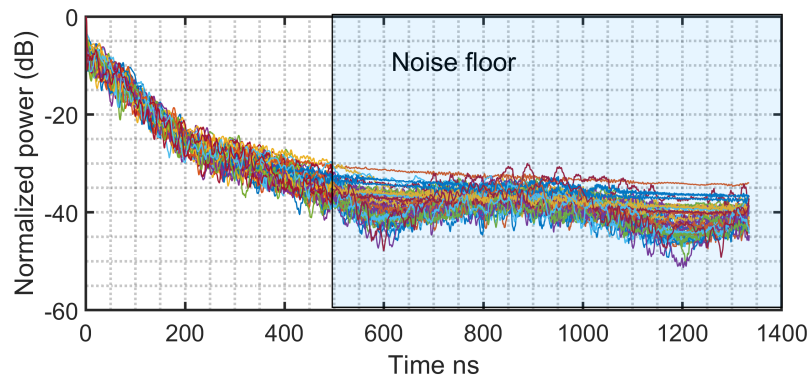


Figure 5.6: A normalized *PDP* of all 49 locations in 2D.

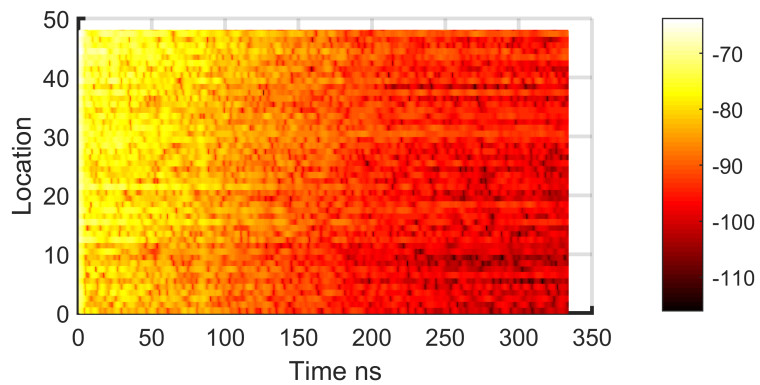


Figure 5.7: A heat-map of 49 *PDP*.

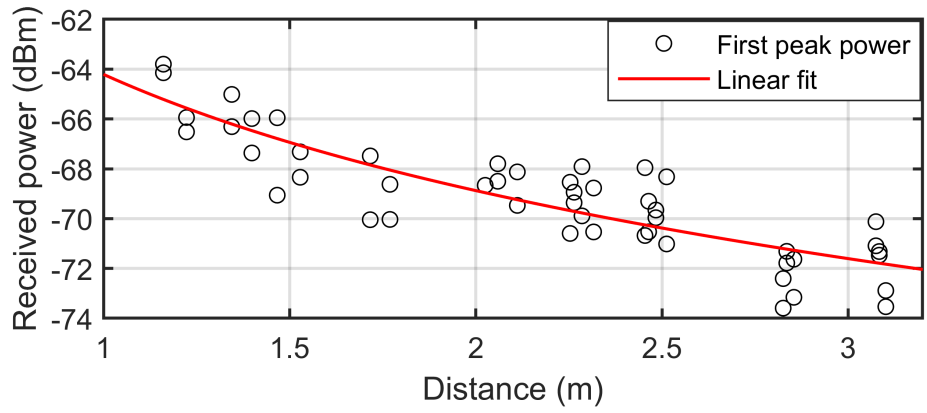


Figure 5.8: The first peak power at $t = 0$ of all 49 locations versus distance.

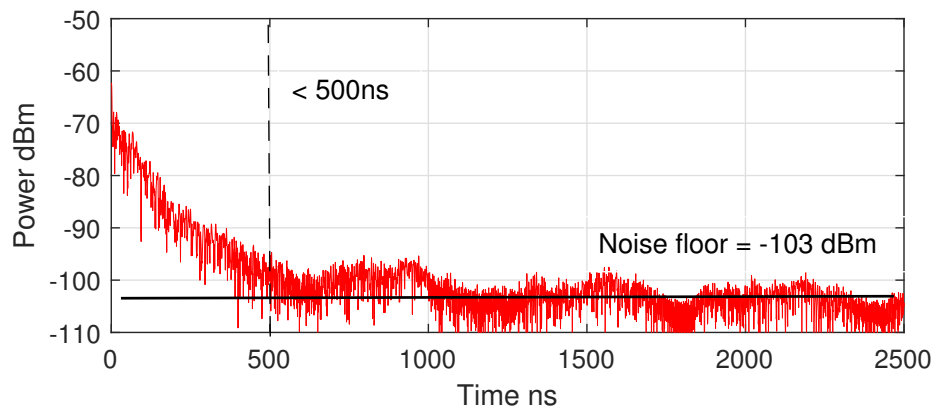


Figure 5.9: Power delay profile of the 49th location.

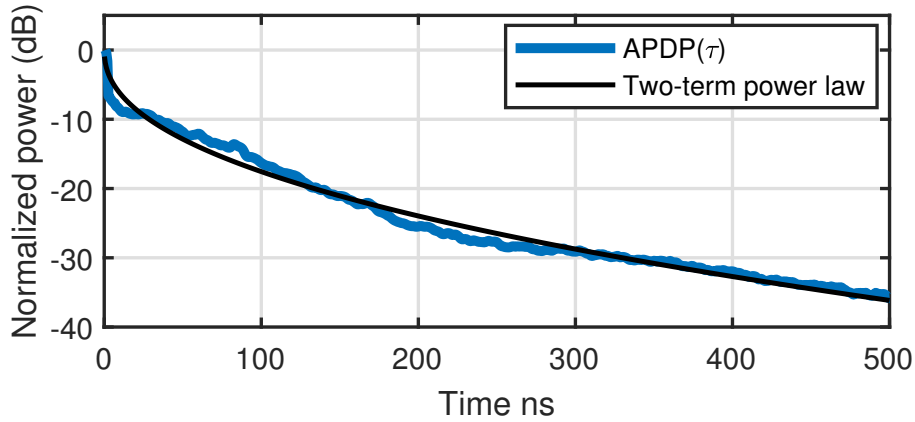


Figure 5.10: The $APDP(t)$ with Two-component power law fit.

5.3.2 RMS delay spread

A transmitted signal propagating in a multipath environment will spread in time owing to the reflection and scattering phenomenon. In a compact environment such as a vehicle, which is dense with objects made of reflective materials, the interaction of a transmitted signal with the environment will cause the received signal to spread, or lengthen in time. A metric called the root mean square (*rms*) delay spread (τ_{rms}) is commonly used to quantify the degree of spread. In digital communications, the performance of a communication system will be impacted when the *rms* delay spread is significantly greater than the symbol period of the transmitted signal.

The *rms* delay spread is determined by finding the mean excess delay $\bar{\tau}$, which is given in Eq. (5.4) as [109]:

$$\bar{\tau} = \frac{\sum_k a_k^2 \tau_k}{\sum_k a_k^2} \quad (5.4)$$

where a_k and τ_k represent the measured *PDP* amplitude and time of the k th path, respectively. The $\bar{\tau}$ is then used to calculate the *rms* delay spread τ_{rms} :

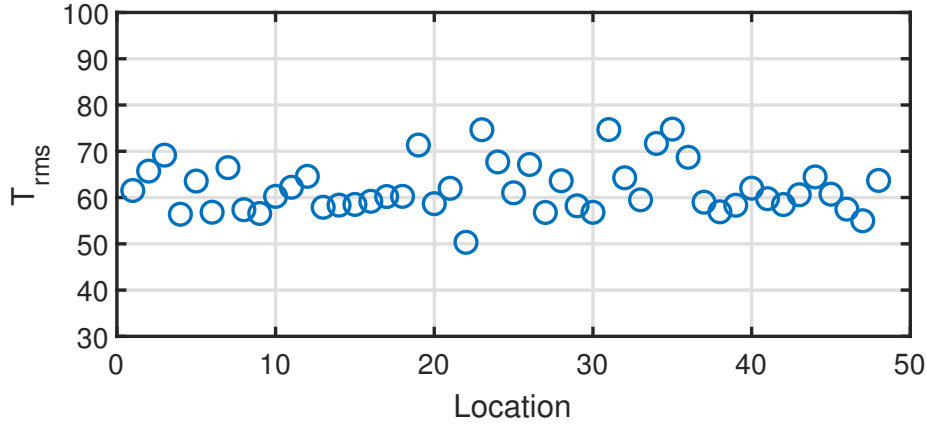


Figure 5.11: RMS delay spread against different location.

$$t_{rms} = \sqrt{\tau^2 - \bar{\tau}^2} \quad (5.5)$$

The estimated *rms* delay spread, as shown in Fig.5.11, varied from 50 to 75 ns among the locations with an average τ_{rms} of 60.72 ns. The *rms* delay spread signifying the degree of multipath has been investigated in various settings. A summary of different measurement campaigns, including this work (engine to passenger compartment), is shown in Table 5.1. Among the various environments tested, the τ_{rms} measured in this study within the vehicle is higher than most indoor settings. However, the *rms* delay spread in the tested environment is significantly lower than that of a reverberation chamber. Several work has proposed that the intra-vehicle channel can be modelled as a reverberation chamber. However, our work suggests that an intra-vehicle channel behaves more like an indoor channel with heavy multipath than a reverberation chamber.

Apart from analysing the dependency of τ_{rms} on location, the Pearson correlation coefficient ρ metric was used to determine the relationship of τ_{rms} with distance. As demonstrated in Fig.5.12, the low correlation coefficient ρ of -0.02 suggests that

Table 5.1: A table of *rms* measurement campaign in different environments

Environment	f (GHz)	B (GHz)	τ_{rms} (ns)
Engine to passenger compartment	2.5	1	50-75
Beneath vehicle chassis [110]	6.85	7.5	17.73
Outdoor [109]	4.3	2.2	2.6-23
Residential [111]	5	6	4.7-8.2
Indoor lab [112]	5.3	4	8-20
Commercial [111]	5	6	5.5-8.2
Steel mill [113]	1.89	0.5	298
Paper mill [113]	1.89	0.5	23
Mine tunnel [114]	2.4	0.5	14
Mine tunnel [115]	3.5	3	11-29
Basement tunnel [116]	3.5	2	3-16
Industrial mechanical room [117]	1.75	1.9	14-30
Indoor room(NLoS) [118]	11	0.4	6-21
Indoor hall(LOS) [118]	11	0.4	2-39
Reverberation chamber [119]	5	0.2	2946-3121
Reverberation chamber [120]	3.5	0.25	1984.3
Within passenger compartment [61]	7	8	5.6-9.7
Indoor corridor [121]	3.5	1	0.8-3.5
Incinerator hall(Industrial) [106]	6.85	7.5	29-51

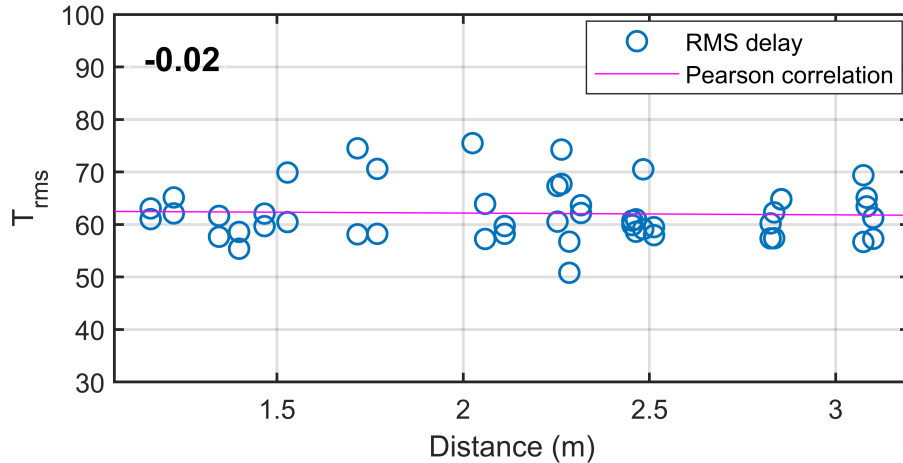


Figure 5.12: *rms* delay spread against distance.

there is little or no correlation between *rms* delay spread and distance. The analysed results indicate that τ_{rms} does not vary significantly with distance or location.

5.3.3 Coherence bandwidth

The coherence bandwidth B_c estimates the channel capacity and determines whether a signal will experience flat fading or frequency-selective fading. A channel is considered frequency-selective when the transmitted signal bandwidth is higher than the B_c of the channel. Signals within a channel with frequency separation equal to or higher than B_c can be considered independent from one another [122].

Two methods are commonly used to estimate the coherence bandwidth of a channel. In the first method, the coherence bandwidth is determined from the *rms* delay spread τ_{rms} using the following equation [123]:

$$B_c = \frac{1}{\alpha \cdot \tau_{rms}} \quad (5.6)$$

where α is selected based on the shape of the *PDP* [124]. While τ_{rms} is inversely proportional to B , their relationship is not exact and varies with the method used to extract τ_{rms} [9].

The second method for estimating B_c , is to apply the frequency correlation function *FCF* to the measured $H(f)$, in other words, the autocorrelation of the complex channel $H(f)$ [125].

The coherence bandwidth has been widely studied in outdoor and indoor environments. However, only a few works have been conducted in a vehicle environment, particularly analysing the dependency of B_c on distance and location (i.e. spatial analysis).

An investigation of coherence bandwidth will help in selecting a suitable channel and bandwidth for a wireless intra-vehicle network. In this analysis, the coherence

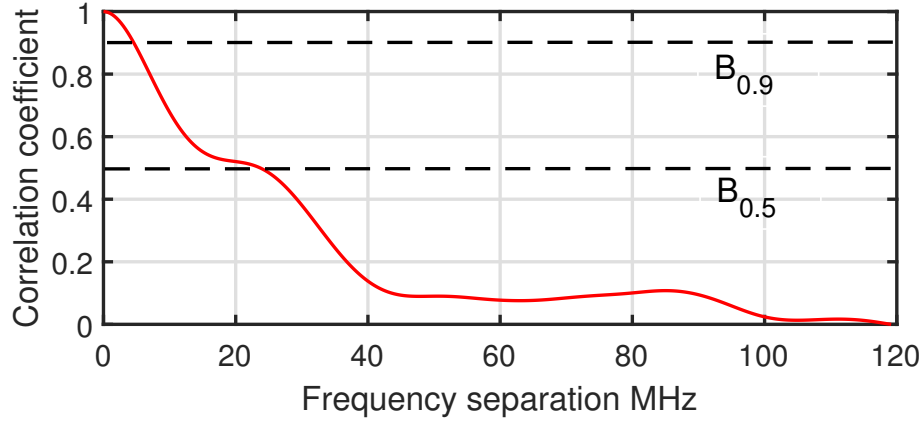


Figure 5.13: Frequency correlation function of the 21st location.

bandwidth was determined using the *FCF* as given by [126]:

$$R(\Delta f) \approx \int_{-\infty}^{\infty} H(f)H^*(f + \Delta f)df \quad (5.7)$$

where Δf and $H^*(f)$ represent frequency shift and the complex conjugate of the channel $H(f)$, respectively. The generally accepted correlation coefficients for estimating the coherence bandwidth are $0.5(B_{0.5})$, $0.7(B_{0.7})$ and $0.9(B_{0.9})$.

In our analysis, the coherence bandwidth was determined when the correlation coefficient reaches 0.5 and 0.9, as shown in Fig.5.13. The *FCF* is applied on all of the 49 locations, the evaluated coherence bandwidth for $B_{0.5}$ and $B_{0.9}$ is shown in Fig.5.14. The *FCF* was applied to all 49 locations; the evaluated coherence bandwidth for $B_{0.5}$ and $B_{0.9}$ is shown in Fig.5.14.

The coherence bandwidth in $B_{0.5}$ varied between 8.7 and 24 MHz with an average $\bar{B}_{0.5}$ of 12.95 MHz. This suggests that wireless communication technologies with channel bandwidth higher than the measured coherence bandwidth, such as WiFi, will experience frequency-selective fading. In contrast, wireless communication technologies, such as 802.11p, Bluetooth, and Zigbee, which have transmission

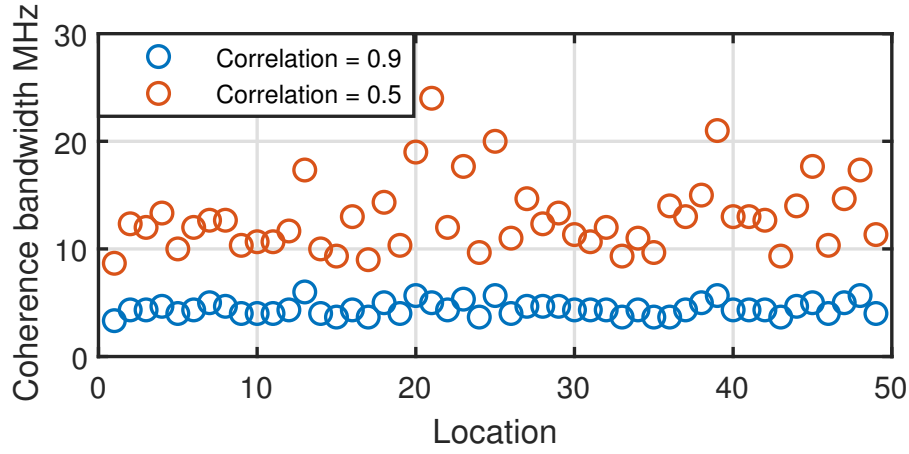


Figure 5.14: The coherence bandwidth at different locations.

bandwidth lower than the coherence bandwidth, will operate under flat-fading channel conditions. In addition, the $B_{0.5}$ varied significantly with location, as depicted in Fig.5.14 (location 18-27). Other studies conducted in the engine compartment have found $B_{0.5}$ to be generally higher than 7 MHz and up to 100 MHz [94].

Similar to the previous analysis, the dependence of coherence bandwidth on distance was evaluated using the Pearson correlation method, as shown in Fig.5.15, resulting in a ρ of -0.1031 and -0.1939 for $B_{0.9}$ and $B_{0.5}$, respectively. This suggests that there is a low correlation between coherence bandwidth and distance.

5.4 Summary and conclusions

In this work, a test was conducted to investigate the multipath characteristics of intra-vehicle channels within engine and passenger compartments. The results show that the power delay profile exhibits a somewhat consistent shape across all the locations measured. This suggests that the general trend of PDP will be similar in any location within the vehicle. In addition, the general trend of PDP show that the multipath components arrived in a single cluster, as compared to other

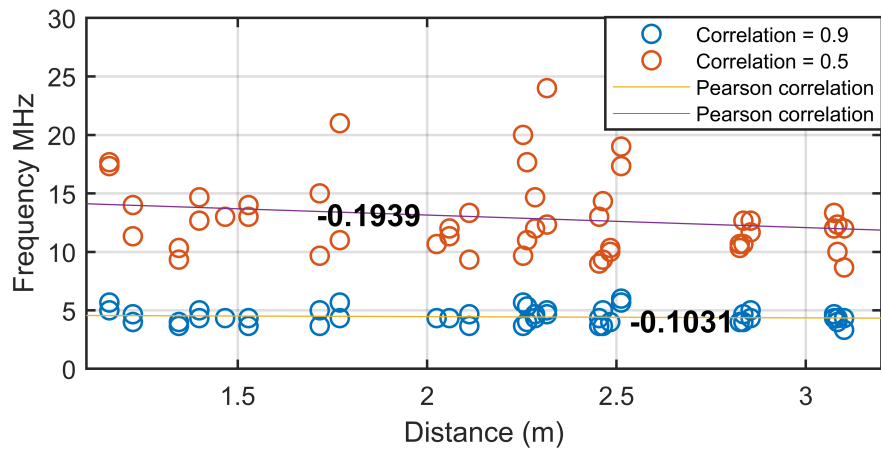


Figure 5.15: The coherence bandwidth against distance.

environment where the multipath component arrives in multiple clusters.

The *rms* delay spread of the channel was determined to range from 50 to 75 ns. This value within the vehicle is slightly higher than most indoor environments. Although the vehicle is made up of reflective material (i.e. metal), the result does not show the channel to be similar to a reverberation chamber. Instead, the result suggests that an intra-vehicle channel is more comparable to an indoor environment. In addition, an analysis performed on the *rms* delay spread and distance revealed that they are uncorrelated. The investigation on the coherence bandwidth shows that it is spatially dependent and varies between 8.7 and 24 MHz with an average of 12.95 MHz. Overall, this study highlights the multipath propagation characteristics of the intra-vehicle channel, which show that some communication technologies such as 802.11p, Bluetooth, and ZigBee will operate in a flat-fading channel condition.

Chapter 6

Electromagnetic interference (EMI)

Vehicles are equipped with a multitude of sensors that have various functions. A reduction in wired networks, or the replacement of these networks with wireless solutions, can reduce weight, save physical space and alleviate complexity in cable management. However, despite these benefits, there are concerns over the reliability, bandwidth and latency of wireless solutions.

When deploying a wireless communication system in a vehicle, it is essential to ensure the required reliability and robustness so that the targeted benefit can be justified. The performance can be achieved by understanding the characteristics of intra-vehicle channels before applying suitable technologies to establish reliable and sustainable wireless connectivity in this environment. In the previous Chapters (4 & 5), the channel loss properties of vehicles were investigated. Another factor that affects wireless communications in a vehicle is electromagnetic interference (EMI).

Electronic systems inside vehicles are much more complicated now than they were decades ago. Current systems are equipped with many types of sensor, such

as those for regenerative braking, advanced driver assistance, autonomous driving, assistant parking and vehicle telematics. This change has led to increased network complexity and higher radiated emissions, which create a noisier and harsher electromagnetic environment in modern vehicles. The present commercial off-the-shelf technologies are not built to operate in such a harsh environment. As a result, proper design or control is needed to allow wireless communication systems to work reliably.

In the past few decades, several studies have investigated EMI in industrial and commercial environments at various frequencies. However, to the best of our knowledge, there had been no other published work that investigate the potential level and influences of the EMI radiated by a vehicle electronic devices in relation to the requirements specified by the standards in this field. The work conducted in [127] uses hypothetical simulation scenarios to demonstrate the impact of EMI on network performance. In comparison, this work was present the characteristic of a vehicle EMI which was conducted through real world measurement. The investigation was carried out over the unlicensed 433 MHz, 2.4 GHz and 5.9 GHz frequency band s because several wireless protocols, such as IEEE 802.15.4, 802.11x and Bluetooth, operate within these bands.

Beside studies on the impact of EMI on intra-vehicle wireless network performance. There have been some related work on radiated emission from individual components or modules, such as spark plugs, Controller Area Network (CAN) buses and automotive Ethernet Multi-Gig cables in vehicles [128, 129]. However, to the best of our knowledge, specific and detailed investigations on vehicle EMI and its impact on intra-vehicle wireless communications have not been reported.

Additionally, the growing interest in renewable energy has led to the electrification of vehicles, and the number of electric vehicles on roads is expected to increase

soon. Such electrification poses new challenges because moving from conventional oil-fuel vehicles to high-power electric drive systems increases radiated EMI. In a oil-fuel vehicle, the major source of EMI is from the ignition of a spark plug [128]. In contrast, in an electric vehicle, an electric motor is used. The electrical motor operates whereby an alternating current is induced through the electrical motor winding using an inverter [130]. An alternating current is generated using high power semiconductor switches which produce EMI [130]. The high-power switching in an electric vehicle presents a challenge to wireless communications because it can cause burst errors which affects the transmission reliability.

The chapter is organised as follows. Section 6.1 provides a discussion of EMI in relation to current standards and its potential impact on wireless communications. Section 6.2 describes the testbed built for this study and related settings for measurement collection. Test results and analysis are presented in Section 6.3, where the impulse noise and EMI characteristics are discussed. Finally, the chapter is concluded in Section 6.4.

6.1 EMC standards

Electromagnetic compatibility (EMC) is the ability of a component to function satisfactorily in an electromagnetic environment without introducing intolerable electromagnetic disturbances to anything in the environment [131]. The EMC standards define the limits and methods to ensure compliance between devices and systems. These standards are published by several organisations, such as the International Electrotechnical Commission (IEC), the International Organization for Standardization (ISO) and the Comité International Spécial des Perturbations Radioélectriques (CISPR). The standards used by each country can differ from one another.

In the European Union (EU), the EMC directive 2014/30/EU (EMCD) is adopted

[132]. The primary purpose of the EMC Directive is to ensure that equipment does not disturb devices (including radio instruments) and that such equipment is immune to interference. For vehicles in the EU, UNECE (United Nations Economic Commission for Europe) Regulation 10 is applied. This regulation refers to various other standards. However, because the current study focuses on the impact of EMI on wireless communications, only the CISPR-related standards will be discussed. Although a vehicle must follow the requirements and specifications of the regulation, a vehicle manufacturer will have its internal standard, which is usually much more stringent. In CISPR, two standards specify the limits of devices in a vehicle:

- CISPR-12: Limits and methods of measurement of radio disturbance characteristics for vehicles, motorboats and spark-ignited engine-driven devices [133].
- CISPR-25: Limits and methods of measurement of radio disturbance characteristics for the protection of receivers used on board vehicles [134].

The main difference between these two standards is that CISPR-12 is for the protection of external receivers, such as TV antennas in a residential area. In contrast, CISPR-25 aims to protect and ensure the performance of receivers mounted inside or on a vehicle.

6.1.1 CISPR-25

The latest revision of CISPR-25 only covers frequencies of up to 2.5 GHz [134]. However, some vehicle manufacturers will have an internal standard that includes higher frequencies. The standards specify a limit for the peak, quasi-peak and average at different frequency bands. The radiated-emission limit published in the standard is further categorised into classes from 1 to 5, with class 5 being the most stringent. The peak and average limits for class 5 are shown in Figs.6.1 and 6.2,

respectively. These limits are used as a guideline for assessing electrical devices in a vehicle to ensure that they comply with the regulations. A device is evaluated for its EMC by performing a radiated-emission measurement, with the device being tested placed 1 metre from the receiving antenna.

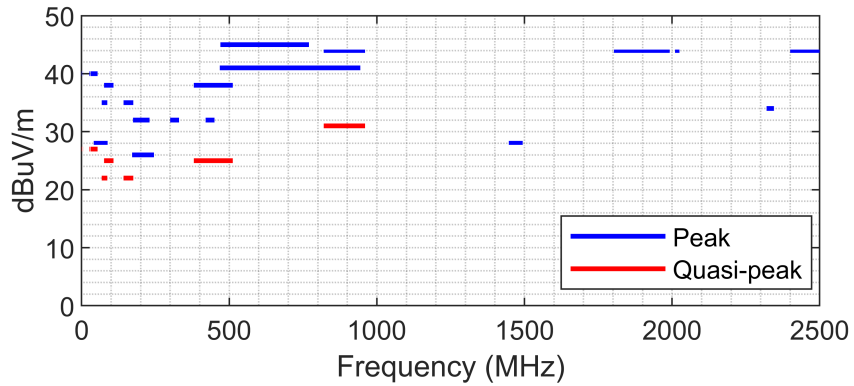


Figure 6.1: CISPR-25 class 5 peak and quasi-peak limits.

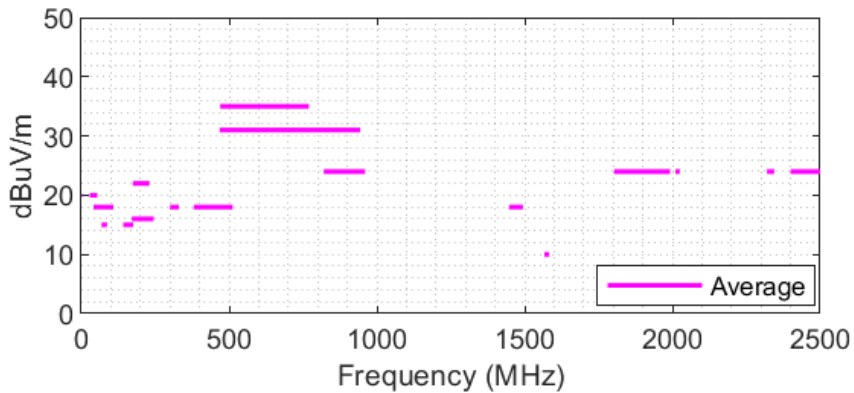


Figure 6.2: CISPR-25 class 5 average limits.

In real world operating condition, it is likely an intra-vehicle wireless node will be placed at a distance of less than 1 metre from a source of EMI. The potential EMI noise when a wireless node is placed close to an EMI source were analysed by first

converting the peak and average limits of the electric-field strength (in dBuV/m) into power (in dBm) [135] using Eqs.(6.1-6.3):

$$\frac{PG}{2\pi D^2} = \frac{E^2}{Z_0} \quad (6.1)$$

where E, P, G, D, Z_0 are the electric-field strength (in V/m), the power (in watts), the antenna gain, the distance from the measuring point to the electrical centre of the antenna, and the free-space propagation impedance (377Ω), respectively.

In this analysis, the antenna gain G is equal to 1 and the distance D is 1 metre as specified in CISPR-25. Hence, the electric-field strength (in V/m) is related to the power (in dBm) by:

$$P = \frac{E^2}{30} \quad (6.2)$$

$$P_{dBm} = 20 \log_{10}(E) - 44.771 \quad (6.3)$$

The peak and average class 5 limits were converted to dBm using Eq.(6.3), and shown in Fig. 6.3 and 6.4.

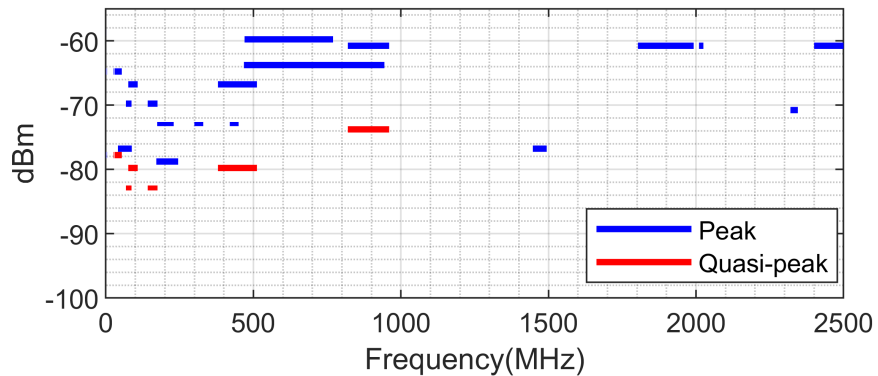


Figure 6.3: CISPR-25 class 5 peak and quasi-peak limits in dBm.

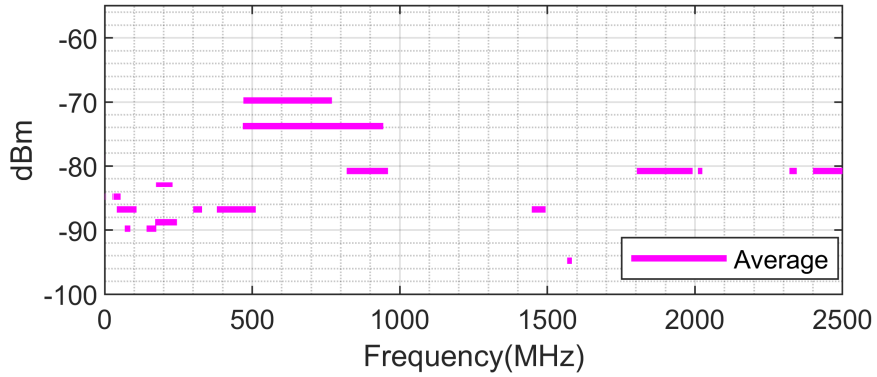


Figure 6.4: CISPR-25 class 5 average limits in dBm.

The estimated noise level for a distance less than 1 metre, EMI_{est} , is calculated using the free-space path loss L_{FS} and the radiated-emission limit EMI_{cispr} as follows:

$$L_{FS,i} = 20\log_{10}(d_i) + 20\log_{10}\left(\frac{4\pi}{c}\right) \quad (6.4)$$

$$EMI_{est,i} = EMI_{cispr} + L_{FS,1m} - L_{FS,i} \quad (6.5)$$

where d_i , c , $EMI_{est,i}$, $L_{FS,i}$, $L_{FS,1m}$ are the i th distance, the speed of light in a vacuum, the i th estimated received EMI, the free-space loss at the i th distance, and the free-space loss at a reference distance of 1 metre, respectively.

Figs. 6.5 and 6.6 show the estimated average-noise and peak-noise levels, respectively, for an on-board receiver at varying distances from an EMI source. These figures demonstrate that a receiver will experience a higher noise level when placed nearer to an EMI source. The CISPR-25 limit is tested on a single electronic device; consequently, the noise level will be higher than the peak limit in an environment containing multiple devices.

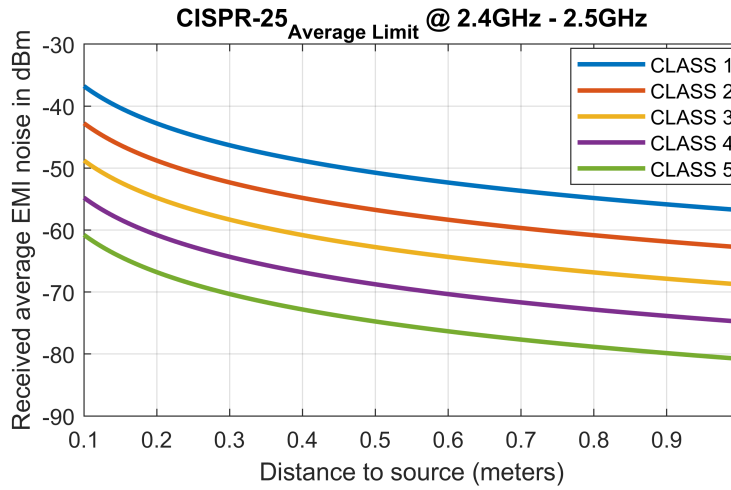


Figure 6.5: Estimated received average noise power based on CISPR-25.

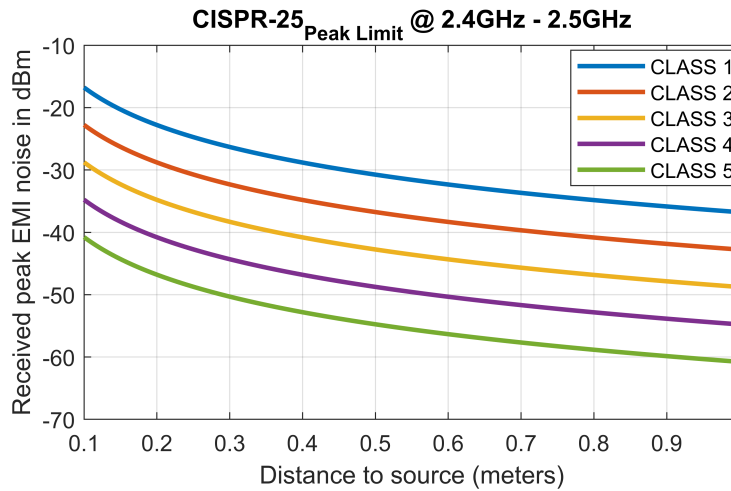


Figure 6.6: Estimated received peak noise power based on CISPR-25.

It is beneficial if more stringent limits are put in place, whereby both peak and average limits are applied, this will make the environment more predictable and the impact of EMI on wireless transmission can be controlled.

Impact on ultra-wideband

Several studies have proposed implementing ultra-wideband (UWB) for intra-vehicle wireless sensor networks due to its better immunity to multipath than narrowband solutions [51, 136]. The maximum power that is allowed to be transmitted by a UWB system is lower compared to narrowband- or wideband-based transmission. The limit specified by the European Telecommunications Standards Institute (ETSI) for UWB operating in the frequency band from 1.6 GHz to 2.7 GHz is -45 dBm [83]. Given the maximum ETSI power limit and the estimated noise level based on CISPR-25, a UWB-based solution will experience significant interference from EMI, compared to the narrowband- or broadband-based solutions, in which higher transmitter power is allowed.

6.2 Testbed and experiment

A purpose-built testbed was developed to perform the EMI measurements. A single Universal Software Radio Peripheral (USRP) device attached to a laptop was used as an EMI receiver. Three different omnidirectional antennas were used to conduct measurements at 433 MHz, 2.4 GHz and 5.9 GHz, as listed in Table.6.1. These measurements were made on two vehicles:

- Jaguar Land Rover Discovery Sport
- Skoda Fabia

A frequency-spectrum scan was performed before the start of each measurement to ensure that the chosen channel was free from interference.

The measurement campaign was divided into two tests. Test 1 was conducted on two types of vehicle to investigate and compare the EMI radiated in the engine,

Table 6.1: USRP settings at 433 MHz, 2.4 GHz and 5.9 GHz

Frequency	433.1 MHz	2.46 GHz	5.9 GHz
Antenna	ANT-STUB-433SM	ANT-2.4-LCW-SMA	TG.35.8113
Sample Rate	20 Msps	20 Msps	20 Msps
Directionality	Omnidirectional	Omnidirectional	Omnidirectional

passenger and boot compartments. Test 2 was performed on a single vehicle to determine the level of EMI radiated in the engine compartment.

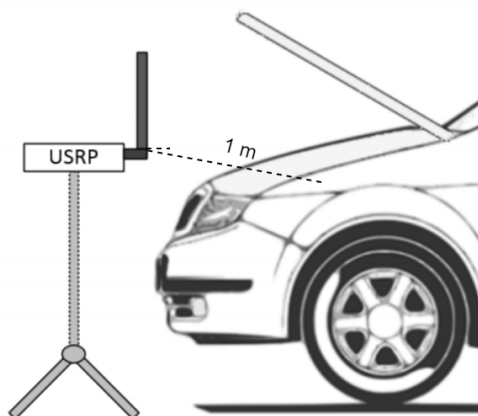


Figure 6.7: Engine-compartment measurement (Test 1).

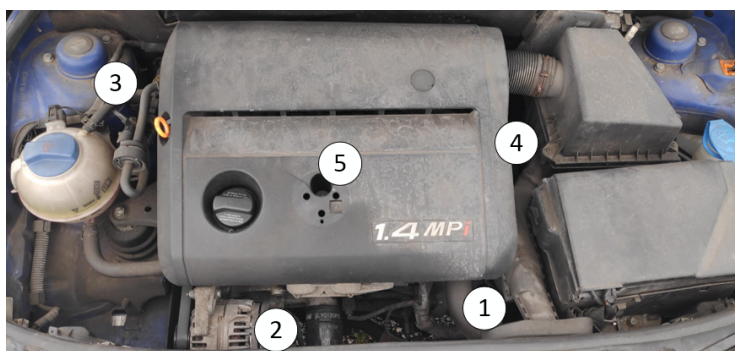


Figure 6.8: Engine compartment measurement (Test 2).

Test 1

This test aimed to examine the EMI radiated in the engine, passenger and boot compartments at 433 MHz and 2.4 GHz. The passenger- and boot- compartment measurements were performed with the EMI receiver placed on the floor inside the vehicle. The engine-compartment measurement was made by placing the EMI-receiver antenna at approximately 1 metre from the centre of the engine compartment, as shown in Fig.6.7. The hood of the vehicle was kept open throughout the test. The USRP was set to record for 3 minutes with the engine turned on and was configured to capture the waveform at a sample rate of 20 Msps.

Test 2

The purpose of this test was to identify the scale of EMI noise at five different locations in the engine compartment, as shown in Fig.6.8. The measurement was performed using a single antenna connected to the USRP through a coaxial cable. The antenna was moved to a different location after completing each measurement. The USRP was configured to capture the waveform for 30 seconds at a sample rate of 20 Msps.

6.3 Result and analysis

6.3.1 Impulsive noise

Impulsive noise refers to relatively short pulses that typically occur as a consequence of fast switching of power in electronic circuits. The results of Test 1 were investigated with a focus on the impulsive noise present in the measurements. In the measurement campaign, the vehicle engine was turned on for part of the time. Fig.6.9 shows a measurement performed at 433 MHz in the engine compartment,

demonstrating that the impulsive noise is not present when the engine is turned off.

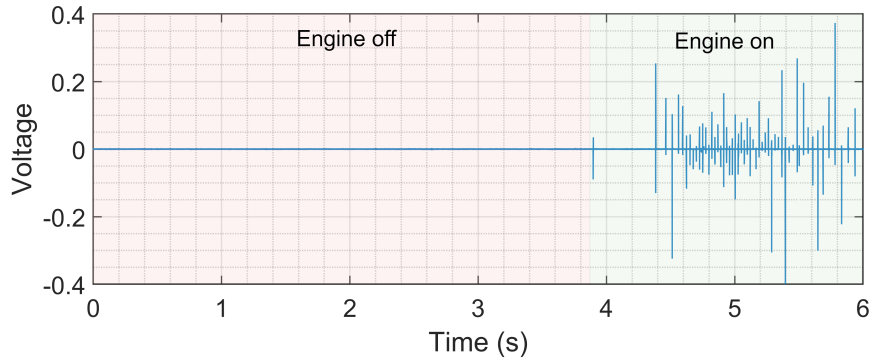


Figure 6.9: Time-series measurement performed at location 1 when the engine is turned off and on.

The time-series measurements conducted in the Land Rover Discovery Sport at 433 MHz and 2.4 GHz are shown in Figs.6.10 and 6.11, respectively. Although the two measurements have different noise patterns, they both show an increase in noise level in the passenger and boot compartments. The impulsive noise is much more present at 2.4 GHz than at 433 MHz.

The overall noise distributions for the 433 MHz and 2.4 GHz results are shown in Figs.6.12 and 6.13, respectively. Impulsive noise can be identified by a heavy tail in the probability density function of the noise [137]. It is evident from the distributions that impulsive noise is present for some locations and frequencies. The exceptions are the boot and passenger compartments at 433 MHz, for which the distribution is more similar to a Gaussian distribution.

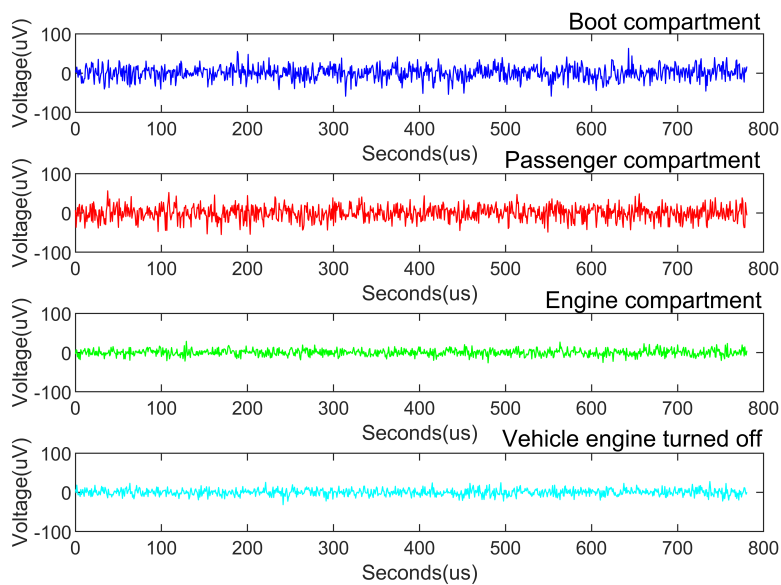


Figure 6.10: Time-series measurement at 433 MHz for the engine, passenger and boot compartment.

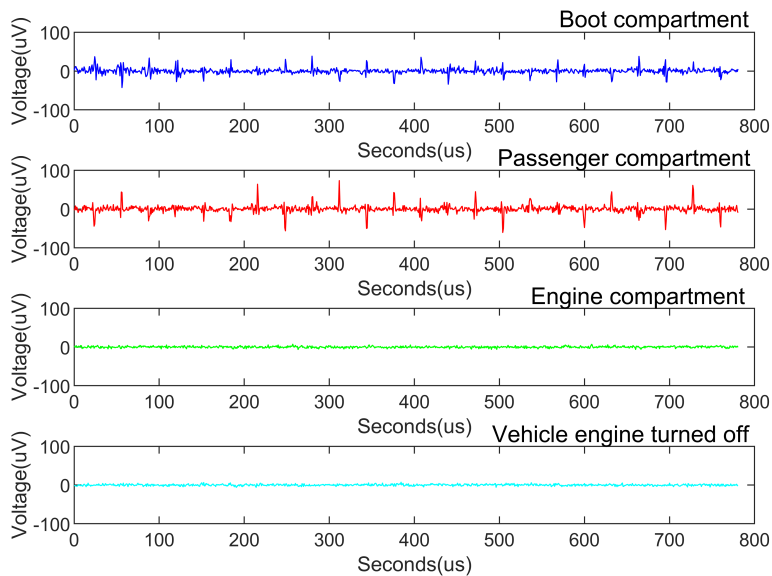


Figure 6.11: Time-series measurement at 2.4GHz for the engine, passenger and boot compartment.

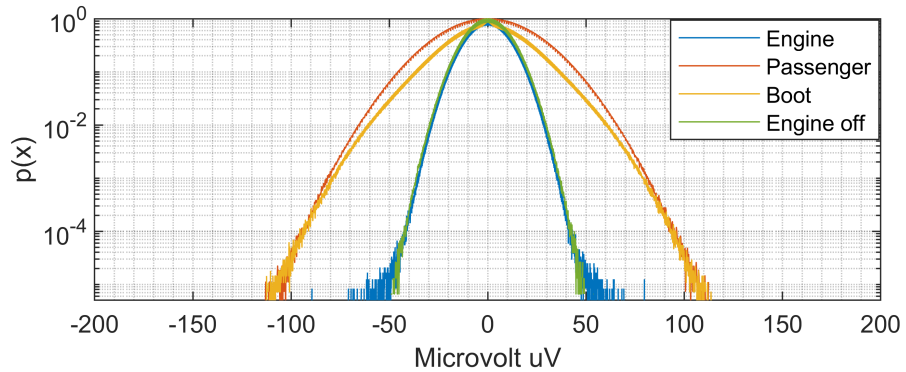


Figure 6.12: Probability density of the time-series measurement at 433 MHz.

Summaries of the peak EMI measured in the two types of vehicle are given in Table.6.2 and 6.3.1. The peak EMI in the Land Rover Discovery Sport is similar at both 433 MHz and 2.4 GHz. At 433 MHz, the boot compartment has the highest peak noise, whereas the passenger compartment has the lowest peak noise. At 2.4 GHz, the passenger compartment has the highest noise, whereas the boot compartment has the lowest. A high noise measured in the passenger compartment could be attributed from the ECU's and wired networks throughout the compartment. The Discovery Sport has a dual battery system in which the battery is located in the engine and boot compartments. For that reason, the high noise in the boot compartment could be caused by electronics and wire harnesses in the boot compartment.

Table 6.2: The peak EMI measured in the engine, passenger and boot compartments of a Land Rover Discovery Sport.

Frequency	Location		
	Engine	Boot	Passenger
433 MHz	-72.41 dBm	-71.77 dBm	-78.02 dBm
2.4 GHz	-75.64 dBm	-75.75 dBm	-71.50 dBm

Table 6.3: The peak EMI measured in the engine, passenger and boot compartments of a Skoda Fabia.

Frequency	Location	
	Engine	Passenger
433 MHz	-12.03 dBm	-43.94 dBm
2.4 GHz	-49.34 dBm	-63.12 dBm

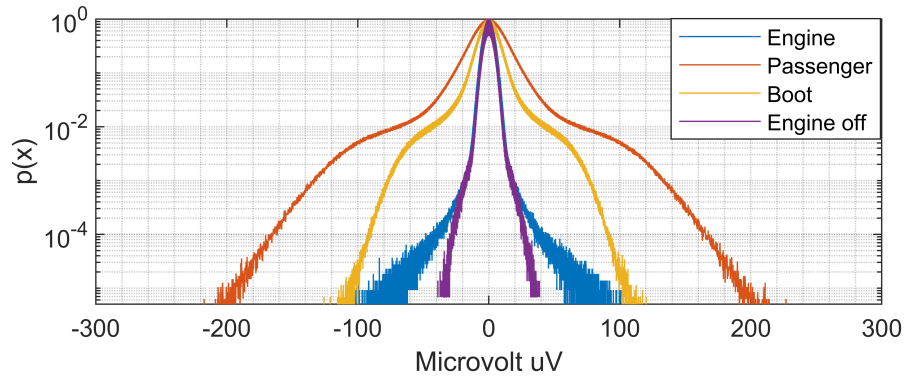


Figure 6.13: Probability density of the measurement at 2.4 GHz.

The peak EMI in the Skoda Fabia is much higher than in the Discovery Sport. For the Skoda Fabia, there was no impulsive noise in the boot compartment. The peak EMI in the engine compartment on the two vehicles is significantly higher than the ambient noise on both frequencies. The impulsive noise in the engine compartment is further investigated in the next section.

6.3.2 Investigation on the impulsive noise radiated in the engine compartments

Test 1 showed that the engine compartment has the highest peak noise. The EMI noise in the engine compartment were further investigated through a measurement (Test 2) at different locations within the engine compartment. These measurements were conducted at 433 MHz, 2.4 GHz and 5.9 GHz, and are summarised in Table.6.4.

Comparing the results from Test 1 and Test 2 confirms that the noise is higher when the antenna is located nearer to the source. The small variation in the measured peak EMI does not support the conclusion that a particular location will experience a higher noise level than other locations. The highest peak noise measured at 433 MHz and location 5 is likely due to the noise emitted by the engine's spark plug. Previous work has shown that a spark plug can cause EMI with frequencies of up to 1 GHz [128, 138]. The peak noise measured at 2.4 GHz and 5.9 GHz is much more varied than that of 433 MHz, which could be explained by the components which have different radiated-emission characteristics. In general, the results measured in this environment demonstrate that the peak EMI noise is lower at higher frequencies. The decrease in peak EMI noise at higher frequencies can be attributed to the atmospheric loss, which is known to increase with frequency [9].

6.3.3 Characterising the measured EMI

The topic of impulsive noise which includes the modelling and characterisation of this noise has been widely studied in other environments such as indoor and industrial environments. In this work, the impact of impulsive noise to wireless communications in the intra-vehicle environment was evaluated by analysing the burst length, burst gap and amplitude probability density of the captured time-series measurements. The pulses from these measurements were examined individually to extract

Table 6.4: Peak EMI measured at five locations and different frequencies.

Location	Frequency (MHz)		
	433	2400	5900
1	-14.3 dBm	-45.5 dBm	-50.4 dBm
2	-11.6 dBm	-48.2 dBm	-50.3 dBm
3	-12.9 dBm	-56.5 dBm	-56.3 dBm
4	-11.5 dBm	-47.9 dBm	-54.5 dBm
5	-8.3 dBm	-49.3 dBm	-50.4 dBm
Max	-8.3 dBm	-45.7 dBm	-50.3 dBm
Average	-11.7 dBm	-49.5 dBm	-52.4 dBm

the burst length and gap, as shown in Fig.6.14.

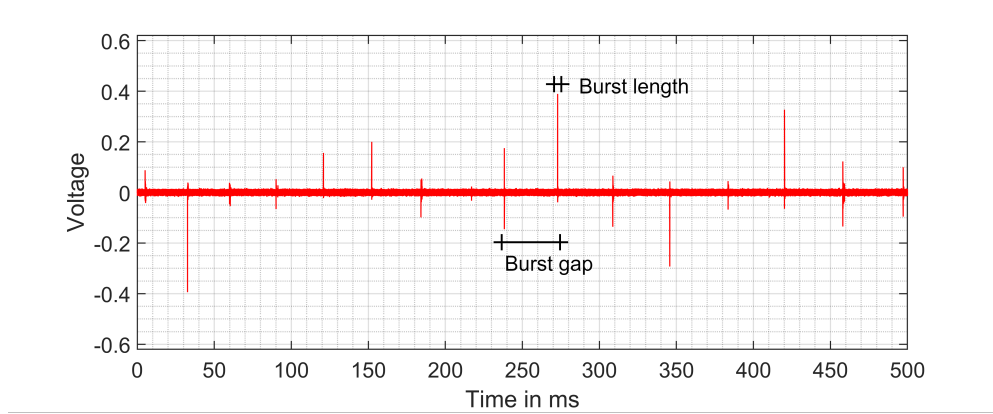


Figure 6.14: Burst length and burst gap of impulsive noise.

The probability denoted as f_{EMI} of an EMI pulse to occur at a specific burst length which for various frequencies and locations are analysed. The f_{EMI} of burst length for five different locations in the engine compartment at 433 MHz, 2.4 GHz and 5.9 GHz are shown in Figs.6.15, 6.16 and 6.17, respectively. The results shows that the pulses have a varying burst length, with the highest number of burst occurring with a burst length of 50 ns. In addition, a highest burst length of upto 2.7 us was recorded at 433 MHz measurement. In short, the impulse noise measured

in a vehicle has a short burst length. The varying burst length seen in the results demonstrate that the noise are emitted from multiple EMI source (radiators) and it varies with frequencies.

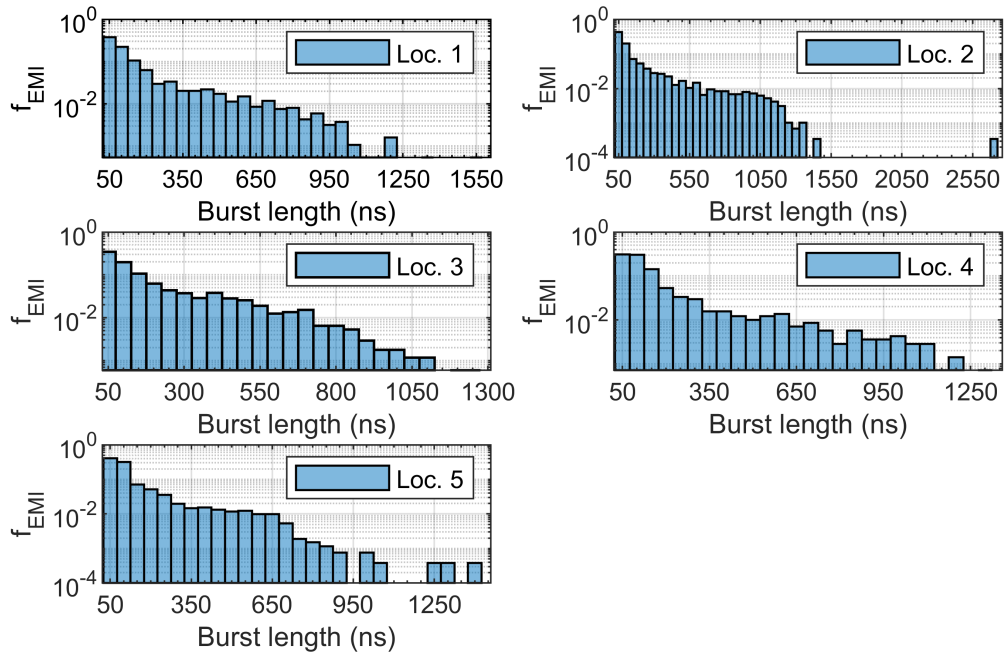


Figure 6.15: Distribution of EMI burst length at 433 MHz.

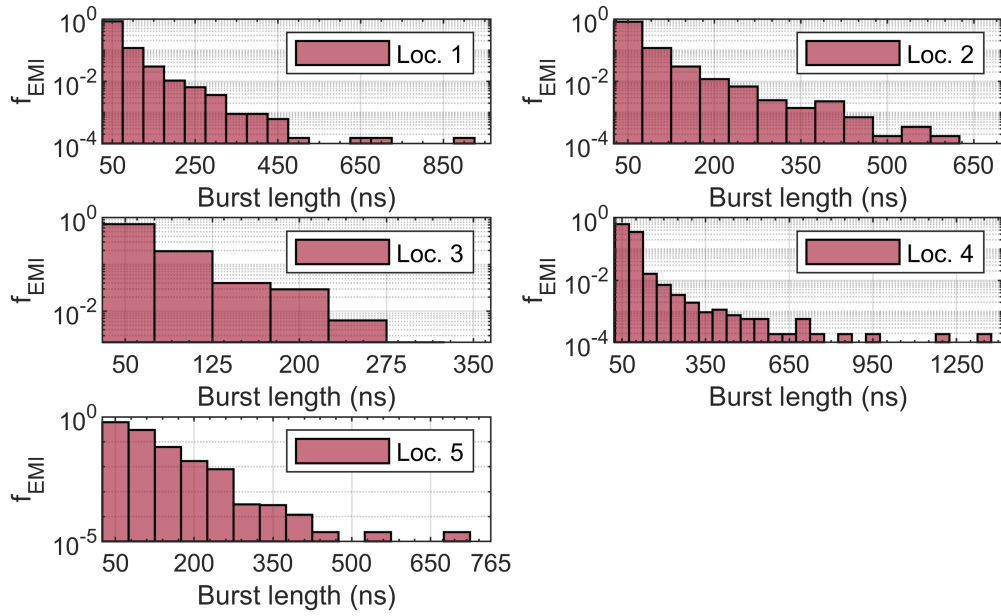


Figure 6.16: Distribution of EMI burst length at 2.4 GHz.

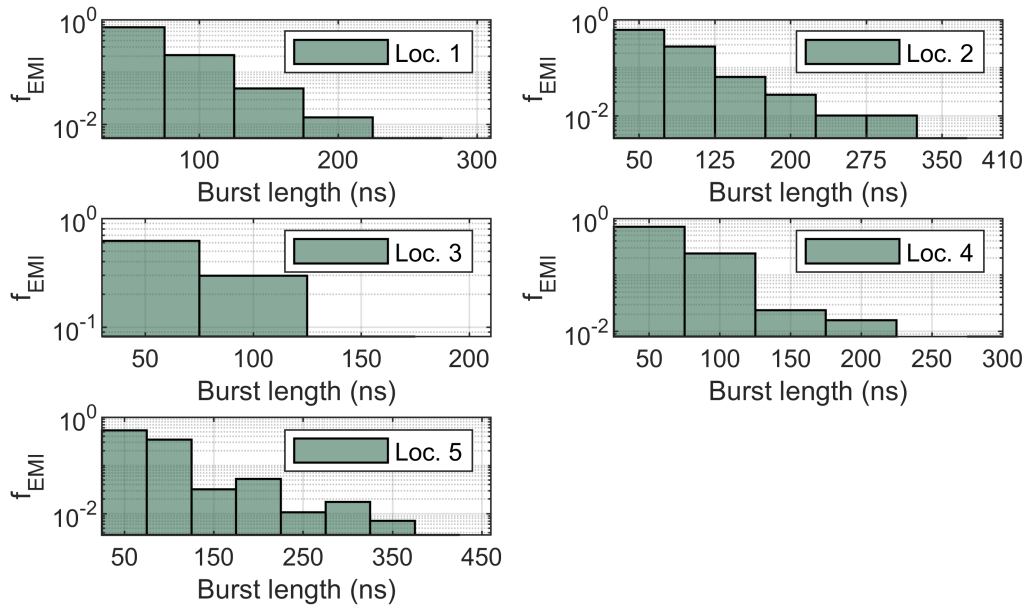


Figure 6.17: Distribution of EMI burst length at 5.9 GHz.

The f_{EMI} of burst gap between each pulses for 433 MHz, 2.4 GHz and 5.9 GHz were evaluated and are shown in Figs.6.18, 6.19 and 6.20, respectively. The distribution of burst gap does show any specific types of distribution pattern. It demonstrate a random like nature and the pattern vary with frequency and location. Although the characteristic of the burst gaps are different between measured frequencies, most of the pulses occur with a gap of 50 ns for different locations and frequencies tested.

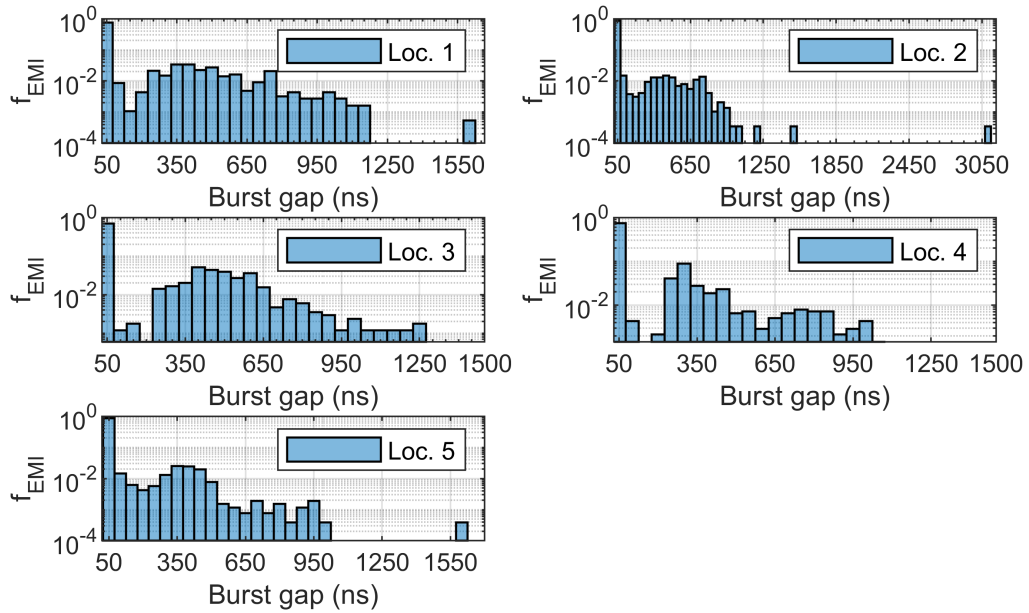


Figure 6.18: Distribution of EMI burst gap at 433 MHz.

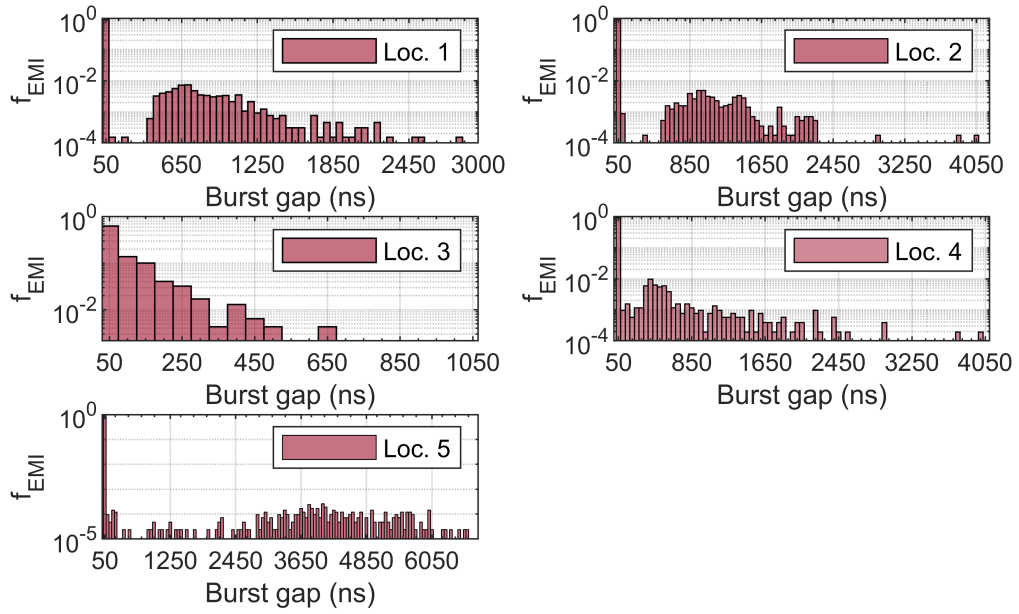


Figure 6.19: Distribution of EMI burst gap at 2.4 GHz.

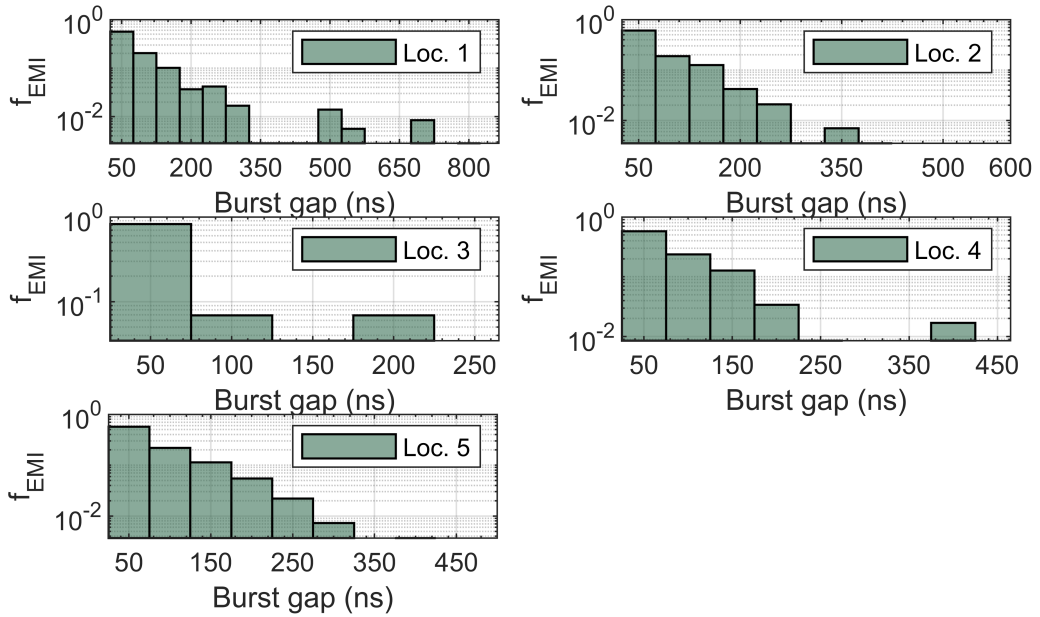


Figure 6.20: Distribution of EMI burst gap at 5.9 GHz.

Amplitude probability distribution

The amplitude probability distribution (*APD*) is commonly used to evaluate the impact of EMI on the performance of wireless communications and has been investigated in other types of environments [139, 140]. The *APD* is directly correlated with the bit error rate performance of a wireless systems [141, 142]. To the best of our knowledge, the *APD* for intra-vehicle environment has not been reported. The *APD* in this work represent the probability of a measured signal (x) exceeds a particular threshold (a_{thr}) in dBm, i.e.

$$APD(x) = p(x > a_{thr}) \quad (6.6)$$

The measured EMI of location 2 was used in this analysis. Figs.6.21, 6.22 and 6.23 depict the *APD* at 433 MHz, 2.4 GHz and 5.9 GHz, respectively. The heavy-tail characteristic of impulsive noise is present in all of the frequencies evaluated. In addition, the tail of the distribution is much wider at 433 MHz than other frequencies. A transmitted signal will be attenuated with distance as it travels through a channel. In brief, the lower the received signal power, the higher the probability of impulsive noise impeding the received signal. The EMI noise in the vehicle can be mitigated by controlling power of the signal received by the receiver. This could be achieved by managing the channel loss characteristics i.e. through frequency and diversity techniques or increasing the power of the transmitting signal.

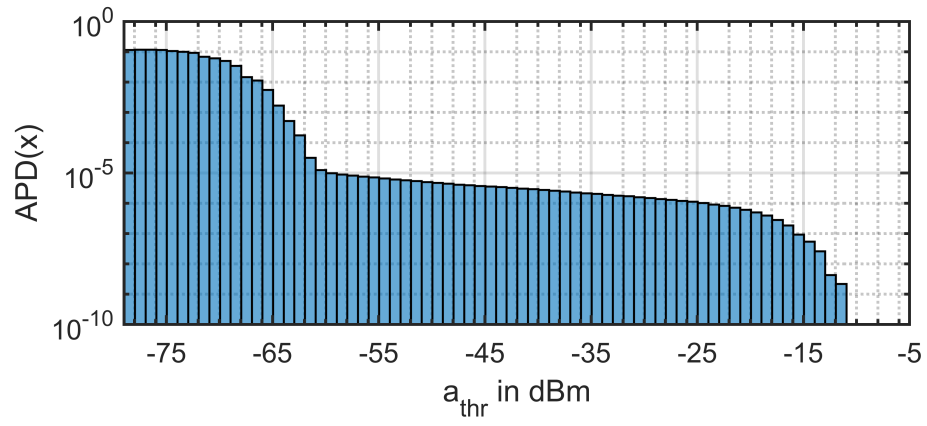


Figure 6.21: *APD* of location 2 at 433 MHz.

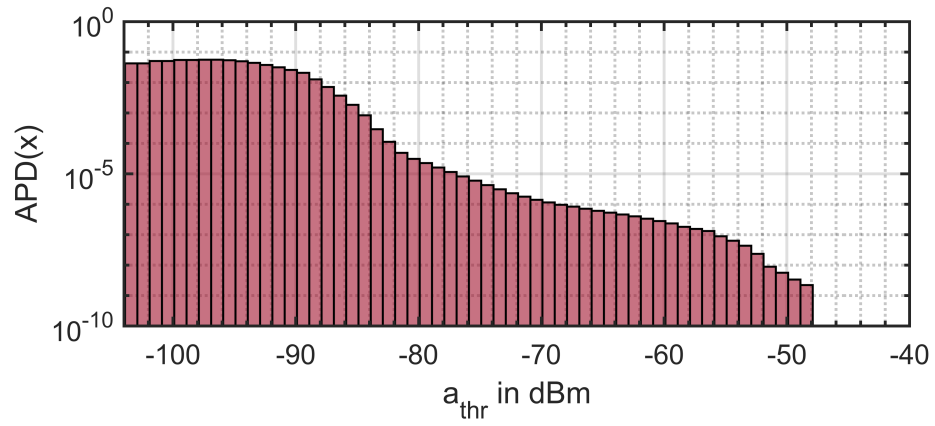


Figure 6.22: *APD* of location 2 at 2.4 GHz..

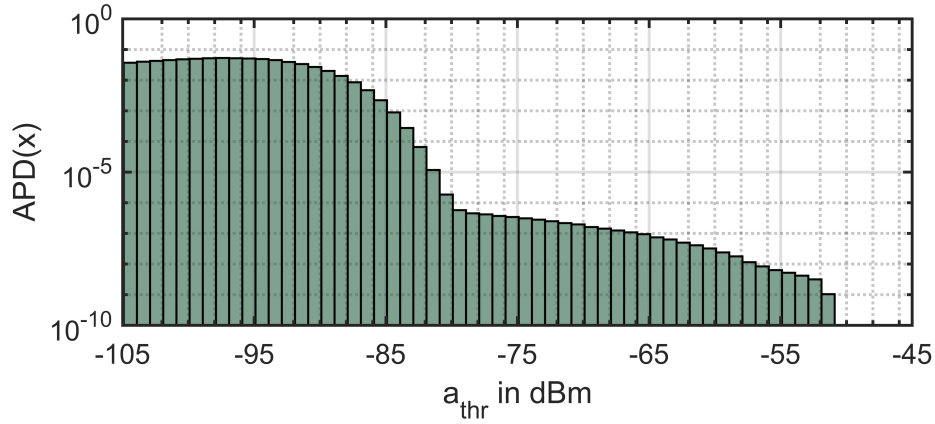


Figure 6.23: *APD* of location 2 at 5.9 GHz.

6.4 Summary and conclusions

In this chapter, the EMC standard and its potential impact on the performance of wireless communications in a vehicle were discussed. Based on the conducted investigation, it is likely that EMI will play a significant part in achieving reliable communications. It is recommended that vehicle manufacturers implement a more stringent EMC requirement to make the environment more predictable. In addition, this work also highlights the vulnerability of UWB relative to narrowband- and broadband-based communications.

A measurement campaign was performed on two different vehicles. The peak noise was measured in different sections of the vehicles, showing that the engine compartment has the highest EMI noise. Additionally, parameters such as the burst length and burst gap, and the frequency of the interfering pulse, were characterised. The findings on this work will help in the design of a suitable communication system under this unique environmental condition. An increased in EMI noise level is seen when the antenna is placed more closely to the source. In consequence, antennas

need to be carefully placed to reduce the impact of EMI on the performance. Furthermore, a vehicle is confined environment and dense with electronic devices. As such, a time-diversity technique such as multiple antenna systems and cooperative relaying technique has the potential of lessening the impact of EMI.

Chapter 7

Time-varying and cooperative communication in IVWN

There are several challenges in the realisation of a wireless intra-vehicle network that can match the performance of a wire-based network in terms of reliability, data rate, and latency [143]. To achieve the required performance, the time-variance nature of the channel must be assessed. In this chapter, the time-varying characteristics of the vehicle channels and the performance of cooperative relay in a vehicle environment are discussed.

This chapter is organised as follows. Section 7.1 covers the time-varying characteristics of the vehicle environment, including the channel variation and coherence time. An investigation on the performance of cooperative relaying as compared to direct transmission and retransmission is analysed and discussed in Section 7.2. Finally, the chapter is concluded in Section 7.3.

7.1 Time-varying channel characteristic

Multipath propagation is an inherent feature of radio propagation where the transmitted signal interacts with the environment, which results in multiple delayed copies to be received and dispersed in time [17]. In other words, the received signal strength is dependent on the environment in which the signal travels. In a non-stationary environment, the effect caused by the movement of scatterer i.e. objects that reflect, scatter, or diffract, give rise to time variation of the wireless channel [144]. Time-varying channel has been studied in other environments such as high-speed train, vehicle-to-vehicle communication, and indoor environment [145–147]. However, the study on time-varying channel characteristic in an intra-vehicle environment is limited.

In a vehicle environment, the transmitter and receiver nodes are expected to be placed fixed at particular locations within the vehicle. As a result, there is no relative change in distance between nodes which can cause a shift in the channel due to Doppler effect [144]. However, the movement made by passengers and signals reflected from external structure whilst the vehicle is in motion may influence the time-variance of a channel in a manner consistent with a non-stationary placement of the nodes.

The time-variance of a wireless channel can be evaluated by measuring the channel's coherence time which describes the expected time duration over which the channel can be considered as time-invariant [148]. While channel loss-related statistics are often the subject of discussion, there are relatively few studies addressing the time-varying characteristics of intra-vehicle channels. The study in [78] has shown that a vehicle in stationary and in non-moving conditions, the channel can be considered time-invariant with a measured coherence time of more than 20 seconds. However, in driving conditions, the movement of the vehicle and the occupants

results in a lower coherence time less than 20 seconds [89].

The effects of vibration from the engine and road conditions have been shown to be nominal when compared to the effects of occupant motion [91]; a study that looked at the effect of human motion in environments other than a vehicle determined that human motion causes a significant variation in channel characteristics [149]. A review of literature on the time-varying channel of the intra-vehicle environment has shown that the channel is highly influenced on the motion of the passengers [90, 149].

In chapter 4, our work has shown that the channel performance is highly dependent on the reflected paths rather than the direct path. As a consequence, motion made by the vehicle's occupant can have an impact on either one or both the direct and reflected transmission paths. In any case, the channel will vary in time due to passenger motion, even when a passenger does not obstruct the direct path. For that reason, it is beneficial to investigate the time-varying characteristics of an intra-vehicle channel.

It is known that the performance degradation caused by the time-varying characteristic of a channel could be mitigated through cooperative relaying or multi-array antenna systems [150]. In general, the independent channel or paths provided by cooperative relaying and multi-array antenna system is exploited whereby each channel experiences different time-varying channel characteristics.

To the best of our knowledge, we believe this is the first work which investigates the correlation of time-varying characteristic and the variation of coherence time across two locations within an intra-vehicle environment. This study is aimed toward answering whether a relaying channel can be considered independent from other paths in terms of its time-varying channel characteristics; which allows the diversity gain from cooperative relaying and multi-array antenna systems to be exploited

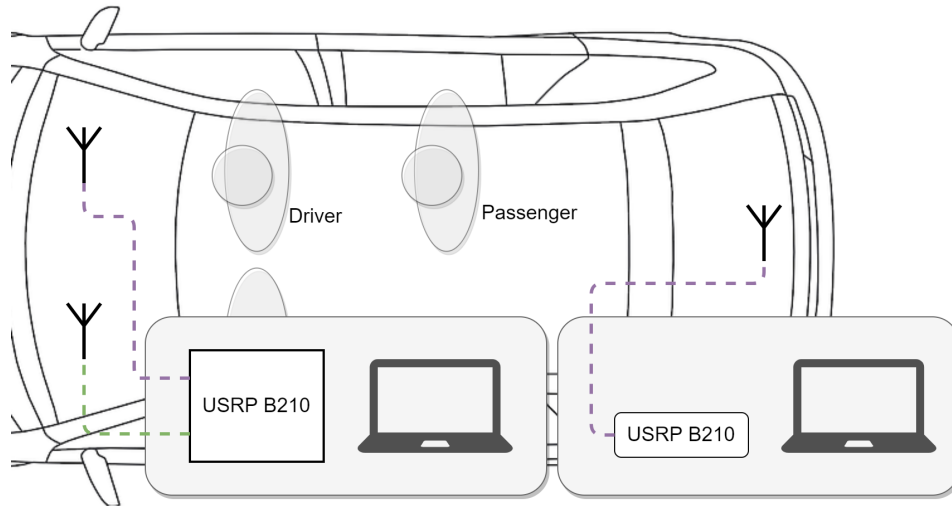


Figure 7.1: The time variation measurement (Test 1) experiment setup.

[150]. As the human component in vehicles is a required condition of operation, an exploration of the effect of human presence on an intra-vehicle wireless network, and potential avenues of mitigation are warranted.

7.1.1 Testbed setup: Time variation measurement

A testbed was developed using two Universal Software Radio Peripheral (USRP) B210 SDRs from National Instruments; one was used as a transmitter and the other as a receiver. Each of the SDR was connected to a laptop for signal generation and processing. An omnidirectional antenna manufactured by Linx Technologies was used throughout the test. The receiver, as depicted in Fig.7.1, is connected to two antennas through a coaxial cable to allow simultaneous measurement from two different paths or locations. The antennas were placed on the floor of both the driver and passenger sides of the vehicle. The transmitter antenna was placed in the centre of the boot compartment, between and equidistant from the two receivers and transmitter antennas.

The SDRs were configured to operate at within the 5.7 GHz frequency band. The frequency band is chosen as it is common to the 802.11p (OCB) and 802.11n/ac/ax operating frequency band. The transmitter output power was set to 0dBm (1mW). The testbed measurement was calibrated in a laboratory environment with a Tektronix spectrum analyser. The receiver measures a complex signal at a sample rate of 250k samples per second, which was converted to received power in dBm.

In this experiment, the speed of the vehicle was not controlled. However, it has been shown in [91] that the speed of a vehicle has a negligible impact on the time-varying characteristic of an intra-vehicle channel. In addition, the work conducted in [55] demonstrates that the external environment also has a negligible effect on the channel. As a consequence, an assumption is made based on the work in [55,91] where the variation of received power is mainly caused by passengers motion.

The measurements were taken while the vehicle was in motion following a predetermined route. The route taken covers typical city environmental scenarios such as stopping at traffic lights, driving along a straight route, and driving with multiple vehicles in the vicinity of the test vehicle. In a realistic driving scenario, there can be more than one occupant in a vehicle; for this reason, the measurements were taken with three occupants in the vehicle driver and two passengers. The relationship between the number of passengers and the time-varying characteristic was not studied in this work. A study conducted in an indoor environment has shown that channel is impacted by the number of people and people's movement speed [151]. Further investigation is needed to understand the relationship between the number of passengers with time-varying characteristics.

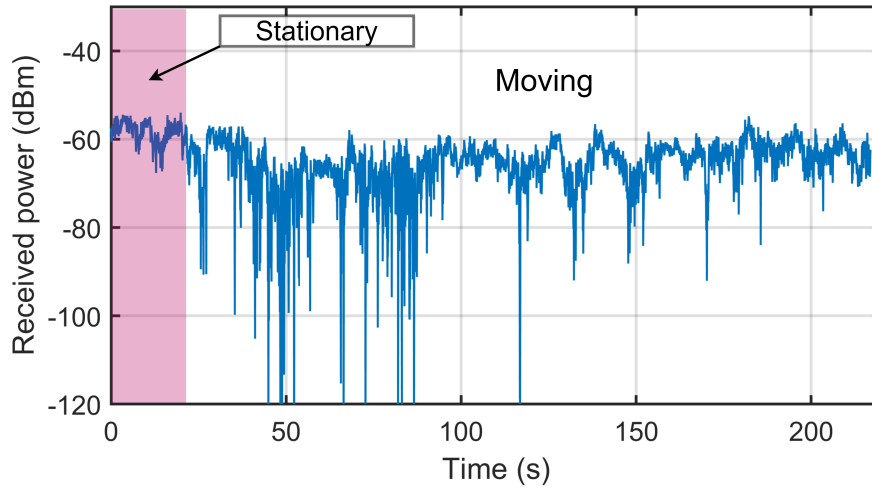


Figure 7.2: The measured received signal power (dBm) against time (s) of the antenna located on the driver side.

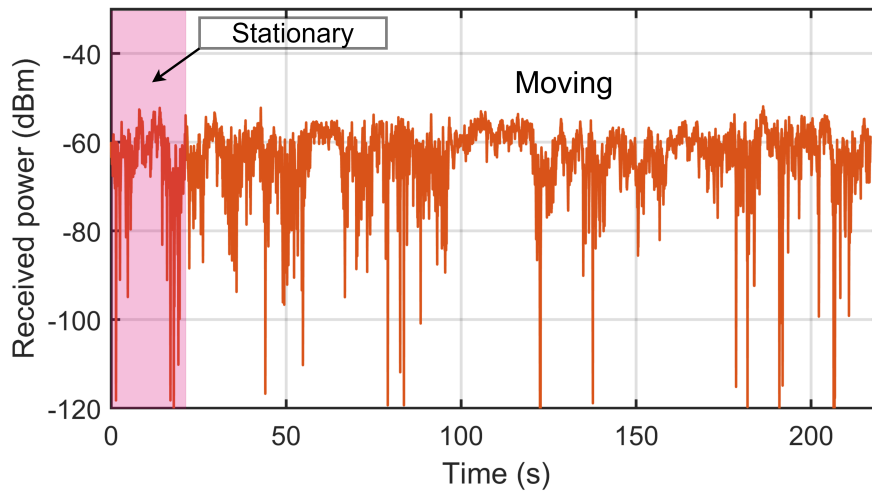


Figure 7.3: The measured received signal power (dBm) against time (s) of the antenna located on the passenger side.

7.1.2 Experimental results and data analysis

Time variation

The time-variance measurement was taken over two independent paths: driver-side floor to boot and passenger-side floor to boot. The received signal strength over time for each path is shown in Figs.7.2 and 7.3. The vehicle is in a stationary parked condition for the first 20 seconds of the measurement. As expected, the channel characteristics changed with time under both moving and stationary conditions. The change in channel condition across time can be attributed to passenger motion.

Fade depth (F_α) is a measure of the variation of power from the local mean due to small-scale fading [152]. Fade depth defines the fade margin required for designing a system with low outage probability [153]. According to [152], fade depth is defined as the three times the standard deviation (3α) of channel energy. The calculated fade depths for the antenna located on the driver and passenger sides of the vehicle are 15.94 dB and 15.6 dB, respectively.

The received signal strengths measured in the two channels from transmitter antenna to driver side antenna and from transmitter antenna to passenger side antenna show a different pattern of received signal strength. The two-sample Kolmogorov-Smirnov (KS) non-parametric test was used to evaluate the correlation between the two channels. The KS test result shows the probability-value $\rho = 0$, which supports and confirms that the time-varying characteristic is independent for each channel.

Coherence Time

Another essential channel parameter is coherence time which measures the length of time the channel can be considered time-invariant or unchanged [14]. Evaluating this parameter helps in determining whether the channel is subjected to slow or fast fading conditions. Coherence time has been widely studied in different environments,

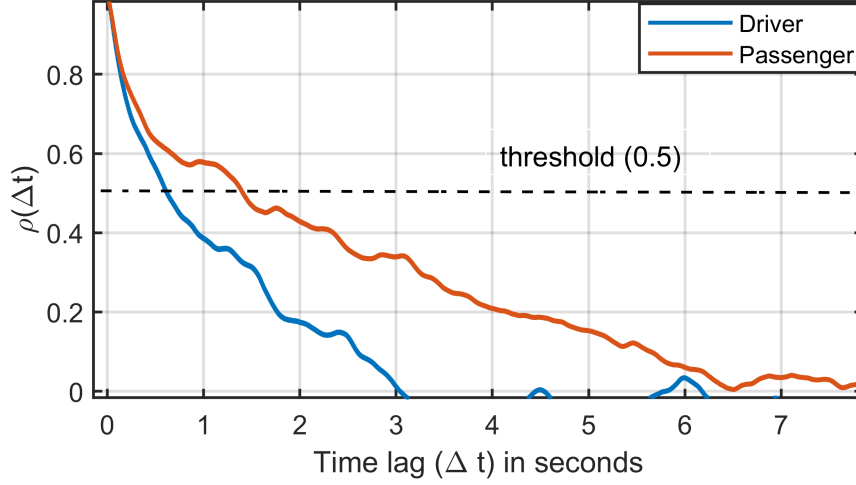


Figure 7.4: The autocorrelation of the measured received power for antennas located on the driver side and passenger side.

including indoors and outdoors environments [154–156].

In this work, the coherence time was extracted through the autocorrelation method, described in [157] as:

$$\rho(\Delta t) = \frac{\frac{1}{N} \sum_{n=1}^{N-\Delta t} (r(n) - n_x)(r(n + \Delta t) - n_x)}{\sqrt{\sum_{n=1}^{N-\Delta t} (r(n) - n_x)^2} \sqrt{\sum_{n=1}^{N-\Delta t} (r(n + \Delta t) - n_x)^2}} \quad (7.1)$$

where $r(n), n_x$ and Δt represents the received signal power of n samples, the average power of all of the samples and the separation time between two consecutive samples, respectively. Coherence time for the experiment was determined when the correlation coefficient ($\rho(\Delta t)$) reached a correlation threshold of 0.5. Using the entire recorded samples from driver and passenger sides, the estimated coherence times, as shown in Fig.7.4, are 0.6 seconds and 1.4 seconds, respectively.

Human motion, which includes fast and slow movements, is irregular and difficult to predict. This behaviour causes the channel to dynamically change over

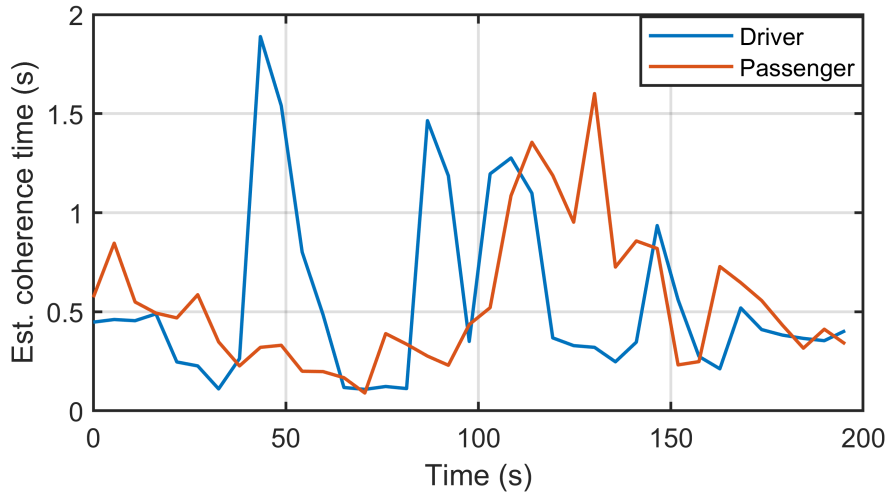


Figure 7.5: The coherence time against time in seconds.

time. As a consequence, to further analyse the variations in coherence time, the running window method was used. Samples were derived from a 20-second time window incrementally evaluated at 10-second intervals. The time window method was selected based on the study in [78], where the coherence time of the channel while in a stationary condition ranged from 5 to 25 seconds.

The results of the running window method are shown in Fig.7.5. The coherence time of the channel on the passenger side varied between 0.2 to 1.6 seconds and on the driver side, varied 0.2 to 1.84 seconds. These results support previous findings where the non-parametric test applied on the fading statistics shows that both channels experience independent time-related fading. With an average coherence time of 0.5 seconds, the results also suggest that intra-vehicle channels can be assumed to be slow-fading. The coherence time measured is lower than measured in [74, 78]. Human movement is difficult to predict, and any move made by the passenger within a vehicle is bound to cause a change in the channel condition. The lower coherence time measured in this work could be due to a higher number of passengers in the

test conducted. Investigation on the correlation of the number of passengers with the coherence time has not been studied; however, it has been shown in an indoor environment that temporal fading increases with the number of people [158].

7.2 Cooperative relaying in IVWSN

Having discussed channel loss statistics, electromagnetic interference, and time-variance of vehicle channels in previous chapters, it is evident that to achieve reliable communication within the vehicle environment, these factors that contribute to the degradation of wireless communication performance must be mitigated. One method of mitigation may lie through incorporating path and time diversity techniques such as cooperative relaying.

Cooperative communication is a growing area of interest due to its ability to improve communication capacity, speed, and performance [159]. In cooperative communication the informations are transmitted through independent paths ($h_n(t)$) through a relaying node, as shown in Fig. 7.6. In general, the distance between the relay node is kept multiple wavelengths apart to ensure independent channel characteristics [150].

In the previous work, we have shown that a vehicle in an environment with high EMI noise, severe multipath fading and slow time-varying characteristic. The performance of wireless communication inside a vehicle will be affected under such environmental condition. In order to mitigate the impact of EMI, multipath fading and time-varying characteristic, a cooperative communication technique could be implemented which offers both time and spatial diversity [160]. Cooperative offers similar benefits with multiple-antenna array systems without requiring addition antenna on each wireless node [150].

In a time-varying channel with severe multipath fading, there is a probability

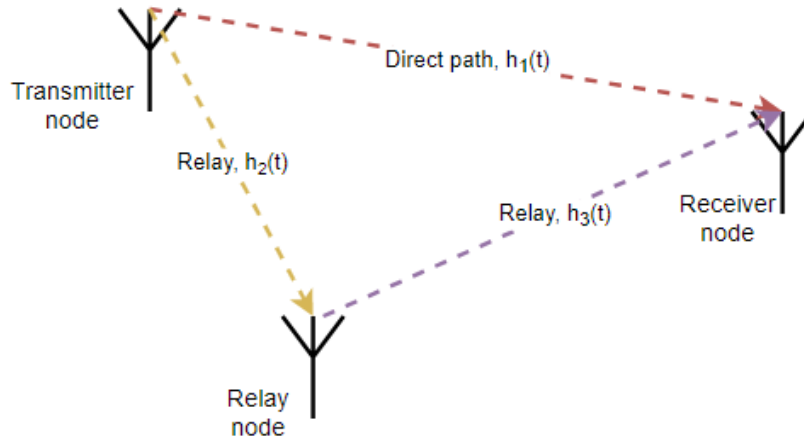


Figure 7.6: Transmitter, relay and receiver node in cooperative relaying configuration.

that a channel will be in deep-fade for a significant amount of time. In such a situation, multiple consecutive packets that are transmitted on the same channel will be lost [161]. In other words, error control techniques such as retransmission would not be able to correct errors or packet loss in deep-fade condition [162]. The path diversity from cooperative communication allows the information to be transmitted through a different channel which experiences different channel characteristics. In a situation where one of the paths is under deep-fading condition, information can be successfully received through the other path. In addition, the time-diversity of cooperative communication further improves the performance of wireless communication where the information received by the receiver arrived at a different time [150]. Thus, each information experiences different EMI noise, time-related fading effects and co-channel interference.

To the best of author's knowledge, there is no previously published work evaluating the performance of cooperative communication for the wireless intra-vehicle network. However, the performance of cooperative communication has been assessed

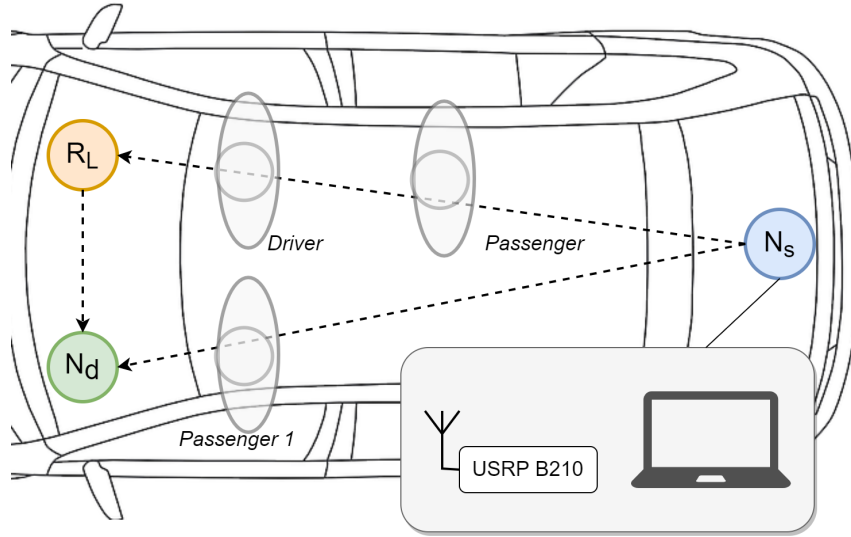


Figure 7.7: The cooperative and retransmission (Test 2) experimental setup.

in other fields such as vehicle to vehicle communication, where it shows significant performance improvement over direct and retransmission schemes [163, 164].

There are several cooperative relaying protocols proposed in the literature [150]; these include the amplify-and-forward (*AF*) relaying protocol and the decode-and-forward (*DF*) protocol. In the *AF* protocol, the relay node receives the transmitted signal, which is then amplified and transmitted to the destination node. By comparison, in *DF* protocol, the relay node decodes and then re-encodes before sending the transmitted packet to the destination. In this work, the *DF* protocol is utilised as it can be easily implemented on off-the-shelf devices such as 802.11x, 802.15.4 (Zigbee) and Bluetooth [165–167].

7.2.1 Testbed setup: Cooperative relaying and retransmission scheme

The performance of a cooperative relaying scheme that exploits a channel’s spatial and time diversity was investigated. In this work, a *fixed DF* scheme is implemented where the relay node transmits even under severe fading condition [150]. In

contrast, in the *selective DF* scheme, the relay node does not transmit the relayed information when the channel is under a severe fading condition which is evaluated from the channel state information [150].

The cooperative relaying scheme was compared against direct transmission and retransmission schemes. There are a number of options for evaluating *DF* based cooperative communication. The IEEE 802.11p/OCB was selected for this work as it is readily available and has been widely deployed for the vehicle to vehicle and vehicle to infrastructure communications [168]. An SDR-based 802.11p/OCB testbed with cooperative relaying was developed, and its performance was then evaluated under realistic driving conditions.

The IEEE 802.11p/OCB-based cooperative relaying testbed was developed using three USRP B210 SDRs with the testbed system configuration, as shown in Fig.7.7. The SDRs were attached to a laptop set up as a source, (N_s); a relay, (R_L); and a destination node (N_d). The parameters, as configured in this test, are shown in Table 7.1.

The testbed events direct transmission, relay, and retransmission are illustrated in Fig.7.8. In the first event, N_s transmitted a packet which was then received and decoded by both R_L and N_d nodes. In the second event, R_L decoded and forwarded the received packet to N_d node. Finally, the same packet was retransmitted from N_s to N_d . This series of events occurred at 90 ms intervals, and a total of 26,000 packets were transmitted throughout the test. Upon implementation, the relay node detected, re-encoded, and transmitted the packets to the destination node. The destination node received two copies of the packets, one from the source, and one from the relay node.

The test was conducted while the vehicle is driven along a predetermined route with a distance of 6.5 km. There were three occupants in the vehicle; the driver and

Table 7.1: USRP settings for N_s , R_L and N_d nodes.

Frequency Setting	5.7 GHz
Antenna	ANT-2.4-LCW-SMA (omnidirectional)
Tx Power	-35 dBm
Modulation	16-QAM
Coding rate	$\frac{1}{2}$
Packet Size	100 bytes
Transmission Interval	90ms

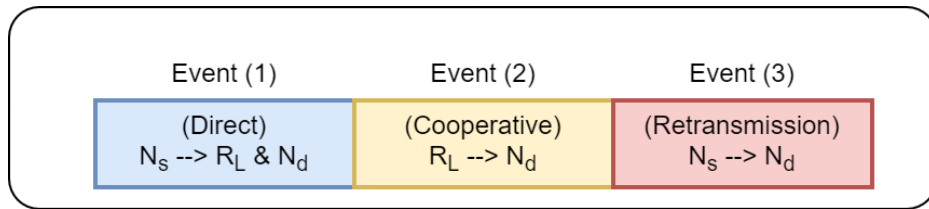


Figure 7.8: The testbed event diagram.

two passengers.

7.2.2 Performance evaluation

Previous tests demonstrated that the intra-vehicle channel is subject to slow fading. As a result, there is a possibility that the channel will stay in deep-fade for an extended period of time which can cause multiple consecutive packet losses. In this work, the performance of cooperative relaying scheme in an intra-vehicle environment is presented. A cooperative relaying scheme provides two or more independent channels, thus providing path diversity and leads to reduced packet loss.

The transmission performance in this work is evaluated by measuring the percentage of packet successfully received (*PPSR*) of each transmission schemes, as shown in Fig.7.9. At 99.25%, cooperative relaying scheme demonstrates the highest *PPSR*, followed by retransmission and direct transmission, which result in *PPSR* of 97.95% and 93.80%, respectively.

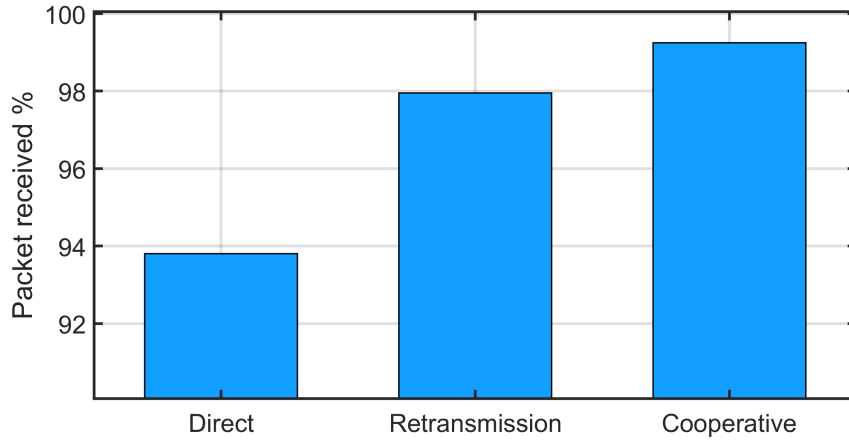


Figure 7.9: The percentage of packet received for direct, cooperative relaying and retransmission.

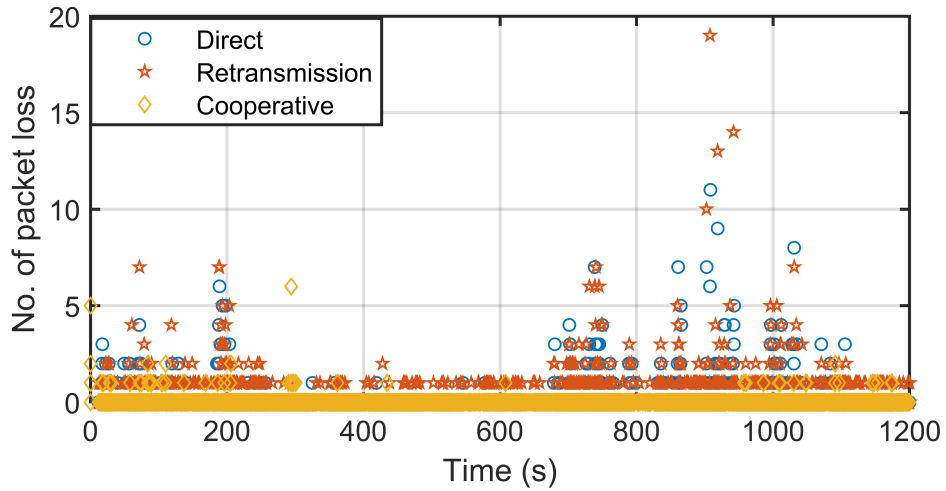


Figure 7.10: The number of consecutive packet losses against time in seconds for direct, retransmission, and cooperative relaying.

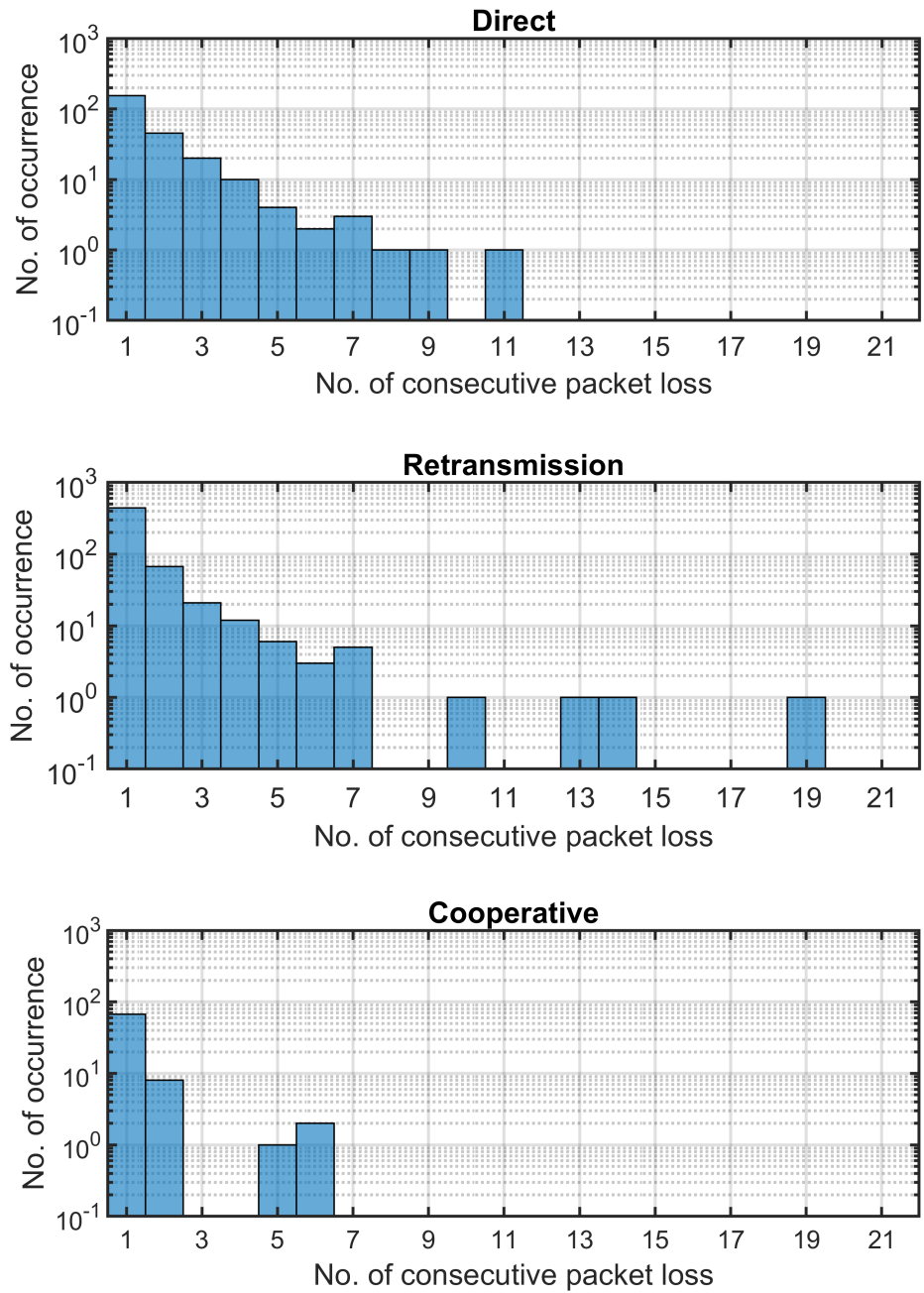


Figure 7.11: The distribution of the number of consecutive packet losses for direct, retransmission, and cooperative relaying.

The number of packet loss event that occurred consecutively is shown in Fig. 7.10. The packet loss for direct and retransmission scheme show a similar pattern and a high number of packet losses occur between time (t) = 700 to 1100 seconds. In contrast, the cooperative relaying results demonstrate a more consistent as well as a lower rate of packet loss throughout the test. The similarity in pattern between the retransmission and direct scheme is due to the channel in deep fading for an extended amount of time, hence causing multiple consecutive packet loss. The retransmission scheme does not result in significant improvement in performance, as the information is retransmitted over the same channel that is still in deep-fading condition.

The distribution of consecutive packet losses and how often it occurs in direct transmission, retransmission, and cooperative relaying is shown in Fig.7.11. The results show that direct transmission and retransmission have a higher number of consecutive packet losses at 11 and 19, respectively, while the highest number of consecutive packet losses with cooperative relaying was just 6.

Overall, the results of these tests demonstrate that cooperative relaying performs better than both direct transmission and retransmission. Through the cooperative relaying, a *PPSR* of 99.25% can be achieved. The transmit power setting in this test is set to -35 dBm (316uW), which shows that a high *PPSR* can be achieved even with a low transmit power setting. The advantages of implementing cooperative relaying are twofold; it will improve the overall *PPSR*, and will lead to reduced latency through lower number of consecutive packet losses.

7.3 Summary and conclusions

In this chapter, the time-varying nature of a vehicle is discussed. Coherence time was evaluated and found to vary between 0.2 to 1.84 seconds, with the average equal

to 0.5 seconds. Our result is lower than the coherence time measured in [74, 78], which could be caused by the number of occupants in our test being higher than in other work. Based on these results, the vehicle environment can be treated as a slow-fading channel. Through observing the fading patterns and applying the *KS*-test, it is clear the channels can be treated as independent from one another.

To ensure reliable communication within a vehicle, the investigations and assessments performed in the previous chapters have shown the impact of frequency-selectivity, electromagnetic interference (EMI), and time-related fading must be mitigated. Time and spatial-diversity in cooperative communication offer a distinct advantage over other methods tested. When the performance of the cooperative relaying protocol is compared to the performances of direct and retransmission protocols, the results of foregoing tests show that cooperative relaying, with a *PPSR* of 99.25% has a distinct advantage over the 93.80% for direct transmission and 97.95% for retransmission protocols.

Although the cooperative relaying result shows an increase in performance over the other schemes, this is at the expense of lower bandwidth efficiency and increased end to end latency [150]. As such, different cooperative relaying scheme could be explored, such as *AF* which has better latency at the expense of complexity. Furthermore, Non-Orthogonal Multiple Access (*NOMA*) has gained ever-growing attention from the research community, where it offers increased spectral efficiency, improved outage, and high throughput [169]. Cooperative relaying using *NOMA* could potentially be used in intra-vehicle wireless communications. Exploratory work on the different cooperative relaying scheme is needed to evaluate and justify the trade-offs between each scheme.

Chapter 8

Conclusions and future work

This chapter concludes the thesis and discusses some potential research directions following the work presented here. In summary, the thesis presents an essential work with extensive results on intra-vehicle channel characteristics and highlights the factors that could affect the performance of wireless communications in a vehicle. The wireless communication channel in a vehicle can be described as frequency-selective with a high level of EMI noise and slow fading dominance. The reliability of wireless communications for an in-vehicle setting can be improved by introducing frequency or spatial diversity to mitigate frequency selectivity, and by employing time-diversity to minimise the impacts of both EMI and the time-variant nature inside a vehicle.

8.1 Summary

In Chapter 3, a thorough review of current vehicle network is presented. Given the rising complexity and costs of vehicle networks, there is pressing need for a lighter and more flexible network solution. Wireless technologies may prove increasingly useful. They offer significant benefits, allowing the wire harness to be reduced

in size or eliminated altogether from vehicle network architecture. An extensive literature review on research related to wireless communications in a vehicle shows that there are currently no standards, nor indeed a definitive answer regarding the most suitable technology for the vehicle environment. Therefore, it is beneficial to investigate the channel properties from a broad perspective.

Chapter 4 discusses the measurement campaign conducted to investigate the propagation characteristics of narrowband signals. A path loss model with the large-scale and small-scale fading. Based on an analysis of the result, this study demonstrates that the small-scale fading effect is not statistically dependent on the carrier frequency. In addition, small-scale fading is much more influential than large-scale fading in this environment. Furthermore, the Rician K -factor, which is the ratio of the spectral component over the scattered path, shows that the K -factor decreases with distance. The low K -factor value indicates that the multipath component is comparable to the specular component, even when there is a direct LOS path. Thus, the multiplicative gain from a LOS path in a vehicle environment would not be significant as compared to other environments such as indoor and outdoor settings .

Following the investigation of narrowband characteristics, the propagation characteristics of the wideband channel are presented in Chapter 5. The vehicle environment is dense with objects such as seats and panels. It is expected that multipath propagation characteristics to vary by locations. However, the measurement campaign shows a consistent PDP exponential decay trend at each location measured. The rms delay spread of each location is evaluated, which facilitates a comparison of the multipath characteristics of each location and other environments; We found this value to be slightly higher than in most indoor environments. The rms delay spread varies slightly with location and is not correlated to distance. Determining

the coherence bandwidth shows that a wireless technology with a channel bandwidth higher than 12.95 MHz will experience frequency-selective fading.

A vehicle is equipped with numerous electronic devices that are potential sources of EMI. The number of electronic devices in a vehicle increases each year. Along with the electrification of vehicles, this has led to a noisier and harsher electromagnetic environment. In Chapter 6, the impact of EMI on the performance of wireless communications in a vehicle is investigated. The standards regarding the protection of on-board radio instruments which regulate the level of EMI that can be radiated by a component are reviewed. The combined noise emitted by each module is multiplicative, creating a harsh EMI environment. The vulnerability of UWB compared to the narrowband system is highlighted. A series of measurements to characterise the noise generated in the vehicle environment. This study demonstrates that EMI will be a significant factor in achieving reliable communication in a vehicle.

In Chapter 7, the time-variant nature of the vehicle channel is investigated. This work presents the time-variation statistics and the coherence time of a vehicle channel. The results show that the coherence time of a vehicle in motion with passengers varies from 0.2 to 1.84 seconds, with an average of 0.5 seconds. This suggests that the vehicle environment can be considered as a slow-fading channel.

8.2 Future work

Several topics have not been covered in this study and merit further research. This list presents subjects for future work:

- Vehicles are classed into various segments: small, medium, large, luxury, and more. Furthermore, vehicles have various compartments such as the engine, passenger and boot compartments, each with different dimensions. It is im-

portant to investigate whether the volume or dimensions of a vehicle play a significant role in multipath statistics.

- Similarly, the impact of objects such as seats and panel linings on the delay spread should be investigated. Understanding the significance of the materials used in, and the sizes of objects would simplify the creation of vehicle channel models.
- A channel investigation would be enhanced by investigating the correlation between transmission bandwidth and channel fading statistics.
- There have been several attempts to model the vehicle channel using the empirical method. A simple propagation model based on ray-tracing should be investigated and developed.
- For this research, the work was conducted using an omnidirectional antenna. A directional antenna could potentially improve the performance of a wireless system in a vehicle by increasing the LOS path gain while simultaneously reducing multipath. The advantages of using a directional over an omnidirectional antenna should be investigated.
- The performance of wireless communications in a vehicle can be improved by introducing spatial diversity using a MIMO (Multiple-Input and Multiple-Output) antenna. The design of wireless communications in a vehicle would benefit from further knowledge of the coherence distance of the channel.
- It is known from literature that the separation distance of antenna in which it's channel characteristic can be considered to be independent from one another is related to the carrier frequency [170]. Hence, as carrier frequency increases, the antenna separation distance decreases. Millimetre waves (mm-waves) that

operates at a frequency band in the tens of gigahertz has an antenna separation distance in the range of millimetres. Thus, the benefits of mm-waves frequencies could be exploited in a small environment with severe multipath, where a compact multi-array antenna could be used to introduce channel diversity and improve the wireless network performance. However, the channel characteristic of mm-waves band is different to sub-6 GHz band, and known to suffer from atmospheric absorption [171]. An investigation can be performed to investigate the benefits of multi antenna system operating at sub-6 GHz against mm-wave band.

- A wireless network operating in a vehicle environment will experience EMI [172]. It is known from the literature that EMI can cause burst errors, which can be mitigated through channel coding and interleaving techniques [173,174]. An investigation could be performed to investigate the performance benefits of different coding techniques in mitigating vehicle's EMI.
- At the moment, there is no definite answer on the optimum channel bandwidth for intra-vehicle communications. A frequency response measurement could be performed, and its K -factor at varying channel bandwidths (narrowband, wideband and ultra-wideband) analysed. Through this study, the advantage and disadvantages of various transmission bandwidths can be justified.

Bibliography

- [1] S. Tuohy, M. Glavin, C. Hughes, E. Jones, M. Trivedi, and L. Kilmartin, "Intra-Vehicle Networks: A Review," *IEEE Transactions on Intelligent Transportation Systems*. 2015, doi: 10.1109/TITS.2014.2320605.
- [2] D. Paret, *Flexray and its Applications: Real Time Multiplexed Network*. 2012.
- [3] IHS, "Automotive ECU Intelligence Service ," IHS Markit, 2019.
- [4] Deloitte, "Semiconductors – the Next Wave Opportunities and winning strategies for semiconductor companies," Deloitte, 2019.
- [5] Chenfei Wang and Filippos Pappasavvas, "What lies ahead for the automotive harness industry? a white paper." CRU, Wire and Cable Conference 2019
- [6] *Radio Wave Propagation for Telecommunication Applications*. 2005.
- [7] R. H. Clarke, "A Statistical Theory of Mobile-Radio Reception," *Bell Syst. Tech. J.*, 1968, doi: 10.1002/j.1538-7305.1968.tb00069.x.
- [8] Vijay Garg, *Wireless Communications & Networking*, Morgan Kaufmann Publishers Inc., 2007
- [9] T. S. Rappaport, *Wireless communications: principle and practice*. New Jersey: Prentice Hall PTR, 2002.

- [10] B. Sklar, "Rayleigh fading channels in mobile digital communication systems Part I: Characterization," *IEEE Commun. Mag.*, 1997, doi: 10.1109/35.620535.
- [11] J. Salo, L. Vuokko and P. Vainikainen, "Why is Shadow Fading Lognormal?" in *Proc. International Symposium on Wireless Personal Multimedia Communications*, Aalborg, Denmark, Sept. 18-22, 2005, pp. 522-526
- [12] Z. Hongmei, Y. Hailong, and G. Shuting, "Research on path loss and shadow fading of ultra wideband simulation channel," *Int. J. Distrib. Sens. Networks*, 2016, doi: 10.1177/1550147716679847.
- [13] A. Bensky, *Short-range Wireless Communication: Third Edition*, Newnes, 2004.
- [14] F. Hlawatsch and G. Matz, *Wireless communications over rapidly time-varying channels*. 2011.
- [15] E. Greenberg and E. Klodzh, "Comparison of deterministic, empirical and physical propagation models in urban environments," *2015 IEEE International Conference on Microwaves, Communications, Antennas and Electronic Systems (COMCAS)*, Tel Aviv, 2015, pp. 1-5, doi: 10.1109/COMCAS.2015.736039
- [16] J. W. Wallace, *Modeling Electromagnetic Wave Propagation in Electrically Large Structures*, Ph.D. thesis, Brigham Young University, Provo, Utah, USA, September 2001.
- [17] A. Grami, *Introduction to digital communications*. 2015.
- [18] Andreas F. Molisch, "Statistical Description of the Wireless Channel," in *Wireless Communications*, IEEE, 2011, pp.69-99, doi: 10.1002/9781119992806.ch5.

- [19] K. A. Bonsu, K. O. Boateng, J. K. Oppong, and K. A. Dotche, "Small-Scale Fading Characteristics in Cellular Networks in Ghana," *Int. J. Interdiscip. Telecommun. Netw.*, 2013, doi: 10.4018/jitn.2013070103.
- [20] A. Doukas and G. Kalivas, "Rician K factor estimation for wireless communication systems," in *Second International Conference on Wireless and Mobile Communications, ICWMC 2006*, 2006, doi: 10.1109/ICWMC.2006.81.
- [21] Dave Pearce, *Getting Started With Communications Engineering*, 2008.
- [22] A. Muqaibel, A. Safaai-Jazi, B. Woerner, and S. Riad, "UWB channel impulse response characterization using deconvolution techniques," in *Midwest Symposium on Circuits and Systems*, 2002, doi: 10.1109/mwscas.2002.1187112.
- [23] H. Kim, *Wireless Communications Systems Design*. 2015.
- [24] T. B. Santoso, E. Widjiati, W. Wirawan, and G. Hendranto, "The evaluation of probe signals for impulse response measurements in shallow water environment," *IEEE Trans. Instrum. Meas.*, 2016, doi: 10.1109/TIM.2016.2519768.
- [25] A. Chehri, P. Fortier, and P. M. Tardif, "Large-Scale Fading and Time Dispersion Parameters of UWB Channel in Underground Mines," *Int. J. Antennas Propag.*, 2008, doi: 10.1155/2008/806326.
- [26] R. B. Boatright, J. Quesnelle, C. M. Kozierok, and C. Correa, *Automotive Ethernet - The Definitive Guide*. 2014.
- [27] R. Bosch, "CAN Specification Version 2.0," Rober Bousch GmbH, Postfach, 1991.

- [28] ISO - INTERNATIONAL ORGANIZATION FOR STANDARDIZATION. ISO 11898-1:2015 Road vehicles – Controller area network (CAN) – Part 1: Data link layer and physical signalling, 2015
- [29] M. Ruff, “Evolution of local interconnect network (LIN) solutions,” in IEEE Vehicular Technology Conference, 2003, doi: 10.1109/vetecf.2003.1286317.
- [30] H. C. Von Der Wense, “Introduction to local interconnect network,” in SAE Technical Papers, 2000, doi: 10.4271/2000-01-0153.
- [31] S. Kobayashi and C. Almeida, ”Fiber optic interconnection devices for in-vehicle communication,” 2017 22nd Microoptics Conference (MOC), Tokyo, 2017, pp. 30-31, doi: 10.23919/MOC.2017.8244481.
- [32] S. Huq and J. Goldie, “An overview of LVDS technology,” Nat. Semicond. Appl. Note, vol. 971, pp. 1–6, 1998.
- [33] OPEN ALLIANCE. BroadR-Reach Specifications. <http://www.opensig.org/about/specifications>, 2016.
- [34] INSTITUTE OF ELECTRICAL AND ELECTRONICS ENGINEERS (IEEE). Time-Sensitive Networking Task Group. <http://www.ieee802.org/1/pages/tsn.html>, 2015.
- [35] W. Zeng, M. A. S. Khalid, and S. Chowdhury, “In-vehicle networks outlook: Achievements and challenges,” IEEE Commun. Surv. Tutorials, vol. 18, no. 3, pp. 1552–1571, 2016, doi: 10.1109/COMST.2016.2521642.
- [36] N. Navet and F. Simonot-Lion, “In-vehicle communication networks: A historical perspective and review,” in Industrial Communication Technology Handbook, Second Edition, 2017.

- [37] Ixia, “Automotive Ethernet: An Overview,” White Paper, ixia, 2014.
- [38] Y. Wang, D. Tian, Z. Sheng, and J. Wang, Connected vehicle systems: Communication, data, and control. 2017.
- [39] SAE J2057/1, Society of Automotive Engineers Std., 2006.
- [40] R. Schmidgall, “Automotive embedded systems software reprogramming,” PhD Thesis. May, 2012.
- [41] IEEE Draft Standard for Ethernet Physical Layer Specifications and Management Parameters for Greater Than 1 Gb/s Automotive Ethernet,” in IEEE P802.3ch/D3.0, November 2019 , vol., no., pp.1-212, 21 Nov. 2019.
- [42] S. Matsushima, T. Matsushima, T. Hisakado and O. Wada, ”Trends of EMC standards for automotive network devices and communication quality of ethernet in relation to parameters of pulse disturbances,” in IEEE Electromagnetic Compatibility Magazine, vol. 7, no. 1, pp. 46-50, First Quarter 2018, doi: 10.1109/MEMC.0.8339542.
- [43] Y. Xu, X. Lu and S. Liu, ”Research and Design on Lightweight Automotive Ethernet FQ-TSS Protocol,” 2018 Chinese Automation Congress (CAC), Xi’an, China, 2018, pp. 1163-1167, doi: 10.1109/CAC.2018.8623458.
- [44] F. L. Soares, D. R. Campelo, Y. Yan, S. Ruepp, L. Dittmann and L. Ellegard, ”Reliability in automotive ethernet networks,” 2015 11th International Conference on the Design of Reliable Communication Networks (DRCN), Kansas City, MO, 2015, pp. 85-86, doi: 10.1109/DRCN.2015.7148990.
- [45] R. M. Metcalfe and D. R. Boggs, “Ethernet: distributed packet switching for local computer networks,” Commun. ACM, vol. 19, no. 7, pp. 395–404, 1976.

- [46] International Cablemakers Federation (ICF), “TRENDS IN AUTOMOTIVE WIRING,” ICF NEWS ISSUE 76, 2015.
- [47] G. Leen and D. Heffernan, “Vehicles without wires,” *Computing and Control Engineering Journal*. 2001, doi: 10.1049/cce:20010501.
- [48] M. Schack, M. Jacob, and T. Kiirner, “Comparison of in-car UWB and 60 GHz channel measurements,” *Antennas Propag. (EuCAP), 2010 Proc. Fourth Eur. Conf.*, pp. 1–5, 2010.
- [49] D. W. Matolak and A. Chandrasekaran, “5 GHz intra-vehicle channel characterization,” *IEEE Veh. Technol. Conf.*, 2012, doi: 10.1109/VTCFall.2012.6399095.
- [50] J. Blumenstein et al., “In-vehicle UWB channel measurement, model and spatial stationarity,” *IEEE Veh. Netw. Conf. VNC*, vol. 2015-Janua, no. January, pp. 77–80, 2015, doi: 10.1109/VNC.2014.7013312.
- [51] W. Niu, J. Li, and T. Talty, “Intra-Vehicle UWB channel measurements and statistical analysis,” *GLOBECOM - IEEE Glob. Telecommun. Conf.*, pp. 3402–3406, 2008, doi: 10.1109/GLOCOM.2008.ECP.653.
- [52] W. Aldeeb, W. Xiang, and P. Richardson, “A study on the channel and BER-SNR performance of ultra wide band systems applied in commercial vehicles,” *2007 IEEE Sarnoff Symp. SARNOFF*, pp. 1–5, 2007, doi: 10.1109/SARNOF.2007.4567331.
- [53] M. Schack, R. Geise, I. Schmidt, R. Piesiewicz, and T. Kurner, “UWB channel measurements inside different car types,” *Antennas Propagation, 2009. EuCAP 2009. 3rd Eur. Conf.*, pp. 640–644, 2009.

- [54] M. Peter, R. Felbecker, W. Keusgen, and J. Hillebrand, "Measurement-based investigation of 60 GHz broadband transmission for wireless in-car communication," *IEEE Veh. Technol. Conf.*, 2009, doi: 10.1109/VETEFCF.2009.5378803.
- [55] F. Bellens, F. Quitin, F. Horlin, and P. De Doncker, "UWB channel analysis within a moving car," *2009 9th Int. Conf. Intell. Transp. Syst. Telecommun. ITST 2009*, no. 3, pp. 681–684, 2009, doi: 10.1109/ITST.2009.5399271.
- [56] W. Niu, J. Li, and T. Talty, "Intra-vehicle UWB Channels in Moving and Stationary Scenarios," *Ieee Milcom*, pp. 1–6, 2009.
- [57] J. Blumenstein et al., "In-vehicle channel measurement, characterization, and spatial consistency comparison of 3-11 GHz and 55-65 GHz frequency bands," *IEEE Trans. Veh. Technol.*, vol. 66, no. 5, pp. 3526–3537, 2017, doi: 10.1109/TVT.2016.2600101.
- [58] L. Liu, Y. Wang, N. Zhang, and Y. Zhang, "UWB channel measurement and modeling for the intra-vehicle environments," pp. 381–384, 2010.
- [59] Y. Katayama, K. Terasaka, K. Higashikaturagi, I. Matunami, and A. Kajiwara, "Ultra-wideband impulse-radio propagation for in-vehicle wireless link," *IEEE Veh. Technol. Conf.*, pp. 232–242, 2006, doi: 10.1109/VTCF.2006.63.
- [60] A. T. Ott, U. Siart, T. F. Eibert, O. Klemp, and R. Steffen, "Enhanced investigations of 433 MHz-10 GHz time invariant wireless in-car communication channels," *Microw. Conf. (GeMIC)*, 2011 Ger., no. March, pp. 1–4, 2011.
- [61] A. Chandra et al., "Frequency-Domain In-Vehicle UWB Channel Modeling," *IEEE Trans. Veh. Technol.*, vol. 65, no. 6, pp. 3929–3940, 2016, doi: 10.1109/TVT.2016.2550626.

- [62] H. Sawada, H. Nakase, K. Sato, and H. Harada, "A sixty GHz vehicle area network for multimedia communications," *IEEE J. Sel. Areas Commun.*, vol. 27, no. 8, pp. 1500–1506, 2009, doi: 10.1109/JSAC.2009.091019.
- [63] J. Blumenstein, T. Mikulasek, T. Zemen, C. Mecklenbrauker, R. Marsalek, and A. Prokes, "In-vehicle mm-wave channel model and measurement," *IEEE Veh. Technol. Conf.*, pp. 1–5, 2014, doi: 10.1109/VTCTFall.2014.6966022.
- [64] R. D'Errico, L. Rudant, and J. Keignart, "Channel characterization for intra-vehicle WSNs in the ISM bands," *Fourth Eur. Conf. Antennas Propag.*, pp. 1–5, 2010.
- [65] Q. Liang, A. Audu, H. Khani, H. Nie, W. Xiang, and Z. Chen, "Measurement and analysis of intra-vehicle UWB channels," *IEEE Radio Wirel. Symp. RWS*, pp. 166–168, 2013, doi: 10.1109/RWS.2013.6486676.
- [66] U. Demir, C. U. Bas, and S. C. Ergen, "Engine compartment UWB channel model for intravehicular wireless sensor networks," *IEEE Trans. Veh. Technol.*, vol. 63, no. 6, pp. 2497–2505, 2014, doi: 10.1109/TVT.2013.2294357.
- [67] I. J. Garcia Zuazola, J. M. H. Elmirghani, and J. C. Batchelor, "High-speed ultra-wide band in-car wireless channel measurements," *IET Commun.*, vol. 3, no. 7, p. 1115, 2009, doi: 10.1049/iet-com.2008.0135.
- [68] F. Bellens, F. Quitin, F. Horlin, and P. DeDoncker, "Channel measurements and MB-OFDM performance inside a driving car," *Proc. 2009 Int. Conf. Electromagn. Adv. Appl. ICEAA '09*, no. 3, pp. 392–395, 2009, doi: 10.1109/ICEAA.2009.5297412.

- [69] C. U. Bas and S. C. Ergen, "Ultra-wideband channel model for intra-vehicular wireless sensor networks," *IEEE Wirel. Commun. Netw. Conf. WCNC*, pp. 42–47, 2012, doi: 10.1109/WCNC.2012.6214404.
- [70] O. Delangre, S. Van Roy, P. De Doncker, M. Lienard, and P. Degauque, "Modeling in-vehicle wideband wireless channels using reverberation chamber theory," *IEEE Veh. Technol. Conf.*, pp. 2149–2153, 2007, doi: 10.1109/VETECONF.2007.451.
- [71] J. Li and T. Talty, "Channel Characterization for Ultra-Wideband Intra-Vehicle Sensor Networks," *MILCOM 2006 - 2006 IEEE Military Communications conference*, Washington, DC, 2006, pp. 1-5, doi: 10.1109/MILCOM.2006.302192.
- [72] M. Ohira, S. Ano, S. Kitazawa, H. Ban, N. Kukutsu, and K. Kobayashi, "Microwave propagation characterization in automotive engine compartment for wireless harness communications," *IEEE Antennas Propag. Soc. AP-S Int. Symp.*, no. 1, pp. 1179–1180, 2014, doi: 10.1109/APS.2014.6904916.
- [73] L. Cheng, J. Casazza, J. Grace, F. Bai, and D. D. Stancil, "Channel Propagation Measurement and Modeling for Vehicular In-Cabin Wi-Fi Networks," *IEEE Trans. Antennas Propag.*, vol. 64, no. 12, pp. 5424–5435, 2016, doi: 10.1109/TAP.2016.2610190.
- [74] A. R. Moghimi, H. M. Tsai, C. U. Saraydar, and O. K. Tonguz, "Characterizing intra-car wireless channels," *IEEE Trans. Veh. Technol.*, vol. 58, no. 9, pp. 5299–5305, 2009, doi: 10.1109/TVT.2009.2022759.
- [75] O. K. Tonguz, H. M. Tsai, T. Talty, A. Macdonald, and C. Saraydar, "RFID technology for intra-car communications: A new paradigm," *IEEE Veh. Technol. Conf.*, pp. 3008–3013, 2006, doi: 10.1109/VTCONF.2006.618.

- [76] R. Liu, S. Herbert, T. H. Loh, and I. J. Wassell, "A Study on Frequency Diversity for Intra-Vehicular Wireless Sensor Networks (WSNs)," *Veh. Technol. Conf. (VTC Fall)*, 2011 IEEE, pp. 1–5, 2011, doi: 10.1109/VETECONF.2011.6092976.
- [77] C. A. M. Costa Júnior et al., "Damper-to-damper path loss characterization for intra-vehicular wireless sensor networks," *Eur. Microw. Week 2017 "A Prime Year a Prime Event"*, *EuMW 2017 - Conf. Proceedings; 47th Eur. Microw. Conf. EuMC 2017*, vol. 2017-Janua, no. c, pp. 1341–1344, 2017, doi: 10.23919/EuMC.2017.8231100.
- [78] H. M. Tsai, W. Viriyasitavat, O. K. Tonguz, C. Saraydar, T. Talty, and A. Macdonald, "Feasibility of in-car wireless sensor networks: A statistical evaluation," *2007 4th Annu. IEEE Commun. Soc. Conf. Sensor, Mesh Ad Hoc Commun. Networks, SECON*, pp. 101–111, 2007, doi: 10.1109/SAHCN.2007.4292822.
- [79] R. D'Errico, L. Rudant, and J. Keignart, "Channel characterization for intra-vehicle WSNs in the ISM bands," *Fourth Eur. Conf. Antennas Propag.*, pp. 1–5, 2010
- [80] P. Kukolev, A. Chandra, T. Mikulášek, A. Prokeš, T. Zemen, and C. F. Mecklenbräuker, "In-vehicle channel sounding in the 5.8-GHz band," *Eurasip J. Wirel. Commun. Netw.*, vol. 2015, no. 1, 2015, doi: 10.1186/s13638-015-0273-x.
- [81] M. Heddebaut, V. Deniau and K. Adouane, "In-vehicle WLAN radio-frequency communication characterization," in *IEEE Transactions on Intelligent Transportation Systems*, vol. 5, no. 2, pp. 114-121, June 2004, doi: 10.1109/TITS.2004.828172.
- [82] R. S. Kshetrimayum, "An introduction to UWB communication systems," *IEEE Potentials*, vol. 28, no. 2, pp. 9–13, 2009, doi: 10.1109/MPOT.2009.931847.

- [83] ETSI EN302 065-1 V2.1.1., “Short Range Devices (SRD) using Ultra Wide Band technology (UWB); Harmonised Standard covering the essential requirements of article 3.2 of the Directive 2014/53/EU; Part 1: Requirements for Generic UWB applications,” vol. 1, pp. 1–32, 2016.
- [84] Irfan Yusoff and Xiaohong Peng, ”Impacts of Channel Loss and Electromagnetic Interference on Intra-Vehicle Wireless Communications,” 2020 IEEE 91th Vehicular Technology Conference (VTC2020-Spring), Antwerp, Belgium , 2020.
- [85] S. Herbert, T. Loh, I. Wassell and J. Rigelsford, ”On the Analogy Between Vehicle and Vehicle-Like Cavities With Reverberation Chambers,” in *IEEE Transactions on Antennas and Propagation*, vol. 62, no. 12, pp. 6236-6245, Dec. 2014, doi: 10.1109/TAP.2014.2363681.
- [86] A. Ruddle, “Validation of simple estimates for average field strengths in complex cavities against detailed results obtained from a 3d numerical model of a car,” *Sci., Meas. Technol., IET*, vol. 2, no. 6, pp. 455–466, Nov. 2008.
- [87] H. Weng, D. Beetmer, T. Hubing, X. Dong, R. Wiese, and J. McCallum, “Investigation of cavity resonances in an automobile,” in *Proc. Int. Symp. Electromagn. Compat.*, 2004, vol. 3, pp. 766–770.
- [88] T. Kobayashi, “Measurements and characterization of ultra wideband propagation channels in a passenger-car compartment,” *IEEE Int. Symp. Spread Spectr. Tech. Appl.*, pp. 228–232, 2006, doi: 10.1109/ISSSTA.2006.311768.
- [89] S. Herbert, I. Wassell, T. H. Loh, and J. Rigelsford, “Characterizing the spectral properties and time variation of the in-vehicle wireless communication channel,” *IEEE Trans. Commun.*, vol. 62, no. 7, pp. 2390–2399, 2014, doi: 10.1109/TCOMM.2014.2328635.

- [90] A. Prokes, J. Vychodil, M. Pospisil, J. Blumenstein, T. Mikulasek, and A. Chandra, "Time-Domain nonstationary intra-car channel measurement in 60 GHz band," *Int. Conf. Adv. Technol. Commun.*, pp. 1–6, 2016, doi: 10.1109/ATC.2016.7764753.
- [91] J. Blumenstein, J. Vychodil, M. Pospisil, T. Mikulasek, and A. Prokes, "Effects of vehicle vibrations on mm-wave channel: Doppler spread and correlative channel sounding," *IEEE Int. Symp. Pers. Indoor Mob. Radio Commun. PIMRC*, no. 1, 2016, doi: 10.1109/PIMRC.2016.7794619.
- [92] J. Blumenstein, A. Prokes, J. Vychodil, M. Pospisil, and T. Mikulasek, "Time-varying K factor of the mm-Wave Vehicular Channel: Velocity, Vibrations and the Road Quality Influence," *IEEE Int. Symp. Pers. Indoor Mob. Radio Commun. PIMRC*, vol. 2017-Octob, pp. 1–5, 2018, doi: 10.1109/PIMRC.2017.8292755.
- [93] P. Overview and T. Applications, "Providing capacity and coverage needed for high-efficiency wireless platforms."
- [94] H. Kamoda, S. Kitazawa, N. Kukutsu, K. Kobayashi, and T. Kumagai, "Microwave propagation channel modeling in a vehicle engine compartment," *IEEE Trans. Veh. Technol.*, vol. 65, no. 9, pp. 6831–6841, 2016.
- [95] A. C. Rencher and G. B. Schaalje, *Linear Models in Statistics*, 2nd ed., Wiley, 2008.
- [96] P. Njemcevic, "A Novel Approach in Determination of the Appropriate Spatial Averaging Signal Length," *Wirel. Pers. Commun.*, 2015, doi: 10.1007/s11277-015-2318-1.

- [97] W. C. Lee, "Estimate of Local Average Power of a Mobile Radio Signal," *IEEE Trans. Veh. Technol.*, vol. 34, no. 1, pp. 22–27, 1985.
- [98] D. de la Vega et al., "Generalization of the Lee method for the analysis of the signal variability," *IEEE Trans. Veh. Technol.*, vol. 58, no. 2, pp. 506–516, 2009.
- [99] A. Abdi, C. Tepedelenlioglu, M. Kaveh, and G. Giannakis, "On the estimation of the K parameter for the rice fading distribution," *IEEE Commun. Lett.*, vol. 5, no. 3, pp. 92–94, 2001.
- [100] R. De Francisco, L. Huang, G. Dolmans, and H. De Groot, "Coexistence of ZigBee wireless sensor networks and bluetooth inside a vehicle," *IEEE Int. Symp. Pers. Indoor Mob. Radio Commun. PIMRC*, pp. 2700–2704, 2009.
- [101] L. J. Greenstein, S. S. Ghassemzadeh, V. Erceg, and D. G. Michelson, "Ricean K-factors in narrow-band fixed wireless channels: Theory, experiments, and statistical models," *IEEE Trans. Veh. Technol.*, vol. 58, no. 8, pp. 4000–4012, 2009.
- [102] B. Mnasri, M. Nedil, N. Kandil, L. Talbi, and I. Ben Mabrouk, "Experimental characterization of wireless mimo channel at 5.8GHz in underground gold mine," *Prog. Electromagn. Res. C*, 2013, doi: 10.2528/PIERC12112707.
- [103] F. Bellens, F. Quitin, J. M. Dricot, F. Horlin, A. Benlarbi-Delaï, and P. De Doncker, "A wideband channel model for intravehicular nomadic systems," *Int. J. Antennas Propag.*, 2011, doi: 10.1155/2011/468072.
- [104] Sasaoka, H., 2000. *Mobile Communications*. Tokyo: Ohmsha.
- [105] H. Arslan, *Cognitive radio, software defined radio, and adaptive wireless systems*. 2007.

- [106] J. Karedal, S. Wyne, P. Almers, F. Tufvesson, and A. F. Molisch, “A measurement-based statistical model for industrial ultra-wideband channels,” *IEEE Trans. Wirel. Commun.*, vol. 6, no. 8, pp. 3028–3037, 2007, doi: 10.1109/TWC.2007.051050.
- [107] Y. Ai, M. Cheffena, and Q. Li, “Power delay profile analysis and modeling of industrial indoor channels,” in *2015 9th European Conference on Antennas and Propagation, EuCAP 2015*, 2015.
- [108] M. Kyrö, K. Haneda, J. Simola, K. I. Takizawa, H. Hagiwara, and P. Vainikainen, “Statistical channel models for 60 GHz radio propagation in hospital environments,” *IEEE Trans. Antennas Propag.*, vol. 60, no. 3, pp. 1569–1577, 2012, doi: 10.1109/TAP.2011.2180349.
- [109] Y. Zahedi and R. Ngah, “RMS Delay Spread and Path Loss Dependency for Mobile Outdoor UWB Channels,” *ICOASE 2018 - Int. Conf. Adv. Sci. Eng.*, pp. 206–211, 2018, doi: 10.1109/ICOASE.2018.8548914.
- [110] C. U. Bas and S. C. Ergen, “Ultra-wideband Channel Model for Intra-vehicular Wireless Sensor Networks Beneath the Chassis: From Statistical Model to Simulations,” in *IEEE Transactions on Vehicular Technology*, vol. 62, no. 1, pp. 14–25, Jan. 2013, doi: 10.1109/TVT.2012.2215969.
- [111] S. S. Ghassemzadeh, L. J. Greenstein, T. Sveinsson, A. Kavčić, and V. Tarokh, “UWB delay profile models for residential and commercial indoor environments,” *IEEE Trans. Veh. Technol.*, 2005, doi: 10.1109/TVT.2005.851379.
- [112] B. Denis, J. Keignart, and N. Daniele, “Impact of NLOS propagation upon ranging precision in UWB systems,” in *2003 IEEE Conference on Ultra Wide-*

- band Systems and Technologies, UWBST 2003 - Conference Proceedings, 2003, doi: 10.1109/UWBST.2003.1267868.
- [113] P. Stenumgaard, J. Ferrer-Coll, P. Angskog, and J. Chilo, "Characterisation of highly absorbent and highly reflective radio wave propagation environments in industrial applications," *IET Commun.*, 2012, doi: 10.1049/iet-com.2012.0028.
- [114] J. Ferrer-Coll, P. Ängskog, J. Chilo, and P. Stenumgaard, "Characterisation of electromagnetic properties in iron-mine production tunnels," *Electron. Lett.*, 2012, doi: 10.1049/el.2011.3133.
- [115] A. Chehri, P. Fortier, and P. M. Tardif, "Characterization of the ultra-wideband channel in confined environments with diffracting rough surfaces," *Wirel. Pers. Commun.*, 2012, doi: 10.1007/s11277-010-0097-2.
- [116] V. Savic, J. Ferrer-Coll, P. Angskog, J. Chilo, P. Stenumgaard, and E. G. Larsson, "Measurement analysis and channel modeling for TOA-based ranging in tunnels," *IEEE Trans. Wirel. Commun.*, 2015, doi: 10.1109/TWC.2014.2350493.
- [117] Y. Ai, J. B. Andersen and M. Cheffena, "Path-Loss Prediction for an Industrial Indoor Environment Based on Room Electromagnetics," in *IEEE Transactions on Antennas and Propagation*, vol. 65, no. 7, pp. 3664-3674, July 2017, doi: 10.1109/TAP.2017.2702708.
- [118] M. Kim, Y. Konishi, Y. Chang and J. Takada, "Large Scale Parameters and Double-Directional Characterization of Indoor Wideband Radio Multipath Channels at 11 GHz," in *IEEE Transactions on Antennas and Propagation*, vol. 62, no. 1, pp. 430-441, Jan. 2014, doi: 10.1109/TAP.2013.2288633.

- [119] X. Zhou et al., “Impacts of absorber loadings on simulating the multipath channel in a reverberation chamber,” *Int. J. Antennas Propag.*, vol. 2017, pp. 1–7, 2017.
- [120] C. L. Holloway, H. A. Shah, R. J. Pirkl, K. A. Remley, D. A. Hill, and J. Ladbury, “Early time behavior in reverberation chambers and its effect on the relationships between coherence bandwidth, chamber decay time, RMS delay spread, and the chamber buildup time,” *IEEE Trans. Electromagn. Compat.*, 2012, doi: 10.1109/TEMPC.2012.2188896.
- [121] A. M. Al-Samman et al., “Comparative study of indoor propagation model below and above 6 GHz for 5G wireless networks,” *Electron.*, 2019, doi: 10.3390/electronics8010044.
- [122] A. F. Molisch, *Wireless Communications*, 2nd Edition. Wiley-IEEE Press, 2011.
- [123] M. S. Varela and M. G. Sánchez, “RMS delay and coherence bandwidth measurements in indoor radio channels in the UHF band,” *IEEE Trans. Veh. Technol.*, vol. 50, no. 2, pp. 515–525, 2001, doi: 10.1109/25.923063.
- [124] M. J. Gans, “A power-spectral theory of propagation in the mobile-radio environment,” *IEEE Trans. Veh. Technol.*, vol. VT-21, pp. 27–37, Feb. 1972.
- [125] A. G. Siamarou and P. O. Box, “Coherence Bandwidth Characterisation at mm-waves,” no. 1, pp. 181–187.
- [126] M. O. Al-Nuaimi and A. G. Siamarou, “Coherence bandwidth characterisation and estimation for indoor Rician multipath wireless channels using measurements at 62.4 GHz,” in *IEE Proceedings: Microwaves, Antennas and Propagation*, 2002, doi: 10.1049/ip-map:20020391.

- [127] V. Kukshya, H. J. Song, H. P. Hsu and R. Wiese, "Impact of Intra-Vehicular Electromagnetic Interference On Tire Pressure Monitoring Systems," 2007 IEEE International Symposium on Electromagnetic Compatibility, Honolulu, HI, 2007, pp. 1-4, doi: 10.1109/ISEMC.2007.35.
- [128] R. R. Burgett, R. E. Massoll, and D. R. Van Uum, "Relationship Between Spark Plugs and Engine-Radiated Electromagnetic Interference," IEEE Trans. Electromagn. Compat., vol. EMC-16, no. 3, pp. 160–172, 1974.
- [129] F. Silva, M. Quilez, J. Llop, X. Torres, and P. Riu, "EMI from an automotive CAN bus," IEEE Int. Symp.
- [130] M. Moon et al., "Modeling and analysis of return paths of common mode EMI noise currents from motor drive system in hybrid electric vehicle," in 2015 Asia-Pacific International Symposium on Electromagnetic Compatibility, APEMC 2015, 2015, doi: 10.1109/APEMC.2015.7175395.
- [131] UNECE, "Addendum 9: Regulation No. 10 Revision 6 - Amendment 1," vol. 1958, no. March 1958, 2019.
- [132] European Parliament and European Council, "Directive 2014/30/EU of the European Parliament and of the council of 26 February 2014 on the harmonisation of the laws of the Member States relating to electromagnetic compatibility (recast)," Off. J. Eur. Union, vol. 29.3.2014, no. February, pp. 79–106, 2014, [Online]. Available: <http://eur-lex.europa.eu/legal-content/ES/TXT/?uri=CELEX:32014L0030>.
- [133] "CISPR-12 Vehicles, boats and internal combustion engines - Radio disturbance characteristics - Limits and methods of measurement for the protection of off-board receivers", IEC, 2007

- [134] "CISPR-25 Vehicles, boats and internal combustion engines - Radio disturbance characteristics - Limits and methods of measurement for the protection of on-board receivers", IEC, 2016
- [135] R. I. Sm and S. M. S. Spectrum, Technical and operating parameters and spectrum use for short-range radiocommunication devices SM Series, vol. 1. 2010.
- [136] T. Tsuboi, J. Yamada, N. Yamauchi, M. Nakagawa, and T. Maruyama, "UWB radio propagation for intra vehicle communications," 2009 Int. Conf. Ultra Mod. Telecommun. Work., 2009.
- [137] T. Shongwe, A. J. H. Vinck and H. C. Ferreira, "A Study on Impulse Noise and Its Models," in SAIEE Africa Research Journal, vol. 106, no. 3, pp. 119-131, Sept. 2015, doi: 10.23919/SAIEE.2015.8531938.
- [138] C. Marczok, U. Maaß, E. Hoene, I. Ndip, K. Lang and D. Hasselberg, "Analysis and improvement of a spark plug for less radiated electromagnetic emissions," 2014 International Symposium on Electromagnetic Compatibility, Gothenburg, 2014, pp. 385-390, doi: 10.1109/EMCEurope.2014.6930937.
- [139] K. Wiklundh, "Relation between the amplitude probability distribution of an interfering signal and its impact on digital radio receivers," IEEE Transactions on Electromagnetic Compatibility, vol. 48, NO. 3, pp. 537-544, Aug. 2006.
- [140] C. Hoffmann, H. H. Slim and P. Russer, "A time-domain EMI measurement system up to 26 GHz with amplitude probability distribution," 2011 International Conference on Electromagnetics in Advanced Applications, Torino, 2011, pp. 448-451, doi: 10.1109/ICEAA.2011.6046382.

- [141] Y. Matsumoto, "On the relation between the amplitude probability distribution of noise and bit error probability," *IEEE Trans. Electromagn. Compat.*, 2007, doi: 10.1109/TEMPC.2007.908280.
- [142] K. Wiklundh, "Relation between the amplitude probability distribution of an interfering signal and its impact on digital radio receivers," *IEEE Trans. Electromagn. Compat.*, 2006, doi: 10.1109/TEMPC.2006.877782.
- [143] W. Niu, J. Li, S. Liu, and T. Talty, "Intra-vehicle ultra-wideband communication testbed," *Proc. - IEEE Mil. Commun. Conf. MILCOM*, 2007, doi: 10.1109/MILCOM.2007.4455143.
- [144] G. Matz and F. Hlawatsch, "Fundamentals of time-varying communication channels," in *Wireless Communications Over Rapidly Time-Varying Channels*, 2011.
- [145] D. Scammell, A. Hammoudeh and M. G. Sanchez, "Estimating channel performance for time invariant channels," in *Electronics Letters*, vol. 40, no. 12, pp. 746-747, 10 June 2004, doi: 10.1049/el:20040508.
- [146] Y. Shui et al., "Vehicle-to-vehicle radio channel characteristics for congestion scenario in Dense Urban region at 5.9GHz," *Int. J. Antennas Propag.*, 2018, doi: 10.1155/2018/1751869.
- [147] H. MacLeod, C. Loadman and Z. Chen, "Experimental studies of the 2.4-GHz ISM wireless indoor channel," *3rd Annual Communication Networks and Services Research Conference (CNSR'05)*, Halifax, NS, Canada, 2005, pp. 63-68, doi: 10.1109/CNSR.2005.33.
- [148] V. Garg, *Wireless Communications & Networking*. 2007.

- [149] J. Das Gupta, H. Suzuki and K. Ziri-Castro, "Effect of Pedestrian Movement on MIMO-OFDM Channel Capacity in an Indoor Environment," in *IEEE Antennas and Wireless Propagation Letters*, vol. 8, pp. 682-685, 2009.
- [150] K. J. R. Liu, A. K. Sadek, W. Su, and A. Kwasinski, *Cooperative communications and networking*. 2008.
- [151] J. S. C. Turner et al., "The study of human movement effect on signal strength for indoor WSN deployment," in *2013 IEEE Conference on Wireless Sensor, ICWISE 2013*, 2013, doi: 10.1109/ICWISE.2013.6728775.
- [152] W. Q. Malik, B. Allen and D. J. Edwards, "Bandwidth dependent modelling of small scale fade depth in wireless channels," in *IET Microwaves, Antennas & Propagation*, vol. 2, no. 6, pp. 519-528, Sept. 2008, doi: 10.1049/iet-map:20080015.
- [153] G. L. Stüber, *Principles of mobile communication: Fourth edition*. 2017.
- [154] G. Makhoul, F. Mani, R. D'Errico and C. Oestges, "Time correlation properties of dynamic mobile to mobile channels in indoor environments," *2016 10th European Conference on Antennas and Propagation (EuCAP)*, Davos, 2016, pp. 1-5.
- [155] S. E. Johnston and P. D. Fiore, "Close-range outdoor wireless channel sounding," *2011 Conference Record of the Forty Fifth Asilomar Conference on Signals, Systems and Computers (ASILOMAR)*, Pacific Grove, CA, 2011, pp. 1919-1923.
- [156] L. Cheng, B. Henty, F. Bai and D. D. Stancil, "Doppler Spread and Coherence Time of Rural and Highway Vehicle-to-Vehicle Channels at 5.9 GHz," *IEEE GLOBECOM 2008 - 2008 IEEE Global Telecommunications Conference*, New Orleans, LO, 2008, pp. 1-6.

- [157] Y. Pan, X. Liu, G. Zheng and K. Guan, "Temporal Autocorrelation of Small-Scale Fading Using Leaky Coaxial Cable in Confined Space," in *IEEE Wireless Communications Letters*, vol. 7, no. 6, pp. 1082-1085, Dec. 2018.
- [158] D. L. Ndzi, N. Savage, and B. Gremont, "Spatial and temporal variation of wideband indoor channels," *Int. J. Antennas Propag.*, 2010, doi: 10.1155/2010/735434.
- [159] A. S. Ibrahim, A. K. Sadek, W. Su, and K. J. R. Liu, "Cooperative communications with relay-selection: When to cooperate and whom to cooperate with?," *IEEE Trans. Wirel. Commun.*, 2008, doi: 10.1109/TWC.2008.070176.
- [160] A. Nosratinia, T. E. Hunter, and A. Hedayat, "Cooperative communication in wireless networks," *IEEE Commun. Mag.*, 2004, doi: 10.1109/MCOM.2004.1341264.
- [161] A. Chockalingam, M. Zorzi, and R. R. Rao, "Performance of TCP on wireless fading links with memory," in *International Conference on Communications - Proceedings*, 1998, doi: 10.1109/ICC.1998.682956.
- [162] A. N. Assimi, C. Poulliat, and I. Fijalkow, "Diversity techniques for single-carrier packet retransmissions over frequency-selective channels," *Eurasip J. Wirel. Commun. Netw.*, 2009, doi: 10.1155/2009/406028.
- [163] G. Brandner, U. Schilcher, T. Andre, and C. Bettstetter, "Packet delivery performance of simple cooperative relaying in real-world car-to-car communications," *IEEE Wirel. Commun. Lett.*, 2012, doi: 10.1109/WCL.2012.033012.120107.
- [164] G. Brandner, U. Schilcher, and C. Bettstetter, "Cooperative relaying in car-to-car communications: Initial results from an experimental study," in *Final*

- Program and Abstract Book - 4th International Symposium on Communications, Control, and Signal Processing, ISCCSP 2010, 2010, doi: 10.1109/ISCCSP.2010.5463432.
- [165] N. Marchenko, T. Andre, G. Brandner, W. Masood, and C. Bettstetter, "An experimental study of selective cooperative relaying in industrial wireless sensor networks," *IEEE Trans. Ind. Informatics*, 2014, doi: 10.1109/TII.2014.2327915.
- [166] T. Andre, G. Brandner, N. Marchenko, and C. Bettstetter, "Measurement-based analysis of cooperative relaying in an industrial wireless sensor network," in *GLOBECOM - IEEE Global Telecommunications Conference*, 2012, doi: 10.1109/GLOCOM.2012.6503170.
- [167] H. Adam, E. Yanmaz, and C. Bettstetter, "Medium access with adaptive relay selection in cooperative wireless networks," *IEEE Trans. Mob. Comput.*, 2014, doi: 10.1109/TMC.2013.97.
- [168] L. Zhao et al., "Vehicular Communications: Standardization and Open Issues," in *IEEE Communications Standards Magazine*, vol. 2, no. 4, pp. 74-80, December 2018, doi: 10.1109/MCOMSTD.2018.1800027.
- [169] M. B. Uddin, M. F. Kader, and S. Y. Shin, "Cooperative Relaying Using MIMO NOMA," in *Proceeding of 2018 4th International Conference on Wireless and Telematics, ICWT 2018*, 2018, doi: 10.1109/ICWT.2018.8527829.
- [170] G. D. Surabhi and A. Chockalingam, "Compact antenna spacing in mmWave MIMO systems using random phase precoding," in *IEEE Vehicular Technology Conference*, 2018, doi: 10.1109/VTCFall.2017.8288021.
- [171] C. Seker, M. T. Güneser and T. Ozturk, "A Review of Millimeter Wave Communication for 5G," *2018 2nd International Symposium on Multidisciplinary*

- Studies and Innovative Technologies (ISMSIT), Ankara, 2018, pp. 1-5, doi: 10.1109/ISMSIT.2018.8567053.
- [172] I. Yusoff and X. Peng, "Impacts Of Channel Loss And Electromagnetic Interference On Intra-Vehicle Wireless Communications," 2020 IEEE 91st Vehicular Technology Conference (VTC2020-Spring), Antwerp, Belgium, 2020, pp. 1-5, doi: 10.1109/VTC2020-Spring48590.2020.9128861.
- [173] R. D. Cideciyan, S. Furrer and M. A. Lantz, "Performance of Interleaved Block Codes With Burst Errors," in IEEE Transactions on Magnetics, vol. 55, no. 3, pp. 1-5, March 2019, Art no. 3100305, doi: 10.1109/TMAG.2018.2866297.
- [174] Y. Q. Shi, X. M. Zhang, Z. C. Ni, and N. Ansari, "Interleaving for combating bursts of errors," IEEE Circuits Syst. Mag., 2004, doi: 10.1109/MCAS.2004.1286985.